UNIVERSITY OF OKLAHOMA

GRADUATE COLLEGE

RESILIENCE ASSESSMENT AND RESILIENCE-BASED RISK MITIGATION FOR COMMUNITY BUILDING PORTFOLIOS

A DISSERTATION

SUBMITTED TO THE GRADUATE FACULTY

in partial fulfillment of the requirements for the

Degree of

DOCTOR OF PHILOSOPHY

By

PEIHUI LIN
Norman, Oklahoma
2018

Downloaded from SHAREOK. Persistent Handle URL: https://hdl.handle.net/11244/54346

RESILIENCE ASSESSMENT AND RESILIENCE-BASED RISK MITIGATION FOR COMMUNITY BUILDING PORTFOLIOS

A DISSERTATION APPROVED FOR THE
SCHOOL OF CIVIL ENGINEERING AND ENVIRONMENTAL SCIENCE

BY

_____
Dr. Naiyu Wang, Chair

_____
Dr. Charles D. Nicholson

_____
Dr. Bruce Ellingwood

_____
Dr. K.K. Muraleetharan

_____
Dr. Amy Cerato

© Copyright by PEIHUI LIN 2018
All Rights Reserved.

Acknowledgements

I would like to express my heartfelt gratitude to my advisor, Dr. Naiyu Wang, for her unconditional support of my doctoral research work. I am greatly honored to be her first Ph. D. student and I appreciate all the opportunities she has given me along the journey. Her patience and encouragement to me and enthusiasm for research motivated me throughout my doctoral program. Without her guidance, I might not have finished this dissertation and certainly would not have enjoyed the great sense of achievement that I feel from my research studies. Besides my advisor, I want to thank the rest of my dissertation committee - Dr. Charles D. Nicholson (Industrial and Systems Engineering, OU), Dr. Amy Cerato and Dr. K.K. Muraleetharan (Civil Engineering and Environmental Science, OU), and Dr. Bruce Ellingwood (Colorado State University) - for their insightful comments and advices.

I also want to thank my colleagues in our CoRe Lab - Dr. Xianwu Xue, Dr. Fuyu Hu, Dr. Weifeng Tao, Weili Zhang, Yingjun Wang, Mohammad Hadikhan Tehrani, Alexander Rodriguez, and Paul Calle Contreras - for offering me lively discussions and friendship. I appreciated and enjoyed the stimulating journey we took together working in the CoRe Lab and look forward to us working together in the future.

Lastly, I would like to thank my parents, brother, and sister for their understanding and support of me in my efforts to pursue a doctorate at the University of Oklahoma.

The research herein was supported by the Center for Risk-Based Community Resilience Planning, funded by the U.S. National Institute of Science and Technology (NIST) Award Number: 70NANB15H044. This support is gratefully acknowledged.

Table of Contents

Acknowledgements iv

List of Tables ix

List of Figures xii

Abstract xvi

Chapter 1 Introduction 1

1.1 Statement of the Problem 1

1.2 Research Objectives and Scope 3

1.3 Organization of Dissertation 5

Chapter 2 Appraisal of State of the Art 7

2.1 The Concept of Community Resilience 7

2.2 Building Portfolio Metrics 10

2.3 Building Portfolios Loss Estimation 12

2.4 Building Portfolios Recovery Modeling 17

2.5 Critical Appraisal 23

Chapter 3 Building Functionality Definition, Metrics and Notations (BPFM) 27

3.1 Building Portfolio Functionality: Definition and Metrics 27

3.2 Notation of Variables in BPLE and BPRM 31

Chapter 4 Building Portfolio Loss Estimation (BPLE) 34

4.1 Probabilistic Framework for BPLE 34

4.1.1 BPLE Formulation 34

4.1.2 Step 1: Spatial Hazard Demand Characterization (IM) 38

4.1.3 Step 2: Spatial Damage Analysis (DS) 39

4.1.4 Step 3: Portfolio Functionality Loss Estimation 41
4.1.5 Uncertainty Propagation in BPLE 46
4.2 An Implementation of Random Sampling Technique in BPLE 49
4.3 Closure 52
Chapter 5 Building Portfolio Recovery Model (BPRM) 54
5.1 Step 1: Building-Level Restoration 56
5.1.1 Discrete-State, Continuous-Time Markov Chain (CTMC) 56
5.1.2 Determination of Transition Probability Matrix (TPM) 61
5.2 Step 2: Portfolio-Level Recovery 73
5.2.1 Portfolio Recovery Trajectory (PRI) 73
5.2.2 Portfolio Recovery Time (PRT) 75
5.3 Uncertainty Propagation and Correlation Quantification 78
5.4 Closure 80
Chapter 6 Assessment of Building Portfolios in Two Testbed Communities 82
6.1 Centerville Building Portfolio Analysis 82
6.1.1 Centerville Building Portfolio Characteristics 82
6.1.2 Seismic Demands and Building Damages 86
6.1.3 Building Portfolio DLR and HDR 92
6.1.4 Building-Level and Portfolio-Level Functionality Loss 102
6.1.5 Building-Level and Portfolio-Level Functionality Recovery 104
6.1.6 Sensitivity Study 112
6.2 Shelby County Building Portfolio Analysis 115
6.2.1 Shelby Building Portfolio Characteristics 115

6.2.2 Seismic Demands 118
6.2.3 Building Portfolio Recovery 119
6.3 Closure 126
Chapter 7 Building Portfolio Decision Support (BPDS) 128
7.1 Pre-Event Risk Mitigation Strategies for Building Portfolios 128
7.2 Decision Support for Building Portfolio Retrofit Planning 132
7.2.1 Problem Description and Assumptions 132
7.2.2 Building Portfolio Performance Goal 134
7.2.3 Formulation of Portfolio Retrofit Plan Optimization 135
7.3 Case Study 138
7.4 Closure 147
Chapter 8 Conclusions and Future Work 149
8.1 Summary 149
8.2 Conclusions 150
8.3 Future Work 152
References 155

List of Tables

Table 2-1. Different social-economic loss metrics and methodologies 12

Table 3-1. Notations of variables in the BPLE and BPRM 31

Table 4-1. Relative error associated with random sampling for different correlation distances and sample sizes 52

Table 5-1. Waiting time conditional on initial damage condition and utility availability, $WT_{i,j}^{n}|ds_p, ua_q$ 72

Table 6-1. Summary of Centerville building types [data source: Lin & Wang (2017b)] 85

Table 6-2. Household characteristics of residential zones (Zone 1- Zone 7) [Data source: Lin & Wang (2017b)] 85

Table 6-3. Structural fragility curve parameters (unit: inch) [data source: HAZUS-MH (FEMA/NIBS, 2003)] 89

Table 6-4. Nonstructural drift-sensitive fragility curve parameters (unit: inch) [data source: HAZUS-MH (FEMA/NIBS, 2003)] 90

Table 6-5. Nonstructural acceleration-sensitive fragility curve parameters (unit: g) [data source: HAZUS-MH (FEMA/NIBS, 2003)] 91

Table 6-6. Building appraised value and fractions of values of structural, nonstructural acceleration-sensitive, nonstructural drift-sensitive components, and building contents [data source: HAZUS-MH (FEMA/NIBS, 2003)] 95

Table 6-7. Mean structural, nonstructural drift-sensitive, nonstructural acceleration sensitive repair cost ratio, $\mu_{DV_i|DS_i}$ for DLR (unit: %) [Data sources: HAZUS-MH (FEMA/NIBS, 2003)] 96

Table 6-8. Standard deviation of repair cost ratio with respect to structural (SD), nonstructural drift-sensitive (ND), nonstructural acceleration-sensitive (NA) components, and building contents (CL), $\sigma_{DV_i|DS_i}$ for DLR (unit: %) [Data source: MAEViz (Steelman et al., 2007)] 97

Table 6-9. Social characteristics of residential zones [Data source: Ellingwood et al. (2016); Lin & Wang (2016)] 97

Table 6-10. Statistics of Delay Time [Data source: REDi^{TM} framework (Almufti & Willford, 2013)] 107

Table 6-11. Statistics of building Repair Time with respect to repair classes (RCs) [synthesized from HAZUS-MH (FEMA/NIBS, 2003) database] 107

Table 6-12. Financing resources for Centerville buildings restoration 108

Table 6-13. Financing resources for Centerville buildings restoration after applying insurance incentives 114

Table 6-14. Residential building portfolio by structural type and seismic design code [Data Source: MAEViz (Steelman et al., 2007)] 116

Table 6-15. Statistics of delay time used in Shelby RBP recovery 120

Table 6-16. Statistics of repair time used in Shelby RBP recovery 121

Table 6-17. Distribution of financing resources in different income levels in Shelby 121

Table 7-1. Community disaster mitigation tools 130

Table 7-2. Summary of the optimization formulation 137

Table 7-3. Alternative portfolio retrofit schemes (RS) for Zone I and Zone II buildings 141

Table 7-4. Damage state probabilities for residential buildings (building type: W1) (FEMA/NIBS, 2003) 141

Table 7-5. Optimal solutions to achieve the target portfolio robustness goal ($\alpha = 90\%$) with minimized *PRC* 146

Table 7-6. Optimal solutions to achieve the target portfolio robustness goal ($\alpha = 90\%$) with minimized *PRT* 146

List of Figures

Figure 1-1. The organization of the dissertation 6

Figure 2-1. Illustration of resilience concept (Lin et al., 2016) 8

Figure 2-2. Steps in the PBEE procedures (Whittaker et al., 2004) 14

Figure 3-1. Functionality states of individual buildings (Lin & Wang, 2017a) 29

Figure 4-1. Flowchart of community-wide probabilistic pre-recovery damage and functionality loss assessment 37

Figure 4-2. Mapping from building damage and utility availability to building functionality states 45

Figure 4-3. Flowchart of the MCS for building portfolio functionality loss estimate 48

Figure 4-4. Illustration of (a) a hypothetical residential zone and (b) random sampling of the houses in this zone 51

Figure 4-5. Convergence of the random sample model using FLR as a portfolio functionality metric 51

Figure 5-1. Schematic representation of building portfolio recovery 54

Figure 5-2. Flowchart of the two-step portfolio functionality recovery modeling 55

Figure 5-3. Discrete state, continuous time Markov Chain $S(t)$ (for buildings with $S(t_0) = S_1$) 57

Figure 5-4. Illustration of building restoration function (*BRF*) of an individual building 60

Figure 5-5. An illustration of the general restoration process of individual buildings 66

Figure 5-6. General restoration paths for individual buildings with initial pre-repair functionality states of a) RE, b) RU, c) RO, and d) BF. 70

Figure 5-7. Illustration of the (a) building damage restoration and (b) utility operability restoration 71
Figure 5-8. Illustration of the mean trajectory of the building portfolio recovery 77
Figure 5-9. Expected outcome of the two-step BPRM - spatial and temporal evolution of portfolio recovery (areas are shaded to indicate level of functionality; darker means lower functionality state) 77
Figure 6-1. Centerville (a) zoning map, and (b) building portfolio 84
Figure 6-2. (a) Expected direct loss and (b) expected direct loss ratio for each building in Centerville 99
Figure 6-3. (a) Expected direct loss and (b) expected loss ratio for each building zone and critical facility in Centerville 100
Figure 6-4. Probability of exceeding (a) Direct Loss Ratio (DLR) and (b) Household Dislocation Ratio (HDR), for Centerville Zones 1, 3 and 7 for the Mw7.8 earthquake 101
Figure 6-5. Spatial variation in the mean damage state of (a) structural components (SD), (b) non-structural drift-sensitive (ND) , (c) acceleration-sensitive components (NA), and (d) the mean initial functionality state a$t\ t_0$ 103
Figure 6-6. Probability assessment of (a) building-level pre-repair functionality state PMF, $\pi^n(t_0)$ (illustrated using W2 in Zone 4); and (b) portfolio-level pre-recovery functionality index, $PRI_j(t_0)$. 104
Figure 6-7. Illustration of building-level restoration: (a) conditional mean restoration process and (b) the building restoration function, BRF (both illustrated using W2 building in Zone 4 as an example). 108

Figure 6-8. Mean portfolio recovery trajectory and recovery time 109
Figure 6-9. An illustration of (a) uncertainty in the portfolio recovery trajectory; and (b) the mean recovery trajectory for each of the seven residential zones (Zone1-Zone7) . 111
Figure 6-10. Spatial variation of functionality recovery at a) $t_0 = 0$; b) 30 weeks; c) 60 weeks; and d) 90 weeks following the hazard occurrence. 112
Figure 6-11. Comparison between recovery resources with and without insurance incentive 114
Figure 6-12. Updated Centerville portfolio recovery trajectory and recovery time respectively for Case 1 and Case 2 115
Figure 6-13. Distribution of (a) the residential buildings in census tracts of Shelby County (Data source: MAEViz, Steelman et al., 2007); (b) annual household income in 2015 inflation-adjusted dollars (Data source: https://censusreporter.org/profiles/05000US47157-shelby-county-tn/) 117
Figure 6-14. Median peak ground acceleration (PGA) with soil amplification 119
Figure 6-15. Financing resources percentage in Shelby RBP 120
Figure 6-16. Spatial variation and temporal evolution of recovery to (a) power service (0-fully available; 100%-not available); (b) water service (0-fully available; 100%-not available); (c) building functionality (1-RE; 2-RU; 3-RO; 4-BF; 5-FF) 124
Figure 6-17. Recovery trajectory of Shelby RBP under (a) extreme level scenario earthquake; (b) expected level scenario earthquake (1-RE; 2-RU; 3-RO; 4-BF; 5-FF) 125
Figure 6-18. Mean recovery trajectory of RBP in Shelby 126
Figure 7-1. Portfolio system reliability (*PSR*) versus portfolio retrofit cost (*PRC*) 144

Figure 7-2. Number of buildings in Zones I (z_1) and II (z_2) that require retrofit (for target portfolio robustness goal $\alpha = 90\%$) 145
Figure 7-3. Boxplot of total number of buildings require retrofit (for target portfolio robustness goal $\alpha = 90\%$) 145
Figure 7-4. Portfolio recovery time (*PRT*) versus portfolio retrofit cost (*PRC*) (for target portfolio robustness goal $\alpha = 90\%$) 146

Abstract

The resilience of a community is determined by its ability to withstand and recover from disruptions due to natural or manmade hazards. While a consensus has developed in disaster-related research in recent years that community infrastructure should be designed, managed and regulated to achieve community-specific resilience goals, there is currently no integrated source of quantitative tools and measurement technologies to support risk mitigation decisions of building owners, city planners, policy makers and other community stakeholders in a coordinated and risk-informed manner.

The on-going efforts in the NIST-funded Center for Risk-based Community Resilience Planning (CRCRP) are aimed at developing a comprehensive computational platform, named IN-CORE, which integrates science-based models of community socio-economic systems and supporting interdependent physical infrastructure (i.e. building portfolios, transportation infrastructure, energy, water/wastewater, and communication networks) in several distinct modules, with an ultimate goal of supporting community risk mitigation decisions and optimizing resilience planning activities. This dissertation work provides the essential components of the IN-CORE module on Community Building Portfolio Resilience Analysis.

This work contributes to the state of the art of resilience assessment of community building portfolios in several aspects. First, a new building portfolio functionality metric (BPFM) is proposed, which is a measureable, scalable, and actionable indicator of a building portfolio's capacity to respond and recover from a hazard event. The BPFM enables the resilience of a building portfolio to be assessed on

a consistent measure at various spatial scales (e.g. parcel, block, census, zone or community) and throughout the time domain of interest (i.e. pre-event planning, immediate post-disaster response, and long-term recovery). Second, a building portfolio functionality loss estimation (BPLE) framework is developed, which provides a probabilistic and spatial loss assessment, measured by the BPFM, across an entire community immediately following a hazard event; this assessment also defines the initial post-event functionality state, which is the starting point for building portfolio recovery modeling. Third, a novel stochastic post-disaster building portfolio recovery model (BPRM) is formulated; this model characterizes the spatial and temporal evolution of a building portfolio's recovery following a hazard event, resulting in projected recovery trajectory and recovery time of the building portfolio, as well as the spatial variation of the recovery outcome within the community. Finally, a building portfolio decision support (BPDS) framework is constructed, underlining that the resilience of a building portfolio (assessed by the BPLE and BPRM) can be enhanced to achieve risk-informed resilience goals through optimized mitigation strategies and recovery planning activities at a community scale.

Chapter 1 Introduction

1.1 Statement of the Problem

The increasing vulnerability of communities to natural hazards, as manifested in recent disaster events such as Wenchuan Earthquake in 2008, Superstorm Sandy in 2012, the Moore, OK Tornado in 2013, and Hurricane Harvey in 2017, has posed significant research challenges in disaster-related science and technology. While there is a consensus among researchers that effective hazard mitigation requires systematic and holistic community-level planning for disaster resilience, to date there are no science-based tools and measurement frameworks to guide the public and private decision makers to assess and enhance resilience of their communities in a quantitative and integrated manner.

Among existing community resilience assessment and planning methodologies being implemented or under development are the San Francisco Planning and Research Association (SPUR) Framework (Poland, 2009), the Oregon Resilience Plan (OSSPAC), the UNISDR Disaster Resilience Scorecard for Cities (UNISDR, 2014), the Rockefeller Foundation City Resilience Framework (CRF) (Arup, 2014), FEMA's HAZUS Methodology (FEMA/NIBS, 2003), and the NIST Community Resilience Planning Guide (NIST, 2015). Each of these methodologies has a different scope of application, focuses on different hazard types, emphasizes different aspects and dimensions of community resilience, and has its own limitations in theory and practice. Although these methodologies have provided partial or comprehensive, qualitative or quantitative tools to guide community resilience planning, most of them lack an integration of resilience assessment models for a whole spectrum of subsystems that

collectively provide the technical, organizational, social and economic functions of a community. The on-going efforts in the NIST-funded Center for Risk-based Community Resilience Planning (CRCRP) are aimed at the development of measurement science and technology to support community resilience planning. The major work product of the CRCRP is a comprehensive computational platform, named IN-CORE, which integrates science-based models of community socio-economic systems and supporting interdependent physical infrastructure (i.e. building portfolios, transportation infrastructure, energy, water/wastewater, and communication networks) in several distinct modules. The ultimate goals of the CRCRP and IN-CORE are to support community risk mitigation decisions and optimize resilience planning activities. *This dissertation work provides the essential components of the IN-CORE module on Community Building Portfolio Resilience Analysis.*

The building portfolio within a community is essential to the day-to-day operation of the community as it provides infrastructure that supports critical community functions such as housing, education, business, health services and government. Physical damages and functionality losses caused by natural hazard events to a community building portfolio, as a system, can lead to multi-scale social-economic impacts that cascade throughout all sectors of the community during and long after the hazard event. Traditionally, the impact of natural hazards on individual buildings has been considered by structural engineers through codes, standards and regulations in building design, construction and management (NEHRP, 2009; ASCE Standard 7, 2016). These codes and standards for individual buildings, however, were developed mainly to protect life safety in the events of extreme hazard events, without considering

the functional dependences among buildings of different occupancies or between a building portfolio and other infrastructure systems that together contribute to the social-economic stability of a community. This lack of a system-level perspective in traditional disaster management has caused communities to experience disproportionate physical damages, economic losses and social disruptions in hazard events notwithstanding that the buildings, individually, had been designed and constructed to comply with codes and acceptable construction practices (Bruneau et al., 2003; Bruneau & Reinhorn, 2006, 2007; Cutter et al., 2008; OSSPAC, 2013; Poland, 2013).

To facilitate community resilience planning, the current engineering practice of design, assessment, and risk management of buildings should move beyond the life-safety focused consideration at the individual building level to a comprehensive portfolio-level approach. This portfolio-level approach must be developed through investigation and modeling of the functionality loss and recovery process of spatially distributed buildings within a community as a whole, as an integrated system, to enable pre-disaster mitigation decisions and post-disaster recovery planning strategies to be optimized under various resources and regulatory constraints in a risk-informed manner.

1.2 Research Objectives and Scope

The objective of this dissertation is twofold: 1) to develop physics-based analysis models that allow the functionality loss and recovery of a building portfolio as a whole to be predicted and assessed in a quantitative and probabilistic manner; and 2) to formulate a risk-informed decision methodology that allows hazard mitigation

strategies and recovery planning activities to be optimized to facilitate resilience goals of a community building portfolio to be achieved.

The dissertation will focus on the following tasks:

- Critically appraise the advances and limitations of existing resilience assessment methodologies for community building portfolios;
- Identify or introduce, if necessary, a definition of and a metric for *the functionality of a community building portfolio* that can be assessed quantitatively as an effective indicator of a portfolio's capacity to respond and recover from a hazard event.
- Develop a framework for building portfolio functionality loss estimation (BPLE) in which the spatial damages and functionality losses across the geographic domain of a community building portfolio are quantified probabilistically.
- Develop a building portfolio functionality recovery model (BPRM) which characterizes the spatial and temporal evolution of the recovery process of a building portfolio from its initial functionality loss, resulting in the estimates of portfolio recovery trajectory and recovery time as well as associated uncertainties at different spatial resolutions.
- Illustrate a complete analysis procedure for building portfolio resilience assessment by applying the BPLE & BPRM framework to two testbed communities.
- Formulate a building portfolio decision support (BPDS) framework which enables the resilience of a building portfolio to be enhanced to achieve risk-informed resilience goals through optimized mitigation strategies and recovery planning activities at a community scale.

1.3 Organization of Dissertation

Consistent with the research tasks listed above, this dissertation includes eight Chapters.

Chapter 2 reviews and critical appraises state-of-the art methodologies on loss estimation and recovery modeling of community building portfolios and identifies research challenges for the dissertation work. In Chapter 3, a new functionality definition and metric for building portfolios (BPFM) is proposed for resilience assessment as an effective indicator of a portfolio's capacity to respond and recover from a hazard event. In Chapter 4, a probabilistic framework for building portfolio functionality loss estimation (BPLE) is developed in which the loss is measured in term of the BPFM. In Chapter 5, a novel simulation-based, two-step stochastic building portfolio functionality recovery model (BPRM) is developed, with the portfolio spatial functionality loss characterized by the BPLE framework as the initial state for recovery. In Chapter 6, the applications of the developed resilience assessment tools for building portfolios - i.e. the BPLE and BPRM - are illustrated through case studies of two testbed communities – one is a hypothetical community called Centerville, and the other is Shelby County, Tennessee, USA. In Chapter 7, a building portfolio decision support (BPDS) framework is formulated, highlighting that the resilience a community building portfolio can be quantified (e.g. using BPLE and BPRM) and subsequently can be enhanced through optimized mitigation strategies and recovery planning activities at a community scale to achieve risk-informed resilience goals. The organization of Chapters 3-7 is illustrated in Figure 1-1. Chapter 8 summarizes the major contributions of this research and suggests future lines of inquiry.

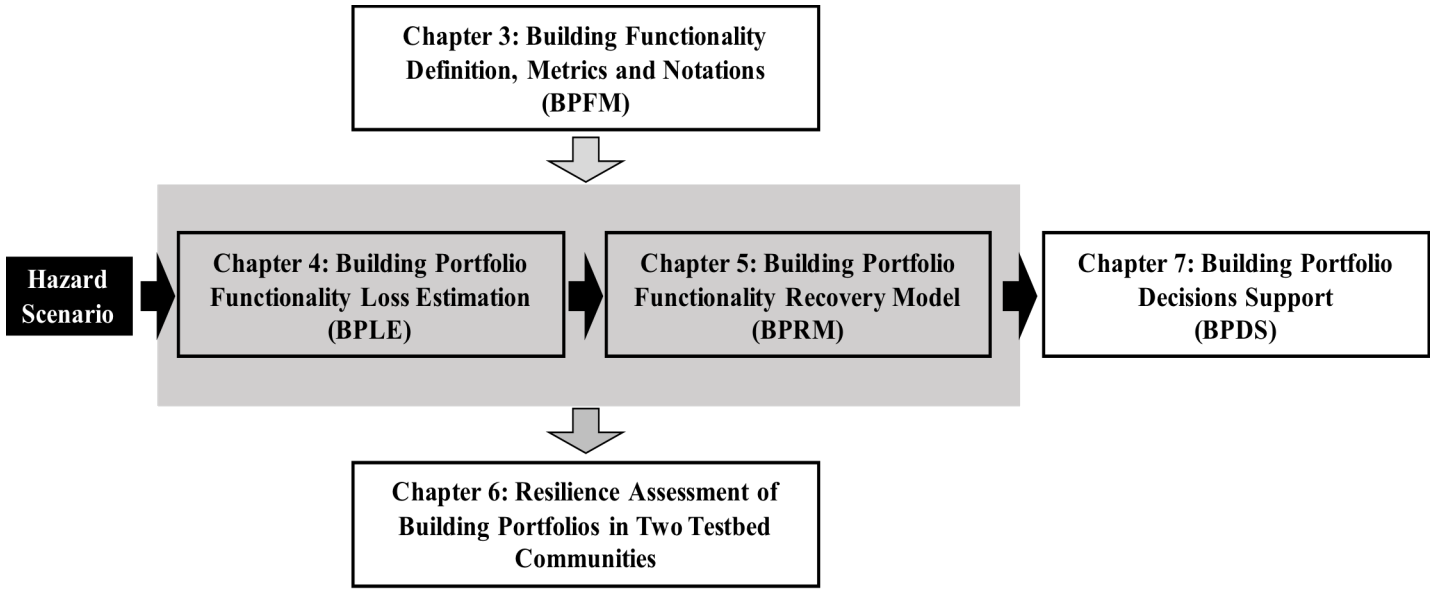


Figure 1-1. The organization of the dissertation

Chapter 2 Appraisal of State of the Art

The concept of enhancing community resilience has evolved in the past decade around the notion that communities should develop strategies for mitigating the impact of natural hazards from the failures of the built environment and supporting social, economic and political institutions, and for organizing post-disaster recovery activities that revitalize communities and restore normalcy within a reasonable period of time. In this chapter, the general concept of community resilience in the context of natural hazards will be reviewed in Section 2.1. Existing resilience metrics relevant to community building portfolios will be summarized in Section 2.2. Existing methods on quantitative resilience assessment of building portfolios (or other physical systems) will be reviewed in Sections 2.3 and 2.4 for loss estimation and for recovery prediction, respectively. Finally, a critical appraisal presented in Section 2.5 will identify existing research gaps in building portfolio resilience assessment.

2.1 The Concept of Community Resilience

A community is an entity designated by geographical boundaries that functions under a common governance structure and has a common culture and historical heritage (NIST, 2015). In the event of severe natural disasters, a resilient community should be able to withstand the resulting physical damages and social disruptions and to facilitate a planned and expedited recovery. We adopt the definition of resilience given in the NIST community resilience planning guide (NIST, 2015) as “the ability of a community or a system to prepare for and adapt to changing conditions, and to withstand and recover rapidly from disruptions”.

The resilience of a community (or a system) is often expressed by functionalities of the community (or system) as a function of time (Bruneau et al., 2003; Bruneau & Reinhorn, 2006, 2007; Bruneau, 2006; Cimellaro et al., 2010a, 2010b; Bocchini & Frangopol, 2011; Lin et al., 2016) as illustrated in Figure 2-1. Bruneau et al. (2003) have identified four essential attributes of resilience: *robustness* - the ability to withstand an extreme event and deliver a certain level of service even after the occurrence of that event; *rapidity* - to recover the desired functionality as fast as possible; *redundancy* - the extent to which elements and components of a system can be substituted for one another; and *resourcefulness* - the capacity to identify problems, establish priorities, and mobilize personnel and financial resources after an extreme event. The assessments of these attributes require quantification and modeling of considerable uncertainties, as indicated by the probability density functions (PDF) in Figure 2-1.

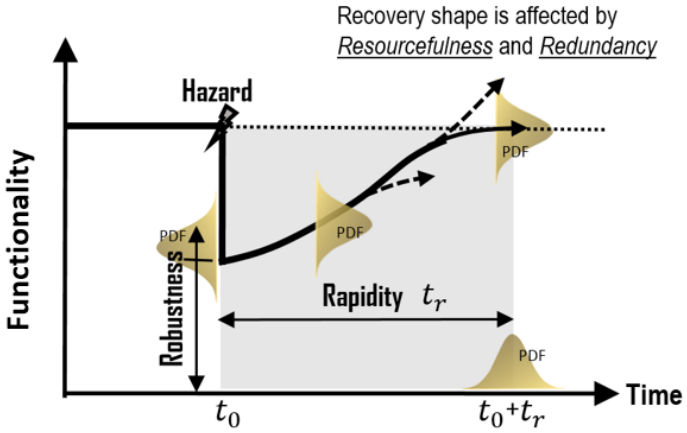


Figure 2-1. Illustration of resilience concept (Lin et al., 2016)

Moreover, the resilience of a community, as summarized in Bruneau et al. (2003), can be conceptualized as encompassing four interrelated dimensions:

technical—the ability of physical systems (e.g. building portfolios, transportation systems and utility networks) to withstand and recovery from hazards; *organizational*—the capacity of various organizations (e.g., government and emergency response agencies) that manage essential facilities to plan, make decisions and take actions prior to, during and following the occurrence of a hazard event; *social*—the ability of people within a community to design measures to lessen the negative social consequences of the disaster; and *economic*—the capacity of community to reduce both direct and indirect economic losses from hazard consequences.

To quantify each of the four abovementioned dimensions of resilience for a community , one needs to identify the community-specific functionality metrics (i.e. the vertical axis of Figure 2-1) that must be measureable, scalable, and actionable indicators of the community' capacity to respond and recover from a hazard and must be associated with a broad spectrum of community systems, e.g. including but not limited to physical damages and recovery of built environment, direct economic losses and recovery, and impact on social well-being (NIST, 2015). Such functionality metrics are indispensable elements of community resilience measurements enabling abstract resilience concepts to be mapped into specific actions. Several studies have provided comprehensive summaries of metrics for different community functions that extent to different attributes of resilience (Bruneau et al., 2003; Cutter, 2008, 2014; Burton, 2015; NIST, 2015). Beyond those, a few studies have focused on the classification and systemization of existing metrics in term of their applicability to communities of different sizes and scales, policy realms, as well as different types of hazards and shocks (Rodriguez-Llanes, 2013; Cimellaro, 2016). Nevertheless, most existing community

functionality metrics summarized in the literature are illustrative and conceptual in nature.

Community resilience planning requires establishing and maintaining resilience of all aforementioned dimensions (i.e. technical, organizational, social, and economic dimensions), thus by nature is a collaborative effort that demands commitments from various community stakeholders, including local government officials for resilience planning, emergency response and social services, public and private owners of buildings, operators of different infrastructure systems, local business and industry owners, and other social and economic organizations (NIST, 2015). Effective community resilience planning must be supported by quantitative resilience assessment in all of the above dimensions, which not only requires clearly defined functionality metrics for each dimension but also demands robust, risk-informed tools and models that can support the resilience assessment in that dimension. The following review focuses on the existing metrics and assessment tools for community building portfolios, which belongs to the technical (or physical) dimension of the community resilience.

2.2 Building Portfolio Metrics

A community's building portfolio is an essential asset of the community and serves as the physical foundation to support critical social and economic functions of the community. A community building portfolio consists of buildings of different of occupancies - residential, commercial, industrial, and many other critical facilities such as education, health care and government institutions. In addition, a building portfolio can represent a group of buildings at various spatial scales and resolutions, e.g. a

building block, a neighborhood, a group of essential facilities (e.g. hospitals and schools), a zone of commercial/retail buildings, or all buildings within a community. The resilience curve (cf. Figure 2-1) of a building portfolio is anchored by its robustness and rapidity of recovery, while the resourcefulness and redundancy of the portfolio as an integrated system affect the shape of the curve. Measuring resilience of a building portfolio requires functionality metrics that can be used not only to measure directly the robustness of a portfolio but also to track (or to monitor) the recovery of the portfolio.

Among widely-accepted metrics that are closely tied to the performance of a community building portfolio are *direct economic loss ratio, DLR* (ratio of losses directly caused by building damage to the total assessed value of buildings, or other losses such as business interruption, rental income loss, etc.), *indirect economic losses* (such as loss of taxes, price increases, increased demand of substitutes, increased supply of labors, etc.), *household dislocation ratio (HDR)*, *casualty* and *building downtime*, as summarized from the literature in Table 2-1. These metrics are mostly social and economic-based metrics. In most cases, they are estimated by regression models derived from empirical observations and field data including building damage as the major input variable along with other demographic characteristics (such as race, age, income, etc.) as associated building attributes, such as the approach in HAZUS (FEMA/NIBS, 2003), the ordinary least-squares model (Peacock et al., 2008), and the logic regression model (Lin, 2009) among others. Moreover, even when field data of past events are available, certain metrics, such as indirect economic loss in terms of GDP, are still difficult to predict due to the intrinsic complexity of the operations of social and economic systems within a community and the various sources of uncertainties involved. Furthermore,

these social and economic oriented metrics in Table 2-1 in fact should be determined jointly by the performances of all subsystems of a community built environment, which, aside from building portfolios, also includes lifelines and other critical facilities; however the conventional methodologies to quantify these metrics (also summarized in the Table 2-1) are often linked solely to the damage levels of buildings, which explicitly neglect the impact of other physical infrastructural systems on the community's social and economic functions.

Unfortunately, a metric that is firmly rooted in the performance of a building portfolio and directly measures the functionality of that building portfolio could not be found in the literature.

Table 2-1. Different social-economic loss metrics and methodologies

Loss Metrics	Methodologies
Direct economic Loss Ratio (DLR)	HAZUS approach (FEMA/NIBS, 2003); Empirical data by RS Means Company (2015)
Indirect economic Loss	Input-output model (Okuyama et al., 2004); Computable General Equilibrium (CGE) model (Rose & Guha, 2004)
Household dislocation Ratio (HDR)	HAZUS approach (FEMA/NIBS, 2003); Ordinary least-squares model (Peacock et al., 2008); Logic regression model (Lin, 2009)
Casualty	Event tree modeling (FEMA/NIBS, 2003)
Building downtime	FEMA P-58 (FEMA, 2012); REDi (Resilience-based earthquake Design Initiative) rating system (Almufti & Willford, 2013)

2.3 Building Portfolios Loss Estimation

Existing models for estimating building-related losses vary with different metrics (such as those identified in Table 2-1) and different building types considered, different hazards investigated, and different resolutions and scales at which the analysis

is performed. Most of existing loss estimation models have incorporated a somewhat probabilistic approach to account for uncertainties, both aleatory and epistemic, associated with hazard intensities, building responses, structural capacities, and physical damages.

At the individual building level, conventional building loss estimation models usually involve a sequence of uncertainty propagations through hazard analysis, structural response assessment, damage evaluation and finally to loss estimation. The Pacific Earthquake Engineering Research Center introduced a Performance-based Earthquake Engineering (PBEE) framework to quantify three loss metrics associated with a building - death (loss of life), dollars (economic losses), and downtime (temporal loss of use of the facility) (FEMA, 1997) as illustrated in Figure 2-2 and expressed as (Cornell & Krawinkler, 2000):

$$\lambda(DV) = \iiint G(DV|DM)dG(DM|EDP)dG(EDP|IM)|d\lambda(IM)| \quad (2\text{-}1)$$

where $\lambda(DV)$ is the mean annual frequency of exceeding the decision variable, DV; $G(DV|DM)$ is the conditional probability that the decision variable (*DV*) exceeds a specified level given the damage measure; $dG(DM|EDP)$ is the conditional probability that the damage measure (*DM*) exceeds a specified level given the engineering demand parameter; $dG(EDP|IM)$ is the conditional probability that the engineering demand parameter (*EDP*) exceeds a specified level given the intensity measure (*IM*); and $|d\lambda(IM)|$ is the mean annual frequency of exceeding hazard intensity *IM*, which is the derivative of the hazard curve.

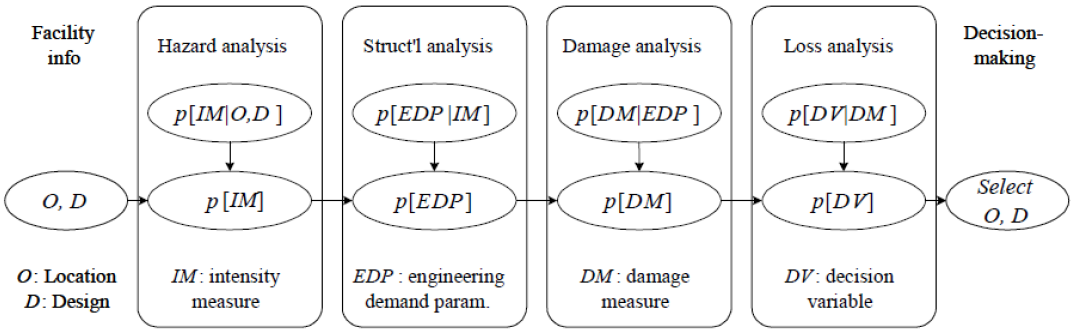


Figure 2-2. Steps in the PBEE procedures (Whittaker et al., 2004)

Eq. (2-1) is a statement of the theorem of total probability, and estimates the annual exceedance rate of a decision variable (death, dollar, and downtime) via integrating a set of sub-analysis: hazard analysis, structural analysis, damage analysis, and loss analysis (see Figure 2-2). In the hazard analysis, one obtains $\lambda(IM)$ through hazard curve which describes the annual frequency with which seismic excitation exceeds a set of predefined threshold levels. The seismic excitation is parametrized by an intensity measure such as spectral displacement or spectral acceleration. In the structural analysis, a structural model of the building is created to obtain the uncertain response (*EDP*) conditioned on a seismic intensity (*IM*) using linear or non-linear time-history structural analysis. In damage analysis, a building's physical damage is generally categorized into several levels (defined relative to the level of repair efforts needed to restore the component to its undamaged state) and the probability of exceeding a specific damage level (*DM*) conditional on a structural response (*EDP*) is calculated. Alternatively, the structural analysis and damage analysis [i.e., the joint term $\int_{EDP} dG(DM|EDP)dG(EDP|IM)$] of Eq. (2-1) can be substituted by a fragility function derived from a hazard-specific vulnerability analysis. A fragility function, defined as the probability that the response of a building equals or exceeds a stipulated

damage state as a function of hazard intensity, is expressed as a lognormal distribution function (FEMA/NIBS, 2003), i.e.:

$$\mathrm{P}[ds|IM] = \Phi[\ln (IM/\overline{IM}_{ds})/\beta_{ds}] \quad (2\text{-}2)$$

where $\overline{IM}_{ds}$ is the median value of seismic intensity IM at which the structure reaches the threshold of the damage state, *ds*; β_{ds} is the standard deviation of the natural logarithm of seismic intensity with respect to damage state, *ds*. The damage states (*ds*) in HAZUS are described as *slight*, *moderate*, *extensive*, and *complete*, each being associated with a set of predefined quantitative performance thresholds (in terms of relevant structural response parameters, e.g. inter-story drift ratio). The fragility function obtained from hazard-specific vulnerability modeling of individual buildings or other structures provides an effective tool to directly relate damage of structures to hazard intensity at a building site. Lastly in loss analysis, the probabilistic estimation of decision variable (*DV*) conditioned on a damage measure (*DM*) is mostly derived from insurance underwriting data, or using empirical data collected from field studies or data suggested by engineering experts.

The loss estimation of spatially distributed building portfolios, however, is more complex than building-specific loss estimation. Unlike building-specific loss estimation which focuses on estimating "deaths, dollars, and downtime" at a specific building site, the analysis of building portfolios aims at predicting losses in terms of system-level metrics that are most suitable for community stakeholders, as those summarized in Section 2.2. When loss is estimated for a building portfolio at a regional or a community scale, the spatial correlations between the random variables modeling the demands and capacities of spatially distributed buildings must be considered. Such

correlations are mainly due to two major sources: the correlation in building responses caused by a common hazard with a large footprint (referred to as site-to-site correlation), and correlation in structural responses caused by common structures materials, common structural design code and enforcement, and/or common construction practice (referred as structure-to-structure correlation). Both correlations tend to be positive in nature, and it has been found that neglecting such correlations can lead to unconservative estimations of losses for spatially distributed building portfolios (cf. Vitoontus & Ellingwood, 2013). Unfortunately, existing loss estimation platforms, such as HAZUS-MH (FEMA/NIST, 2003) and MAEViz (Steelman et al., 2007), have considered either type of correlation.

Some studies have considered the correlation in ground motion intensity for earthquake events, more specifically, focusing on developing site-to-site correlation models for both intra- and inter-event correlations (Wang & Takada, 2005; Lee & Kiremidjian, 2007; Goda & Hong, 2008; Jayaram & Baker, 2009; Miller, 2011; Vitoontus & Ellingwood, 2013; Bonstrom & Corotis, 2014). Wang and Takada (2005) performed a covariance analysis using dense observation data of earthquakes occurred in Japan in recent years, and proposed a macro-spatial correlation model in which the auto-covariance at two separate points was modeled with an exponential decay function with respect to the separation distance between two observations (ranging from 20 to 50 km). Goda and Hong (2008) developed empirical equations to include the spatial separation distance and natural period of vibration of SDOF systems while predicting the correlation of ground motion parameters considering both inter-event and intra-event variability. Jayaram and Baker (2009) used observed ground motions from seven

past earthquakes to estimate correlation between spatially distributed spectral accelerations at various spectral periods and concluded that the rate of decay of the correlation with separation typically decreases with increasing spectral period.

Compared with site-to-site correlation, the structure-to-structure correlation is much less investigated due to its complexity and the lack of available data specific to the system of interest (Lee & Kiremidjian, 2007, Vitoontus & Ellingwood, 2013). Lee and Kiremidjian (2007) accounted for structure-to-structure damage correlations in the seismic risk assessment of bridges by assuming a partial correlation for bridges within a same class grouped by design method, contractor/construction crews, and/or design year; a sensitivity study was performed for the varying levels of damage correlation assumed. Vitoontus and Ellingwood (2013) proposed a mathematical model to estimate the structure-to-structure correlation for the risk assessment of spatially distributed buildings, in which the damage of buildings is described by the joint effects of material, structural type, and building code of the structure, and a noise term.

2.4 Building Portfolios Recovery Modeling

Although many communities have taken the initiative to enhance their resilience through proactive planning and changes to building practices (Poland, 2013, Oregon, 2013, NIST, 2015), there are neither an integrated policy framework nor readily available tools to improve community recovery outcomes owing, in large part, to the lack of practical recovery models. The use of event-specific case studies to describe the recovery process at the local level dominated early research on disaster recovery (Quarantelli, 1982; Rubin, 1985; Rubin, 1991; Haas et al., 1997); those studies

emphasized how local planning and management expedited recovery, and identified which mitigation techniques had been adopted and incorporated in the recovery process successfully (Smith & Wenger, 2007). More recent studies have included the role of recovery in decision making regarding urban planning and policy implementation, and have considered other aspects of community resilience planning, risk mitigation and recovery optimization (Ohlsen & Rubin, 1993; Peacock et al., 1997; Olson, 2000; Peacock et al., 2011; May & Williams, 2012; Peacock et al., 2014; González et al., 2015; Zhang et al., 2017). These studies have provided important insights into our current understanding of disaster recovery. However, a review of these studies has made it apparent that improvements to recovery outcomes will be difficult to achieve unless a quantitative model revealing the fundamentals of recovery processes is developed.

The FEMA National Disaster Recovery Framework defined the recovery phases of a community as having three parts: short-term, intermediate, and long-term (NIST, 2015). Each phase involves certain mitigation and restoration activities to recover the functionalities of all community systems from the consequences of a hazard event. For example, the short-term phase mainly focuses on rescue, stabilization, and preparing for recovery which is expected to last several days to weeks. The intermediate phase mainly focuses on restoring the neighborhoods, workforce and caring for the vulnerable populations, and extends for weeks to months. The long-term phase is related to restoring the community's economy and all social institutions and physical infrastructure, which may last for years (NIST, 2015).

At the early stage of disaster recovery research, recovery was considered in the literature to mainly focus on the fact of recovery itself, in terms of the roles of

restoration activities and restoration time required in each recovery phase (Kates & Pijawka, 1977; Haas et al., 1977; Quarantelli, 1982; Berke et al., 1993). More recently as people's attention has shifted to the questions concerning how to achieve or improve community resilience, much literature has emphasized "conceptualizing disaster recovery as a social process, involving decision-making, institution capacity and conflicts between interest groups" (Berke et al., 1993; Miles & Chang, 2003). Despite the many case studies of disaster recovery examined, key findings and major issues investigated, and various conceptual frameworks proposed, very few quantitative methodologies have been developed to simulate recovery. Modeling the entire recovery process requires a comprehensive understanding of post-disaster circumstances and conditions, including damage and serviceability of buildings and lifelines, their interactions with social and economic systems, availability of human and financial resources for recovery activities, and decisions made by relevant stakeholders at each stage of the recovery (Deshmukh & Hastak, 2012).

Miles and Chang (2003; 2007; 2011) developed a simulation method for urban post-disaster recovery. In this model, a community's built environment was presented by three modules, namely, businesses, households, and lifelines systems, and the analysis was performed across individual, neighborhood and community scales. Functionality attributes of each module were empirically related to the community's social characteristics, pre-event mitigation strategies and post-event recovery activities. Guided by empirical observations, the functionality dependencies within each module and among different modules were identified and a conceptual model simulating the urban disaster recovery process was established. During the simulation process, the

socio-economic recovery of the community was obtained by employing Markov Chains to represent community functions (such as the restoration of buildings and lifelines, business demand and supply recovery, health recovery, etc.) that are dynamic in nature and change over time. This method has provided numerous insights into community recovery modeling, especially including its potential capability to explore spatial decisions support for hazard mitigation and recovery planning. However, it is limited by the assumptions and simplifications embedded in the methodology, which stem from inadequate empirical data and past experience and therefore lead to difficulties in calibrating the necessary modeling variables and in incorporating uncertainties in the simulation algorithm.

Among the various recovery dimensions within a community, the recovery of physical infrastructure systems (buildings, critical facilities, transportation systems, utility networks) serves as the foundation that supports the social and economic functions of a community. Existing recovery models for physical infrastructure systems may be grouped into three categories. 1) Empirically-based models are derived from empirical data of a past event gathered through surveys (Bolin & Stanford, 1991; Shinozuka et al., 1998; Nojima et al., 2001; Zhang & Peacock, 2009; Chang, 2010; Xiao & Van Zandt, 2012; Peacock et al., 2014). Such models are obtained through examining well-known disasters worldwide, summarizing important lessons learnt from post-disaster recovery, providing policy or decision recommendations, and generating recovery trajectories using, most often, a statistical data fitting approach. Moreover, empirically-based models are event- and location-specific, lack the basis for incorporating uncertainty in recovery modeling, and are difficult to generalize to

support risk mitigation decisions. 2) Simulation-based models are developed from a conceptual investigation of the spatial and temporal evolution of the recovery process, and may be guided by empirical observations from past disasters (Hoshiya, 1981; Noda et al., 1981; Isoyama et al., 1985; Isumi et al., 1985; Kozin & Zhau, 1990; Miles & Chang, 2003; Liu et al., 2007； Burton et al., 2015). For example, Kozin and Zhou (1990) employed a discrete-state, discrete-transition Markov Chain to simulate the restoration of interdependent lifelines modeled as one integrated system; the transition probabilities were formulated as functions of rescue resources, geographic conditions, and topological and structural characteristics of the lifelines. Burton et al. (2015) proposed a framework to incorporate probabilistic building performance in an assessment of community building recovery. In this model, a set of building performance limit states (adopted from the building performance categories defined by SPUR) were identified, building recovery functions were developed by quantifying the time spent in each of the probable performance limit states, and the expected recovery functions of individual buildings were then aggregated to obtain the community level recovery trajectory. Such simulation-based models are most compatible with "what-if" scenario analysis to illustrate the impact of different pre-event or post-disaster risk mitigation activities on the recovery of the system under investigation, thus facilitating the comparison between alternative strategies for resilience planning. Finally, 3) optimization-based models, in which recovery simulation is coupled with decision optimization, lead to a set of optimal recovery strategies along with a best recovery process and the shortest recovery time (Nojima & Kameda, 1992; Kameda, 1994; González et al., 2015, Zhang et al., 2017). For instance, González et al. (2015)

formulated an interdependent network recovery model considering both functional and geographical interdependencies, in which the optimal restoration sequence of damaged network components was determined by minimizing the overall network cost. Zhang et al. (2017) optimized roadway network recovery from an earthquake event by incorporating network topology, redundancy, traffic flow, damage states and available resources into a stochastic decision process. The result was an optimal schedule for sequencing post-disaster restoration interventions for all damaged bridges, which led to the fastest (in terms of time) and most efficient (in terms of indirect loss) network recovery process. While the simulation-based models are often used to forecast the recovery time and trajectory of a system probabilistically, the optimization-based models determine the optimal recovery trajectory and the shortest recovery time by searching for the best decisions through optimization regarding priorities, scheduling, resource allocation, etc.

The recovery of building portfolios has been investigated far less than the recovery of lifelines. Lifelines in a community are usually managed by a single entity or a limited number of owners (e.g. the power, water and gas networks in Shelby County, TN, are all maintained by a municipal public utility - Memphis Light, Gas and Water (MLGW); bridges and roadways usually are managed by State, City or County agencies). Accordingly, their recovery is likely to be a top-down process governed by centralized decisions and resources. On the other hand, buildings in a community are owned by a mix of public and private stakeholders. The functionality recovery of a community building portfolio as a whole is determined, collectively, by the decisions that numerous stakeholders make over the recovery phase. Those decisions usually are

uncoordinated and are affected by the financial and social status and risk perception of individual owners, as well as by the overall resourcefulness and preparedness of the community (e.g. insurance coverage, FEMA emergency relief fund, small business loans, private loans, etc.). Consequently, the collective recovery of a community building portfolio is market-driven and decentralized in nature (Peacock et al., 2014). A recovery model that considers a community building portfolio as an integrated system is not found in the literature.

2.5 Critical Appraisal

Current research on quantitative resilience assessment of building portfolios is in a rudimentary state of development. Conventional quantitative tools for assessing building losses at a regional or community scale have treated distinct buildings independently, without considering the functional dependences among buildings of different occupancies as well as dependencies between the building portfolio as a whole and the supporting civil infrastructure systems that together contribute to the social-economic stability of a community. This lack of a system-level perspective in building portfolio analysis has led to cascading deficiencies in several critical aspects of resilience assessment for building portfolios, including metric identification, loss evaluation and recovery modeling.

Building Portfolio Performance Metrics

System-level metrics as clear and direct indicators of the functionality level of a building portfolio in its entirety are not found in the literature. Existing metrics that have been used in the past as indicators of the performance of building portfolios, as

reviewed in Section 2.2, are in fact not effective metrics specifically designed to support resilience assessment of building portfolios. Those metrics measure key community functions supported by built infrastructure, and at the same time, are affected by the communities' socioeconomic infrastructure. The inability to decouple the effect of community social and economic characteristics from these metrics has obscured the ability of these metrics as effective indicators of the functionality of a building portfolio itself. On the other hand, these metrics are often used only as measures of "robustness" (i.e. only being quantified immediately following a hazard event), and are not suitable for "monitoring" or "tracking" the functionality of a building portfolio (or of a community in general) throughout the post-disaster recovery process. First and foremost, a measurable and scalable metric for a building portfolio must be defined as the first step toward developing a comprehensive and quantitative framework for building portfolio resilience assessment. This metric must be firmly rooted in the performance of the building portfolio itself, and at the same time, explicitly reflect the dependence of the building portfolio as a whole on the other infrastructure systems in the same community.

Building Portfolio Loss Estimation

Regarding probabilistic loss estimation of spatially-distributed building portfolios, very limited studies have explicitly modeled both the site-to-site and structure-to-structure spatial correlations, as reviewed in Section 2.3. The neglect or incomplete consideration of these correlations inevitably leads to underestimation of spatial losses and unconservative errors in portfolio resilience assessment. Common deficiencies in existing correlation models include the lack of data for adequate

validation and extrapolation as well as the need of extensive computation efforts to support a fully probabilistic analysis of a large-scale building portfolio. Such deficiencies have confined existing correlation models to be effectively incorporated in even some of the well-accepted loss estimation platforms (e.g. HAZUS–HM; MAEViz). There is a compelling need to develop a systematic and rigorous methodology that is capable of propagating various uncertainties and both types of spatial correlations throughout the entire building portfolio resilience assessment process, including hazard characterization, loss estimation, and recovery modeling. Equally important, sampling techniques to minimize the computational effort must be provided to make it practical to propagate spatially correlated uncertainties through multiple layers of conditional events for full-sized community building portfolios.

Building Portfolio Recovery Modeling

Post-disaster recovery is one of the least understood components in disaster research and risk management. There is neither an integrated policy framework nor readily available tools to facilitate the improvement of community recovery outcomes owing, in large part, to the lack of quantitative recovery models. A building portfolio traditionally is not perceived as an entity of its own; hence, its recovery is rarely investigated from a system perspective. The recovery of a community building portfolio is dependent on the resourcefulness and social-economic characteristics of the community at large and at the same time, is strongly affected by various decisions made by different public and private building owners and stakeholders. In contrast to the recovery of lifeline networks, which often resembles a decision-driven process, the recovery of a building portfolio is essentially market-driven. Thus, the general-purpose

analytical recovery functions assumed in the literature (e.g., uniform cumulative distribution, lognormal distribution or harmonically over-damped functions) are far too simplistic to reflect the intrinsic complexities in the building portfolio recovery process. On the other hand, the empirical recovery models in the literature derived from historical hazard events are often event- and community-specific, making it hard to be generalized to support resilience planning in a quantitative manner. The above literature review has made it apparent that improvements to recovery outcomes of a building portfolio will be difficult to achieve unless quantitative models revealing the fundamental mechanisms of its recovery processes are developed.

In this dissertation work, a building portfolio resilience assessment framework is developed to address the above-identified research gaps systematically.

Chapter 3 Building Functionality Definition, Metrics and Notations (BPFM)

Developing quantitative models to assess building portfolio resilience, i.e. building portfolio functionality loss (BPLE) and building portfolio functionality recovery (BPRM) following a hazard event, is a necessary step toward risk-informed community resilience planning. Such development must begin with clearly-defined metrics that can directly measure both the functionality loss and recovery of a building portfolio, and at the same time, can explicitly reflect the dependency of the building portfolio on other community infrastructure systems in maintaining its desired functionality level.

In Section 3.1, a new building portfolio functionality metric (BPFM) is introduced, and the major characteristics of this metric are discussed. Section 3.2 provides a comprehensive list of notations and symbols to be used in the quantification of the metric using the BPLE and BPRM (detailed in Chapters 4 and 5, respectively).

3.1 Building Portfolio Functionality: Definition and Metrics

Functionality of an individual building can be defined as the availability of the building to be used for its intended purpose, which is a function of its structural integrity and availability of utilities (Almufti & Willford, 2013; Lin & Wang, 2017a). A main cause of building functionality loss in a hazard event is structural or nonstructural damages, as a building relies on its load-resistant system to provide safety and on its nonstructural components (e.g. lighting, heating, elevators, etc.) to provide serviceability. Another primary cause of building functionality loss is the disruption of

basic utilities, i.e., an undamaged building is not functional if critical utilities, such as water and power, are unavailable.

Following an extreme natural hazard, e.g. an earthquake, professional inspections (including structural, nonstructural or hazardous material damage evaluation) will be initiated for damaged buildings, which are often followed by an ATC-20 placard (Green, Yellow or Red) to be tagged to each building, ascertaining the degree of damage and the level of ***building functionality*** prior to building restoration (Oaks, 1990). Considering the definition of building functionality introduced above, five different functionality states are defined in Figure 3-1, ranging from restricted entry to full functionality, each corresponding to a unique combination of building damage condition and utility availability (Almufti & Willford, 2013). For example, if any threats to life-safety are evident, including significant structural damage, exterior falling hazards due to damaged cladding and glazing, interior hazards from damaged components hung from the floor above or severely damaged partitions, a building is tagged with a Red (**R**estricted **E**ntry, *RE*) or Yellow (**R**estricted **U**se, *RU*) placard following inspection, regardless of utility availability. Otherwise, a Green Tag is awarded, meaning that any damage to structural and non-structural building components is minor and does not pose a threat to life safety and that the building is safe to be re-occupied (**R**e-**O**ccupancy, *RO*). Further, a building is considered as having **B**aseline **F**unctionality (*BF*) when it is both structurally safe to occupy and has basic utility supplies (power, water, fire sprinklers, lighting, and HVAC systems) available on the site, or having **F**ull **F**unctionality (*FF*) when it maintains at or restores to its original, pre-hazard functionality level (Almufti & Willford, 2013).

Functionality States (ATC Placard)			Damage Condition	Utility Availability	Building Repair Classes (RC) & Specific Repair Items
5	FF	**Fully Functionality** (Green Placard)	None	All available	N/A
4	BF	**Baseline Functionality** (Green Placard)	Minor cosmetic structural and nonstructural damage	Critical ones available	**Repair Class 4 (RC4)** • Minor structural damage such as shear wall, link beams, reinforced wall; Minor nonstructural damage such as stairs, partition, tiles
3	RO	**Re-Occupancy** (Green Placard)	Minor to moderate structural and nonstructural damage	N/A	**Repair Class 3 (RC3)** • Minor structural damage; Minor to moderate nonstructural damage; Mechanical equipment, electrical systems, emergency backup
2	RU	**Restricted Use** (Yellow Placard)	Moderate structural or nonstructural damage that does not threaten life safety	N/A	**Repair Class 2 (RC2)** • Moderate to heavy nonstructural damage such as glazing, exterior partitions, elevator, pipes, fire sprinkler drops
1	RE	**Restricted Entry** (Red Placard)	Extensive structural or nonstructural damage that threatens life safety	N/A	**Repair Class 1 (RC1)** • Heavy structural damage; Heavy nonstructural damage that threatens life safety

Figure 3-1. Functionality states of individual buildings (Lin & Wang, 2017a)

The building functionality state $S_j, j \in (RE, RU, RO, BF, FF)$ introduced above serves as the functionality metric for individual buildings. This functionality metric explicitly expresses the dependence between buildings and other infrastructure systems in the community, which is not reflected in other typical building-related metrics in the literature, such as deaths, dollar loss, and downtime. Furthermore, this building functionality metric, as presented in Figure 3-1, not only can be used to measure building functionality loss immediately following a hazard event (t_0), but also enables the restoration of a building to be traced throughout the time horizon of its recovery ($t > t_0$). Moreover, the definition of building functionality is engineering-centric and is firmly rooted in the performance of the building itself, which is uncoupled with the complex human-building interactions during or after occurrence of a hazard event. We further define ***building restoration time (BRT)*** as the time that a building takes to regain its full functionality (FF) from the occurrence of the extreme event. It should be

pointed out that the building functionality categorization we introduced in Figure 3-1 is for risk category II buildings as specified in ASCE 7, which generally includes more than 90% buildings in a typical community in the U.S.

Consistent with the functionality metric for individual buildings, the ***building portfolio functionality metric*** (**BPFM**) is defined as the percentages of buildings in a portfolio that are in each of the five functionality states, PRI_j, $j \in$ (*RE*, *RU*, *RO*, *BF*, *FF*). Again, this BPFM not only allows the functionality loss of a building portfolio as whole to be quantified immediately following the hazard event (t_0), but also enables the functionality recovery of the portfolio to be "recorded" continuously as a function of time ($t > t_0$). Accordingly, we define the ***portfolio recovery time (PRT)*** as the time required for a target percentage (e.g. 90%) of buildings in a community to regain a prescribed desired functionality state (e.g. *FF*), e.g., $PRT_{FF,90\%}$. The *PRT* largely depends on resourcefulness as well as the social-economic characteristics of the community.

In Chapter 4, the BPLE framework is developed to estimate functionality state $S(t_0)$ for individual buildings and $PRI_j(t_0)$ for building portfolios, both at time instant immediately following a hazard event, i.e. $t = t_0$. In Chapter 5, the BPRM is formulated to trace the functionality state $S(t)$ for individual buildings and PRI_j(t) for building portfolios as functions of time during the recovery, i.e. $t > t_0$, resulting in probabilistic estimations of *BRT* and *PRT*.

3.2 Notation of Variables in BPLE and BPRM

For easy reference, Table 3-1 includes all the notations used in the BPLE and BPRM, as well as associated interpretative descriptions.

Table 3-1. Notations of variables in the BPLE and BPRM

Variable	Description
BF	Baseline Functionality state
BRF	Building Restoration Function, defined as the probability of a building achieving or exceeding a predefined functionality level S_j at any time t
$BU^{0,n}$	baseline utility availability at the site of building *n* at t_0
DS	Damage State, categorizes the extent of damage to structural and nonstructural components by different damage levels
DS_{SD}^n	hazard-induced damage to structural components of building *n*
DS_{ND}^n	hazard-induced damage to nonstructural drift-sensitive components of building *n*
DS_{NA}^n	hazard-induced damage to nonstructural acceleration-sensitive components of building *n*
ds_i	predefined damage state; i = 1,…,5 denote *none*, *slight*, *moderate*, *extensive* and *complete* damage states, respectively
DV	Damage Value, defined as the losses to individual buildings with respect to the portfolio performance metric of interest as a result of its physical damage
$e_j^n(t_0)$	probability of building *n* achieving or exceeding a functionality state S_j at t_0
FF	Full Functionality state
$FU^{0,n}$	full utility availability at the site of building *n* at t_0
$I_j^n(t)$	functionality state indicator of building *n* with in terms of S_j
IM	seismic intensity measure
N	total number of buildings in community building portfolio
$p_{i,j}^n(t)$	transition probability of building *n* upgrading to functionality state S_j conditional on initial functionality state S_i
$\boldsymbol{\pi}^n(t_0)$	initial (pre-recovery) functionality state probability vector for building *n*
$\boldsymbol{\pi}^n(t)$	functionality state probability vector of building *n*

$PRI_j(t_0)$	initial (pre-recovery) portfolio recovery index, defined as the percentage of building portfolio in the functionality state S_j at t_0
$PRI_j(t)$	Portfolio Recovery Index, defined as the percentage of building portfolio in the functionality state S_j
$PRT_{FF,a\%}$	Portfolio Recovery Time, defined as the time takes for *a*% of community buildings to regain full functionality (*FF*) state
RE	Restricted Entry functionality state
RO	Re-Occupancy functionality state
RU	Restricted Use functionality state
$\rho_j^{m,n}(t)$	correlation coefficient of the functionality state indicators of building pair (*m*, *n*) with respect to functionality state S_j
$\rho_{i,j}^{IM}$	correlation coefficient of the seismic intensities of building pair (*i*,*j*)
$\rho_{i,j}^{DS\|IM}$	correlation coefficient of the damage states of building pair (*i*,*j*) given seismic intensities
r_{ij}	the separation distance between building sites *i* and *j*
$S^n(t_0)$	hazard-induced pre-recovery functionality state of building *n* at t_0
$S^n(t)$	hazard-induced time-variant functionality state of building *n*
S_j	predefined functionality state; $j = 1, \dots, 5$ denote the *RE*, *RU*, *RO*, *BF*, *FF* functionality states, respectively
S_{EQ}	earthquake scenario event, characterized by a specific magnitude M_w and epicenter distance *D*
$T_{Delay,i}^n$	delay time, the time takes to initiate repair for building *n* conditional on pre-recovery functionality state S_i
$T_{Repair,RCi}^n$	repair time, the time takes for building *n* to complete all repair items in repair class, RCi
$T_{Utility}^n$	utility availability, the time takes to bring utility back to building *n*
$T_{INSP,i}^n$	the time takes to inspect the building *n*
$T_{FINA,i}^n$	the time takes to secure funding for repair building *n* conditional on initial functionality state S_i
$T_{CONM,i}^n$	the time takes to commission architects and engineers for building *n* conditional on initial functionality state S_i
$T_{ENGM,i}^n$	the time takes to design and prepare for construction drawings for building *n* conditional on initial functionality state S_i
$T_{PERM,i}^n$	the time takes to obtain permits, and hire and mobilize contractors and construction crews for building *n* conditional on initial functionality state S_i

$\boldsymbol{TPM^n}(t)$	transition probability matrix of building n
$WT_{i,j}^n$	waiting time that $S^n(t)$ stays at state S_j conditional on initial functionality state S_i
Z	portfolio performance metric, performance measure defined for quantifying a community building portfolio's hazard-induced losses

Chapter 4 Building Portfolio Loss Estimation (BPLE)

This chapter develops a probabilistic building portfolio functionality loss estimation (BPLE) framework for a prescribed hazard event, in which the BPFM introduced in Chapter 3 is used as the metric to measure the functionality loss of a portfolio. The building portfolio functionality loss obtained in this chapter serves as the initial state characterization for the portfolio recovery modeling to be discussed in Chapter 5.

Section 4.1 presents the overall framework of the probabilistic BPLE model in three steps of analysis: (i) spatially correlated hazard demand characterization, (ii) spatially correlated damage assessment, and (iii) estimation of spatially correlated functionality loss for individual buildings and the aggregated functionality loss for a building portfolio. In Section 4.2, a random sampling technique is implemented to reduce the computational effort in the BPLE for building portfolios of large size. Section 4.3 summarizes the major contributions of the BPLE.

4.1 Probabilistic Framework for BPLE

4.1.1 BPLE Formulation

While the BPLE framework developed herein is not limited to a specific hazard type, we use a scenario earthquake hazard to present the BPLE formulation due to its relatively mature development in spatial correlation modeling when compared with other types of hazard. Mathematically, the earthquake-induced loss to a community building portfolio in terms of a predefined loss metric Z exposed to an earthquake

scenario event S_{EQ} (characterized by a specific magnitude M_w and epicentral distance D) can be formulated using the total probability theorem as:

$$P\left(Z \le z \middle| S_{EQ}\right) = \int_{\boldsymbol{u}} \int_{\boldsymbol{v}} \int_{\boldsymbol{y}} F_{Z|\boldsymbol{DV}}(z|\boldsymbol{u}) f_{\boldsymbol{DV}|\boldsymbol{DS}}(\boldsymbol{u}|\boldsymbol{v})\, f_{\boldsymbol{DS}|\boldsymbol{IM}}(\boldsymbol{v}|\boldsymbol{y}) f_{\boldsymbol{IM}|S_{EQ}}(\boldsymbol{y}|S_{EQ}) d\boldsymbol{u} d\boldsymbol{v} d\boldsymbol{y} \quad (4\text{-}1)$$

where, reading from right to the left, $f_{\boldsymbol{IM}|S_{EQ}}(\boldsymbol{y}|S_{EQ})$ is the PDF of ground motion intensity measure $\boldsymbol{IM}$[1] at all the building sites conditioned on the scenario event S_{EQ}; $f_{\boldsymbol{DS}|\boldsymbol{IM}}(\boldsymbol{v}|\boldsymbol{y})$ is the PDF of damage state $\boldsymbol{DS}$[2] of all buildings conditioned on $\boldsymbol{IM}$, which for each building is often given by a fragility function as defined in Eq. (2-2); $f_{\boldsymbol{DV}|\boldsymbol{DS}}(\boldsymbol{u}|\boldsymbol{v})$ is the PDF of damage value $\boldsymbol{DV}$[3] of all buildings conditioned on $\boldsymbol{DS}$; and $F_{Z|\boldsymbol{DV}}(z|\boldsymbol{u})$ is the cumulative distribution function (CDF) of portfolio metric Z conditional on $\boldsymbol{DV}$. The dimensions of vectors $\boldsymbol{IM}$, $\boldsymbol{DS}$ and $\boldsymbol{DV}$ are consistent with the number of buildings in the considered portfolio. Finally, $P\left(Z \le z|S_{EQ}\right)$, the CDF of $Z|S_{EQ}$, is given by the convolution of conditional probability distributions associated with the three intermediate variables (i.e. $\boldsymbol{IM}|S_{EQ}$, $\boldsymbol{DS}|\boldsymbol{IM}$, and $\boldsymbol{DV}|\boldsymbol{DS}$), which intermediately relate Z to S_{EQ}.

[1] Ground motion intensity is the ground motion characteristic that can be related to the response of structural systems, nonstructural components, and building contents through engineering analysis, such as peak ground acceleration, peak ground velocity, peak ground displacement, or a spectral response quantity such as spectral displacement, velocity or acceleration.

[2] The damage state categorizes the extent of damage to structural and nonstructural components by different damage levels (often related to the structural system deformation or acceleration). In HAZUS-MH (FEMA/NIBS, 2003), four damage states (i.e., slight, moderate, extensive, and complete) to structural and nonstructural components of a building and their relationships with building response threshold are identified.

[3] The damage values are defined as the losses to individual buildings with respect to the portfolio performance metric of interest as a result of its physical damage. The damage values can be direct *dollar* losses, *downtime* (or restoration time), and *deaths* (causalities) (FEMA, 2012). In this study, the damage value is the functionality loss.

Specifically, for quantifying functionality losses of building portfolios, in term of the BPFM PRI as defined in Chapter 3, Eq. (4-1) can be written as:

$$P\left(PRI \le z \middle| S_{EQ}\right) = \iiint_{PRI(\boldsymbol{S}) \le z} f_{\boldsymbol{S}|\boldsymbol{DS}}(\boldsymbol{u}|\boldsymbol{v}) f_{\boldsymbol{DS}|\boldsymbol{IM}}(\boldsymbol{v}|\boldsymbol{y}) f_{\boldsymbol{IM}|S_{EQ}}(\boldsymbol{y}|S_{EQ}) d\boldsymbol{u} d\boldsymbol{v} d\boldsymbol{y} \tag{4-2}$$

where, as previously introduced in Section 3.1, $\boldsymbol{S}$ is the functionality state (i.e. *RE*, *RU*, *RO*, *BF*, *FF*) of all buildings; and PRI is the percentages of buildings in the portfolio that are in any of the five functionality states of interest.

To estimate the CDF of the PRI three crucial steps of analysis are required: (1) Characterization of the spatially correlated seismic demands, i.e. $f_{\boldsymbol{IM}|S_{EQ}}(\boldsymbol{y}|S_{EQ})$, in which uncertainties in seismic demands at all buildings sites ($\boldsymbol{IM}$) as well as the spatial correlations among those must be modeled; (2) Assessment of spatially correlated building damages, i.e. $f_{\boldsymbol{DS}|\boldsymbol{IM}}(\boldsymbol{v}|\boldsymbol{y})$, in which the uncertainties in building responses conditional on hazard demands ($\boldsymbol{DS}|\boldsymbol{IM}$) as well as the spatial correlations among those must be considered; (3) Estimation of functionality loss for both individual buildings, i.e. $f_{\boldsymbol{S}|\boldsymbol{DS}}(\boldsymbol{u}|\boldsymbol{v})$, and for building portfolio as a whole, i.e. $F(PRI|S_{EQ})$. Each of the three analysis steps is conditional on the previous one. These three analysis steps are illustrated in Figure 4-1, with each step being detailed in section 4.1.1, 4.1.2 and 4.1.3, respectively.

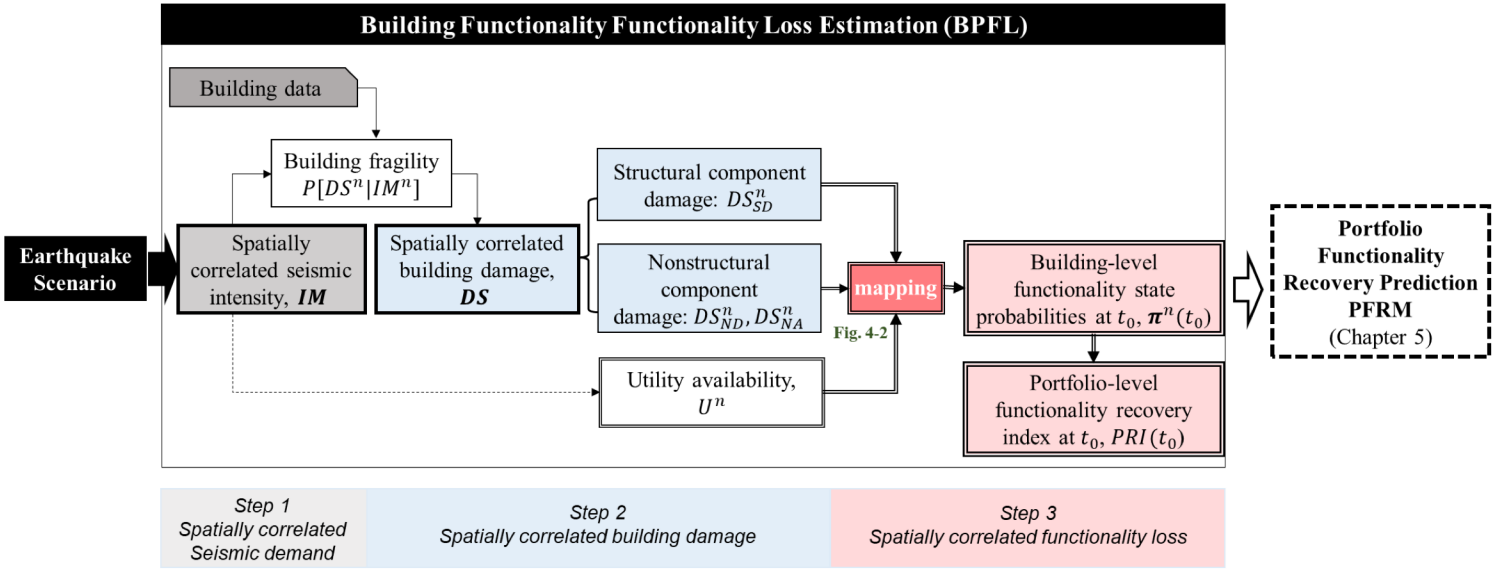


Figure 4-1. Flowchart of community-wide probabilistic pre-recovery damage and functionality loss assessment

*4.1.2 Step 1: Spatial Hazard Demand Characterization (**IM**)*

The scenario-based hazard modeling approach has been widely used in community resilience assessment, planning for emergency response/recovery, and developing hazard mitigation strategies, as it maintains the spatial variation in hazard demand for an interested event, enabling resilience metrics of spatially distributed systems to be assessed on the community scale in a realistic manner. A scenario earthquake is usually characterized by an earthquake magnitude and an epicenter distance. The appropriate scenario event for community resilience planning should be chosen based on the hazard characteristics and the risk tolerance of the specific community being investigated.

For a selected scenario event, the seismic intensity characteristics of buildings are symbolized by a median response spectrum (spectral displacement or spectral acceleration) and a period-dependent dispersion calculated from the ground motion attenuation relationship. The hazard demand characterization must take into account the uncertainty in ground motion intensity at the site of a building for a given earthquake scenario ($\boldsymbol{IM}|S_{EQ}$), as well as the site-to-site correlations in the demands resulted from same seismic source, similar wave propagation path, and similar soil site condition.

The predominant studies have modeled the uncertainty of ground motion intensity at a site of a building (***IM***) with an intra-event error term ξ and an inter-event error term η (Jayaram & Baker, 2009); the latter is not needed for the scenario analysis herein. Accordingly, the ground motion intensity at building site *i* can be written as:

$$\ln(IM_i) = \ln(\overline{IM_i}) + \tau \cdot \xi_i \tag{4-3}$$

where $\overline{IM_i}$ is the expected value of ground motion intensity at building site *i* computed from a selected ground motion attenuation model; ξ_i is often described by a standard normal distribution, and τ represents the standard deviation of ln (IM_i). The joint probability of ground motion intensities at all building sites is a multivariate lognormal distribution.

The correlation between seismic intensities (more specifically, correlation in random variables ξ) of two building sites i and j, $\rho_{i,j}^{IM}$, is often defined as an exponential function with respect to the separation distance between the two sites. As an example to explore the role of correlation in building portfolio loss estimation, the correlation function determined by Wang & Takada (2005) is utilized:

$$\rho_{i,j}^{IM} = \exp\left(-\frac{r_{ij}}{R}\right) \tag{4-4}$$

where r_{ij} is the separation distance between building sites *i* and *j*; and *R* is a parameter denoting the correlation distance, which is related to the characteristics of the earthquake and local site conditions.

*4.1.3 Step 2: Spatial Damage Analysis (**DS**)*

Building damage analysis includes evaluating structural and non-structural damages of buildings using existing fragility functions. Unlike assessment of an individual building which is often focused on detailed and accurate component-level analyses, in a building portfolio loss estimation the physical damage of an individual building is coarsely categorized into two portions: damages of structural component and non-structural component, with the latter being further classified as damages of non-structural drift-sensitive component and acceleration-sensitive component. Fragility

curves with respect to these types of building components for different types of buildings can be found in literature, in existing loss estimation platform such as HAZUS-MH and MAEViz, or in future in the more comprehensive database of IN-CORE.

Such building damage analysis takes into account the uncertainties in both structural and nonstructural damages of a building conditional on the ground motion intensity. Besides uncertainty propagation, the structure-to-structure correlation in the damage states of buildings must be modeled. This correlation is a result of building design according to similar building design codes, similar engineering practices, or similar construction materials. The structure-to-structure correlation has been discussed in only a few studies due to its complexity and the lack of available data for validation. Vitoontus & Ellingwood (2013) modeled the damage state of building i, DS_i, as the sum of the effects of its construction material M_i, structural type T_i, and building code C_i, and a noise term ε_i:

$$DS_i = M_i + T_i + C_i + \varepsilon_i \tag{4-5}$$

Further, let

$$Y_i = M_i + T_i + C_i \tag{4-6}$$

and Y_i is statistically independent of ε_i , then $DS_i = Y_i + \varepsilon_i$. The correlation between Y_i and $Y_j$and the correlation between ε_i and ε_j can be written as:

$$\rho_{Y_i.Y_j} = \rho_{MT_i,MT_j} \cdot \rho_{C_i,C_j} \tag{4-7}$$

$$\rho_{\varepsilon_i.\varepsilon_j} = exp\left(-\frac{r_{ij}}{\beta_\varepsilon}\right) \tag{4-8}$$

where ρ_{MT_i,MT_j} represents the correlation in responses of building *i* and *j* introduced by similar construction type and material; ρ_{C_i,C_j}, represents correlation due to the same (or similar) building code; and β_ε denotes the scale of the correlation due to building separation (buildings in proximity to one another are more likely to be highly correlated because of community development patterns). Accordingly, the structure-to-structure correlation between building *i* and building *j* becomes:

$$\rho_{i,j}^{DS|IM} = \frac{\rho_{Y_i,Y_j}\cdot\sigma_{Y_i}\cdot\sigma_{Y_j}+\exp\left(-r_{ij}/\beta_\varepsilon\right)\cdot\sigma_\varepsilon^2}{\sqrt{\sigma_{Y_i}^2+\sigma_\varepsilon^2}\cdot\sqrt{\sigma_{Y_j}^2+\sigma_\varepsilon^2}} \tag{4-9}$$

where σ_{Y_i} , σ_{Y_j} and σ_ε denote the standard deviation of Y_i , Y_j and ε, respectively. σ_{Y_i} and σ_{Y_j} are computed as the root mean square of the logarithmic standard deviations of all damage values while the σ_ε is often assumed to be a certain percentage of $\sigma_{Y_i}\sigma_{Y_j}$ in the literature (Vitoontus & Ellingwood, 2013).

4.1.4 Step 3: Portfolio Functionality Loss Estimation

Finally, the functionality losses for both individual buildings, i.e. $f_{\boldsymbol{S|DS}}(\boldsymbol{u}|\boldsymbol{v})$, and for the building portfolio as a whole, i.e. $F(PRI|S_{EQ})$ are estimated in this section. The former is obtained by a damage-to-functionality mapping at building-level, the latter is then estimated by establishing a functional form that relates the building-level functionality losses to portfolio-level functionality losses.

4.1.4.1 Building-level damage-to-functionality mapping

To link damage of an individual building (as estimated in 4.1.3) to its functionality state (as introduced in Figure 3-1), we develop a damage-to-functionality mapping through identifying the mechanism by which building components (both structural and nonstructural) are assembled to collectively support the building functionality as well as the dependencies of the building functionality on the availability of critical utilities.

Damage-to-functionality mapping can be constructed by accurate building-level functionality assessment. For instance, Porter & Ramer (2012) identified a diverse set of detailed damage scenarios that can affect building functionality states and implemented a fault tree analysis to relate damage states of building components to a building's post-hazard functionality states. Such functionality assessment, however, needs to be supported by detailed building-specific information (such as vulnerability of roofs, suspended ceiling, HVAC system, etc.), which is often unattainable. Therefore, this method is impractical for the present analysis which is aimed at a far less granular community-level functionality loss estimation.

Accordingly, a mapping using a coarser resolution based on existing studies (FEMA/NIBS, 2003; FEMA, 2012) is introduced in this study to link the damage states of building components (estimated in Section 4.1.2) to the post-disaster building functionality states, as shown in Figure 4-2. The Figure 4-2 depict the assumptions made in the damage-to-functionality mapping that: 1) buildings with no damage to all of the three buildings components (i.e., structural components, nonstructural drift-sensitive components, and nonstructural acceleration-sensitive components) will

achieve *FF*; 2) buildings with no more than slight damage to all of the three components will achieve at least *BF*; 3) buildings with no more than slight damage to the structural components and no more than moderate damage to the two categories of nonstructural components will achieve at least *RO*; 4) buildings no exceeding moderate damage to all of the three building components will achieve at least *RU*[4].

Further, to express the damage-to-functionality mapping probabilistically to facilitate subsequent analysis, let $S^n(t_0)$ denote the functionality status of building *n* at t_0 (t_0 is the time when the prescribed hazard event occurs), which takes one of the five predefined functionality states $S_j, j = 1,2,\dots,5$ (representing *RE, RU, RO, BF, FF*, respectively). Let $e_j^{0,n} = e_j^n(t_0), j = 1,2,\dots,5$ denote the probability of building *n* achieving or exceeding functionality state S_j at t_0. The mapping in Figure 4-2 can be further expressed as:

$$e_1^{0,n} = P[S^n(t_0) \geq RE] = 1 \tag{4-10a}$$

$$e_2^{0,n} = P[S^n(t_0) \geq RU] \tag{4-10b}$$
$$= P\left[DS_{SD}^n \leq ds_{3,SD}, DS_{ND}^n \leq ds_{3,ND}, DS_{NA}^n \leq ds_{3,NA}\right]$$

$$e_3^{0,n} = P[S^n(t_0) \geq RO] \tag{4-10c}$$
$$= P\left[DS_{SD}^n \leq ds_{2,SD}, DS_{ND}^n \leq ds_{3,ND}, DS_{NA}^n \leq ds_{3,NA}\right]$$

[4] There are considerable amounts of nonstructural components suffering from severe damage (such as stairs and suspended ceiling) can threaten life safety and trigger an unsafe placard. However, there are also some nonstructural components that are unlikely to pose threat to life safety (such as elevator, most mechanical equipment and electronical system). In this study we don't distinguish these two types of nonstructural components and assume that the overall nonstructural components with severe damage will threaten life safety and is in restrict entry. This will lead to conservative result in functionality losses.

$$e_4^{0,n} = P[S^n(t_0) \geq BF] = \tag{4-10d}$$

$$\begin{cases} P\left[DS_{SD}^n \leq ds_{2,SD}, DS_{ND}^n \leq ds_{2,ND}, DS_{NA}^n \leq ds_{2,NA}\right], & BU^{0,n} = 1 \\ 0, & , \ BU^{0,n} = 0 \end{cases}$$

$$e_5^{0,n} = P[S^n(t_0) = FF] \tag{4-10e}$$

$$= \begin{cases} P\left[DS_{SD}^n = ds_{1,SD}, DS_{ND}^n = ds_{1,ND}, DS_{NA}^n = ds_{1,NA}\right], & FU^{0,n} = 1 \\ 0, & , \ FU^{0,n} = 0 \end{cases}$$

where DS_k^n is the seismic-induced damage state to component k of building n, $k \in \{SD, ND, NA\}$ denoting structural (*SD*), nonstructural drift-sensitive (*ND*) and nonstructural acceleration-sensitive (*NA*) components, respectively; $ds_{i,k}$ represents a specific damage state i , i = 1,…,5 denoting *none*, *slight*, *moderate*, *extensive* and *complete* damage states, in terms of component $k \in \{SD, ND, NA\}$; $BU^{0,n}$ and $FU^{0,n}$ are binary variables representing baseline utility and full utility, respectively; the binary states (1- available and 0 - disrupted) of baseline utility ($BU^{0,n}$) or full utility ($FU^{0,n}$) at the site of building n at t_0 can be determined by an integrated interdependent utility network damage and cascading failure analysis which is currently performed by other researchers in the CRCRP (e.g. Zhang et al., 2018) or found in the literature (e.g. González et al., 2015).

Let $\boldsymbol{\pi}^n(t_0) = [\pi_1^n(t_0), \pi_2^n(t_0), \pi_3^n(t_0), \pi_4^n(t_0), \pi_5^n(t_0)]$ be the functionality state probability vector of building *n* at t_0, in which the element $\pi_j^n(t_0) = Prob\left[S(t_0) = S_j\right]$ represents the probability of building *n* being in functionality state S_j. Accordingly, the $\boldsymbol{\pi}^n(t_0)$ is obtained by:

$$\boldsymbol{\pi}^n(t_0) = \left\{1 - e_2^{0,n}, e_2^{0,n} - e_3^{0,n}, e_3^{0,n} - e_4^{0,n}, e_4^{0,n} - e_5^{0,n}, \ e_5^{0,n} \ \right\} \tag{4-11}$$

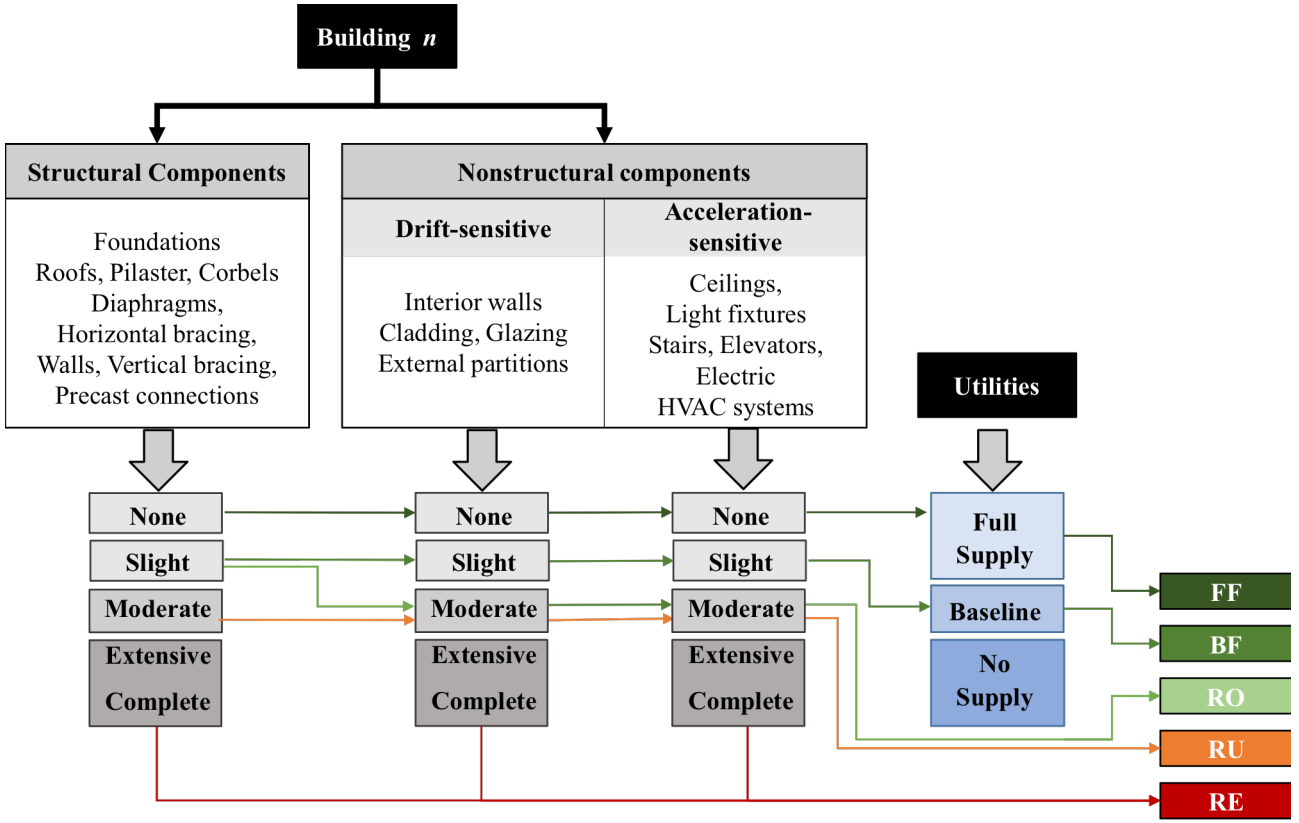


Figure 4-2. Mapping from building damage and utility availability to building functionality states

4.1.4.2 Portfolio-level functionality loss

While the initial functionality state of any building is determined by $\boldsymbol{\pi}^n(t_0)$, the portfolio functionality losses can be estimated as the following.

Let $I_j^n(t_0)$ be the functionality state indicator of any building n at t_0:

$$I_j^n(t_0) = \begin{cases} 0 & S^n(t_0) \neq S_j \\ 1 & S^n(t_0) = S_j \end{cases}, \; n \in 1, 2, \ldots, N \tag{4-12}$$

The $I_j^n(t_0)$ is a binary variable with probability $\text{Prob}\left[I_j^n(t_0) = 1\right] = \pi_j^n(t_0)$ and $\text{Prob}\left[I_j^n(t_0) = 0\right] = 1 - \pi_j^n(t_0)$.

Accordingly, the PRI_j at initial time t_0, denoting the percentage of buildings in a community that are in functionality state S_j at time t_0, is given by:

$$PRI_j(t_0) = \frac{\sum_{n=1}^{N} I_j^n(t_0)}{N}, \qquad j \in 1 \ldots 5 \tag{4-13}$$

4.1.5 Uncertainty Propagation in BPLE

To obtain the probabilistic distribution of portfolio functionality metric investigated under a scenario earthquake, $P\left(PRI \leq z \middle| S_{EQ}\right)$, one needs to solve Eq. (4-2), in which the three conditional probability distributions associated with the intermediate variables $\boldsymbol{IM}|S_{EQ}$, $\boldsymbol{DS}|\boldsymbol{IM}$, $\boldsymbol{S}|\boldsymbol{DS}$ are evaluated in Section 4.1.2, 4.1.3, and 4.1.4, respectively. Note that the relation between functionality state $\boldsymbol{S}$ and damage state $\boldsymbol{DS}$ is obtained from a damage-to-functionality mapping as illustrated in Figure 4-2. This one-to-one mapping implies that the uncertainties associated with the relation modeling between $\boldsymbol{S}$ and $\boldsymbol{DS}$ is neglected. As a result, the distribution function $f_{\boldsymbol{S}|\boldsymbol{DS}}$ in Eq. (4-2) becomes a Heaviside step function.

Eq. (4-2), unfortunately, cannot be evaluated in closed form when a building portfolio consists of thousands or even millions of buildings. To handle the multiple layers of conditional distribution in Eq. (4-2), namely, $f_{\boldsymbol{IM}|S_{EQ}}$ and $f_{\boldsymbol{DS}|\boldsymbol{IM}}$, a numerical solution using Monte Carlo simulation (MCS) is employed for obtaining the distribution of PRI. In the MCS, the two layers of conditional random fields, $\boldsymbol{IM}|S_{EQ}$ and $\boldsymbol{DS}|\boldsymbol{IM}$ [with high dimensions of correlated random variables in each layer, as formulated in Eqs. (4-3)-(4-9)] are simulated to obtain spatially correlated damage states of buildings. Further, through a damage-to-functionality mapping in Figure 4-2, the random samples of functionality state of individual buildings are obtained and the probabilistic outcome, $\boldsymbol{\pi}^n(t_0)$, for each individual building can be derived. Note that the correlation in building damage $\boldsymbol{DS}$ will automatically be propagated into the correlated initial functionality states at t_0, $\boldsymbol{S}(t_0)$, through MCS. Lastly, the portfolio-level functionality metric at t_0, $PRI_j(t_0)$ is calculated using Eqs. (4-12) & (4-13), with its probability distribution obtained from the MCS samples of *PRI*. The numerical implementation of the overall BPLE using MCS is shown in Figure 4-3. Both the building level functionality state probability vector at t_0, $\boldsymbol{\pi}^n(t_0)$, and the portfolio-level functionality metric, $PRI_j(t_0), j = 1,2,\dots,5$ calculated in this section will serve as inputs of the BPRM to be introduced in Chapter 5.

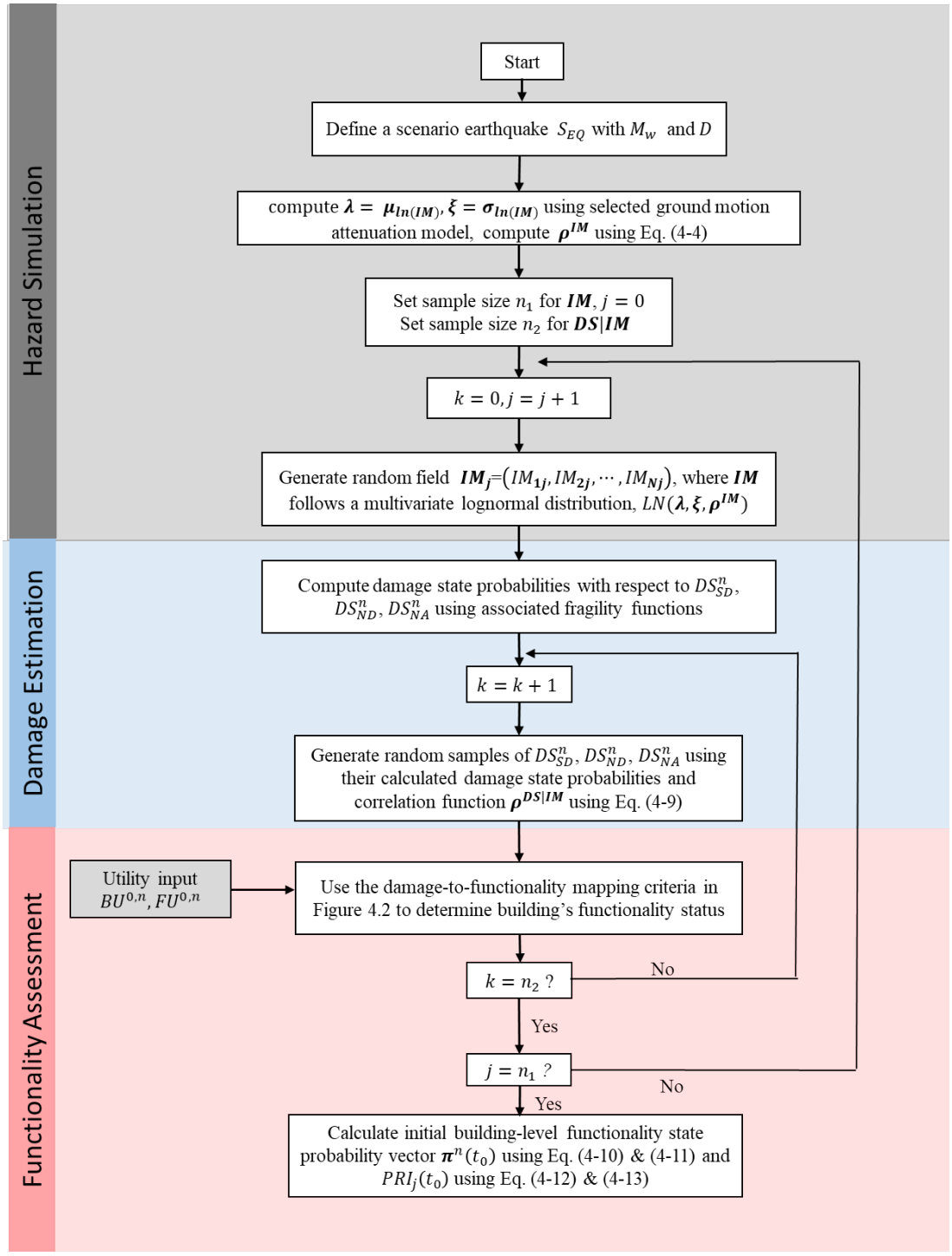


Figure 4-3. Flowchart of the MCS for building portfolio functionality loss estimate

4.2 An Implementation of Random Sampling Technique in BPLE

Despite the MCS can be employed to solve Eq. (4-2), the required computational effort for BPLE is enormous. When the number of buildings (N) is large (e.g. Shelby County, TN, has more than 300,000 buildings), the determination of $\rho_{i,j}^{IM}$ and $\rho_{i,j}^{DS|IM}$, $N \times N$ correlation matrices, is onerous. To ensure the scalability of this BPLE framework to communities of different sizes, a random sampling technique is implemented, i.e., randomly select n samples of buildings to represent the entire building portfolio of N buildings, where $n << N$. The choice of sampling size n depends on the size and topology of the building portfolio, as well as the level of the site-to-site and structure-to-structure correlations (Vitoontus & Ellingwood, 2013).

To validate this sampling technique, a 4km × 1.5km non-homogenous residential zone in the U.S. of 4246 typical residential buildings of three types is anayzed: 2196 non-seismically designed one-story wood frames developed mainly in the 1950s (denoted herein as "pre-code", W1); 2000 seismically designed one-story wood single family dwellings developed during the 1970–1980s ("low-code", W2), and 50 seismically designed wood residential buildings developed in 1990s ("moderate-code", W3). Buildings of the same type developed in a similar period are located in a cluster, representing typical urban development patterns, and within each cluster, they are randomly scattered modeled by Poisson random fields, as shown in Figure 4-4(a); the random sampling applied to each cluster is illustrated in Figure 4-4(b). The relative proportion of the three types of buildings is maintained during the sampling process.

To quantify portfolio functionality losses, a portfolio-level functionality loss ratio (FLR) is proposed and defined as the percentage of buildings in the portfolio that

are non-functional (namely, *RE*, *RU*, *RO*) immediately following a prescribed hazard event. The FLR is calculated by:

$$FLR = \sum_{j=1}^{3} PRI_j(t_0) = \frac{1}{N}\sum_{n=1}^{N}[I_1^n(t_0) + I_2^n(t_0) + I_3^n(t_0)] \tag{4-14}$$

Figure 4-5 displays the empirical CDF of the FLR of this residential zone for a given scenario earthquake (with magnitude $M_w = 7.8$ and epicentral distance $D = 36.5\text{km}$) using different sampling sizes, *n*, ranging from 20 to 2000. When *n* increases to 100, the estimated FLR gradually converges to the "exact" solution which involves all 4246 buildings. To measure the impact of correlation structures on the accuracy of the approximation using this sampling technique, Table 4-1 summarizes the relative error of the approximation associated with different correlation distances and sample sizes, with the relative error defined as:

$$e = \frac{\|\hat{z} - z\|}{\|z\|} \tag{4-15}$$

where $\hat{z}$ is the approximation while z is the "exact". In this particular case, the sample size *n* necessary to ensure accuracy in approximation is not much affected by the correlation distance when *n* is greater than 100. This sampling technique will be further implemented in comprehensive case studies for the two testbed communities investigated.

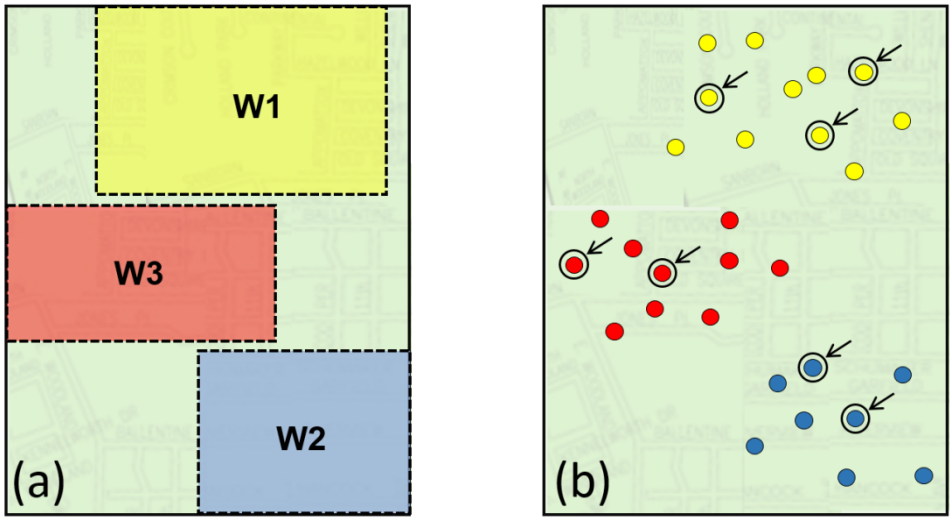


Figure 4-4. Illustration of (a) a hypothetical residential zone and (b) random sampling of the houses in this zone

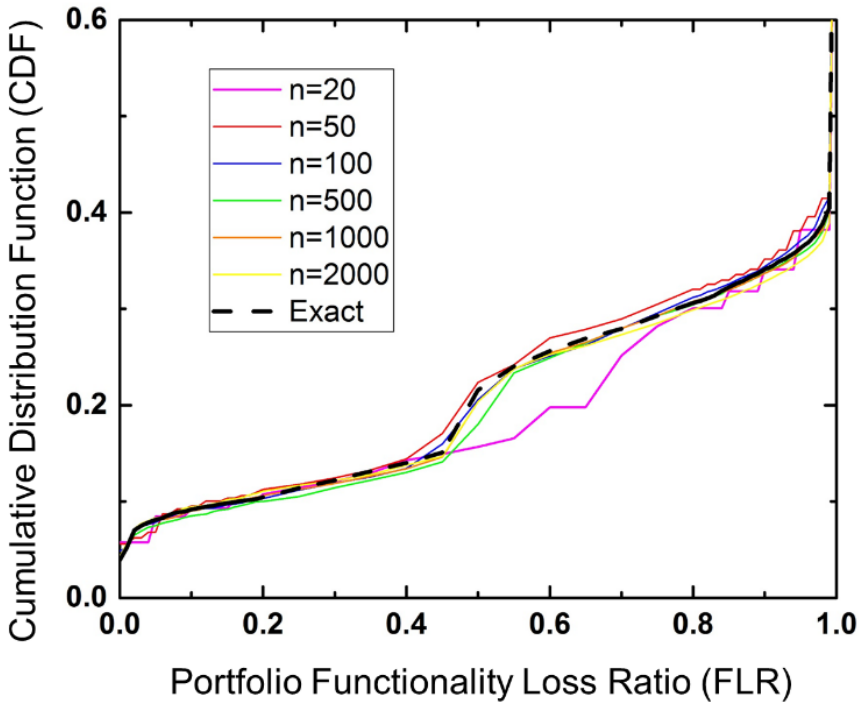


Figure 4-5. Convergence of the random sample model using FLR as a portfolio functionality metric

Table 4-1. Relative error associated with random sampling for different correlation distances and sample sizes

Correlation distance	Sample size, n					
	20	**50**	**100**	**500**	**1000**	**2000**
R=2	0.0356	0.0157	0.0138	0.0115	0.0055	0.0089
R=10	0.0281	0.0116	0.0121	0.0136	0.0098	0.0168
R=20	0.0192	0.0122	0.0105	0.0126	0.0148	0.0139
R=50	0.0377	0.0096	0.0102	0.0272	0.0061	0.0122
R=100	0.0457	0.0227	0.0084	0.0071	0.0199	0.0137

4.3 Closure

In this Chapter, a probabilistic functionality loss estimation (BPLE) framework has been developed for spatially distributed community building portfolios subject to prescribed seismic scenario events. The major characteristics of the BPLE are the following:

(1) The outcome of the BPLE framework is two-fold: the functionality state of individual buildings denoted by the state probability vector $\boldsymbol{\pi}(t_0)$ [cf. Eq. (4-11)] and the aggregated portfolio-level functionality loss, $PRI_j(t_0)$ [cf. Eq. (4-13)] including both mean and its uncertainty. As illustrated in Figure 4-1, these PBLE outcomes will serve as the starting point for the BPRM developed in Chapter 5.

(2) A building-level damage-to-functionality mapping approach [cf. Figure 4-2 and Eqs. (4-10)] is introduced to jointly map the physical damage condition and utility disruption of a building to one of the five building functionality states. The functionality states of individual buildings are then aggregated spatially to obtain the portfolio functionality loss.

(3) The BPLE includes a systematic and rigorous methodology that is capable of propagating various uncertainties and both site-to-site and structure-to-structure spatial correlations throughout all three steps of portfolio loss estimation (i.e. spatial hazard demand characterization, spatial damage analysis, and portfolio functionality loss estimation). This uncertainty propagation is realized through Eqs. (4-2) - (4-13), and implemented with a multi-layer MCS scheme (cf. Figure 4-3).

(4) A random sampling model is implemented to relief the computational effort in uncertainty propagation when dealing with building portfolios of large sizes and scales. The tradeoff between the sampling resolution and the accuracy of estimated portfolio loss is also investigated.

Chapter 5 Building Portfolio Recovery Model (BPRM)

This chapter focuses on developing a stochastic building portfolio recovery model (BPRM) to predict the functionality recovery time and recovery trajectory of a community building portfolio following natural scenario hazard events.

The BPRM is developed in two steps. In Section 5.1, building-level restoration is formulated as a discrete-state, continuous-time Markov Chain (CTMC); and in Section 5.2, portfolio-level recovery is formulated as the spatial aggregation of the CTMC restoration processes of individual buildings over the entire recovery time horizon. Uncertainty propagation associated with the portfolio recovery process and the quantification of time-variant correlations among building functionality states are presented in Section 5.3. The BPRM is conceptually illustrated in Figure 5-1, and detailed model components are illustrated in Figure 5-2.

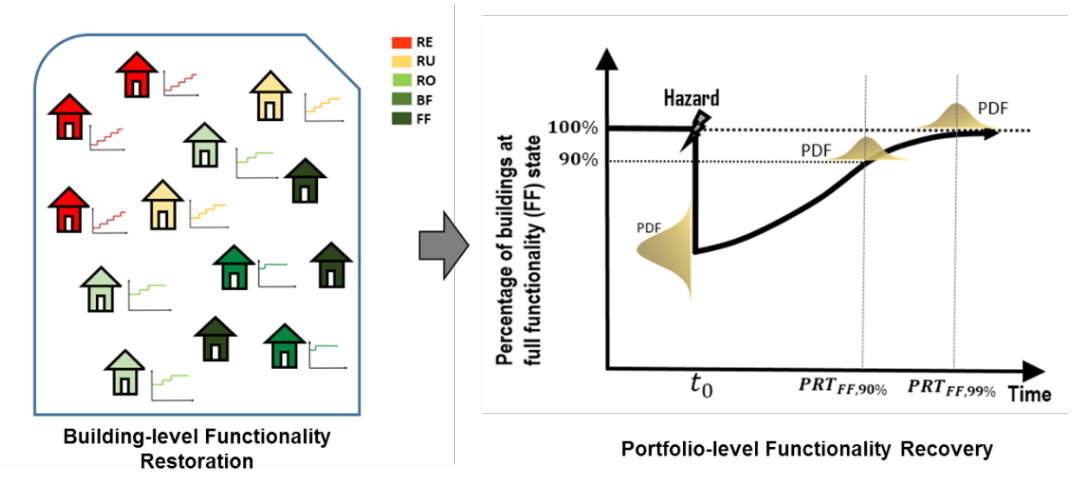


Figure 5-1. Schematic representation of building portfolio recovery

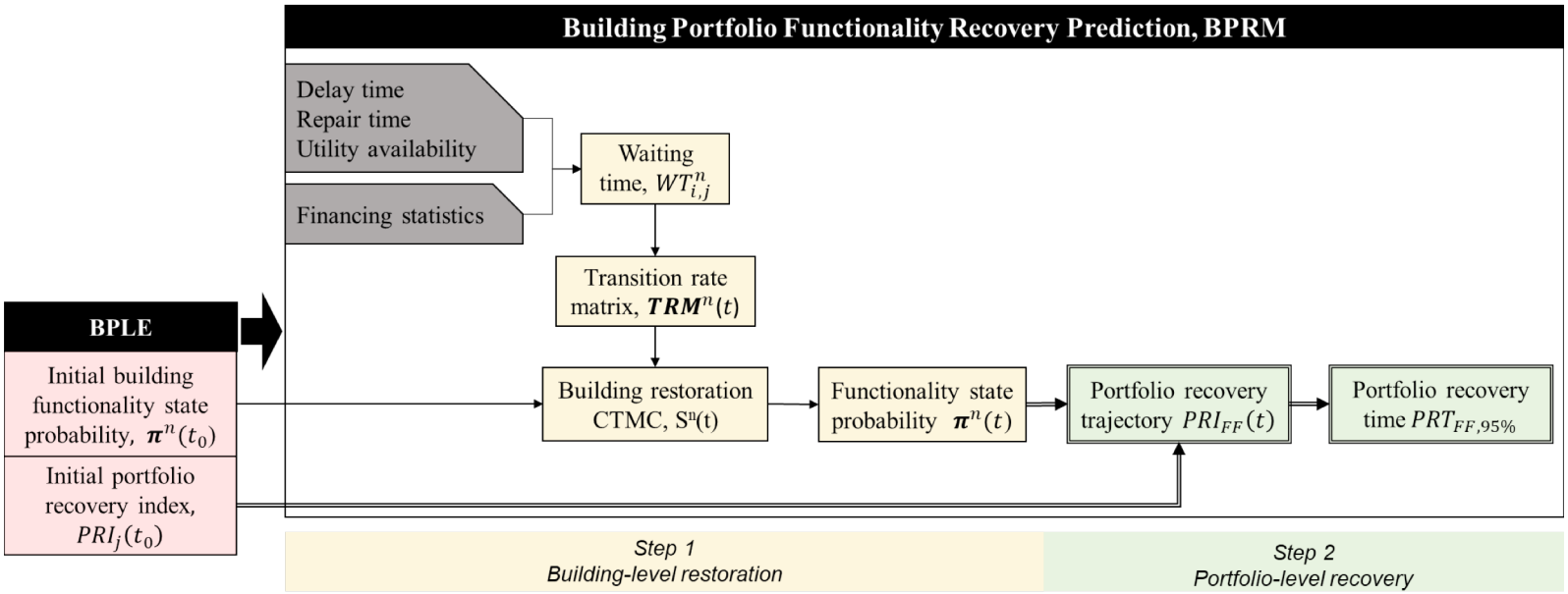


Figure 5-2. Flowchart of the two-step portfolio functionality recovery modeling

5.1 Step 1: Building-Level Restoration

5.1.1 Discrete-State, Continuous-Time Markov Chain (CTMC)

Let $S(t)$ be the stochastic post-disaster restoration process of an individual building, denoting functionality state at any time *t* after hazard occurrence at t_0. $S(t)$ is assumed to take one of the five functionality states in Figure 3-1 at any time, symbolized as $S_1, S_2, \ldots S_5$, representing restricted entry (*RE*), restricted use (*RU*), re-occupancy(*RO*), baseline functionality (*BF*) and full functionality (*FF*), respectively. A building restoration process $S(t)$ starts at time $t_0 = 0$, from its initial pre-restoration functionality state $S(t_0) = S(0)$, and lasts until $t = BRT$ when the building regains *FF* (i.e. S_5). An illustration of the time-dependent building-level restoration process, $S(t)$, is shown in Figure 5-3 for buildings with $S(t_0)$= S_1. Due to the uncertainties in $S(t_0)$, introduced by uncertain hazard intensity and structural performance, as well as the uncertainties in the subsequent $S(t)$ for $t > t_0$, introduced by various decisions of building owners with different social and economic status (which ultimately are affected by the resourcefulness of the community as a whole), the building-level functionality $S(t)$ is modeled as a stochastic random process. Moreover, the next functionality state at any time during a building restoration is only dependent on the current functionality state, hence $S(t)$ is modeled as a *discrete-state, continuous-time Markov Chain (CTMC)*, characterized by the five-state space (i.e. $S_1, S_2, \ldots S_5$) and a transition probability matrix, ***TPM***.

Let $\pi_j(t)$ denote the probability of $S(t) = S_j$ at any time t, i.e. $\pi_j(t) = \text{Prob}\left[S(t) = S_j\right], j = 1, \ldots, 5$, then the state probability vector at any time t is:

$$\pi(t) = [\pi_1(t), \dots, \pi_5(t)\,] \tag{5-1}$$

where $\sum_{j=1}^{5} \pi_j(t) = 1$ for any time t. In particular, the initial ($t = t_0$) functionality state probability vector $\boldsymbol{\pi}(t_0) = [\pi_1(t_0), \pi_2(t_0)\, \pi_3(t_0), \pi_4(t_0), \pi_5(t_0)]$, can be determined by a mapping from the joint effect of building damage and utility disruption following a hazard event to building functionality states (cf. Figure 3-1). For a specific hazard event, this mapping can be done through field inspections as discussed in Section 3.1. For a hazard scenario considered in pre-event planning, one physically-based approach to estimate this joint effect is through a fully coupled building portfolio functionality loss estimation considering utility disruptions, in which the damage-to-functionality mapping scheme introduced in Section 4.1.3 is utilized (Zhang et al., 2018).

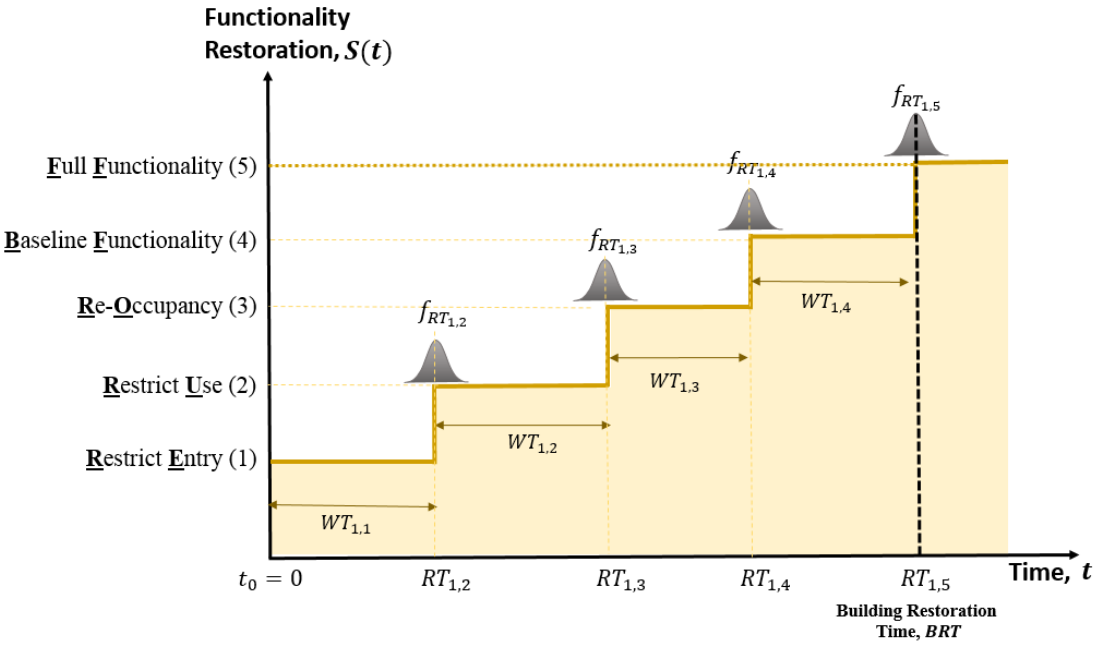


Figure 5-3. Discrete state, continuous time Markov Chain $\boldsymbol{S(t)}$ (for buildings with $\boldsymbol{S(t_0)}$= $\boldsymbol{S_1}$)

Let $\boldsymbol{TPM}(t)$ be the transition probability matrix of the CTMC that represents the building-level restoration process $S(t)$. The non-negative elements of $\boldsymbol{TPM}(t)$, $p_{i,j}(t)$, defined as:

$$p_{i,j}(t) = \text{Prob}\left[S(t) = S_j \middle| S(t_0) = S_i\right] \tag{5-2}$$

describe the probability of the restoration process $S(t)$ transiting to state S_j at any time t given that its initial state at t_0 is S_i. Since at a given time a building's functionality either remains at the present state or shifts to any of its higher states, $S(t)$ is a non-decreasing process and the $\boldsymbol{TPM}(t)$ takes the form:

$$\boldsymbol{TPM}(t) = \begin{pmatrix} p_{1,1}(t) & p_{1,2}(t) & p_{1,3}(t) & p_{1,4}(t) & p_{1,5}(t) \\ 0 & p_{2,2}(t) & p_{2,3}(t) & p_{2,4}(t) & p_{2,5}(t) \\ 0 & 0 & p_{3,3}(t) & p_{3,4}(t) & p_{3,5}(t) \\ 0 & 0 & 0 & p_{4,4}(t) & p_{4,5}(t) \\ 0 & 0 & 0 & 0 & 1 \end{pmatrix} \tag{5-3}$$

As illustrated in Figure 5-3**,** let $WT_{i,j}$ represent the waiting time that $S(t)$ stays at state j (or the waiting time takes $S(t)$ to upgrade from the current state S_j to the next state S_{j+1}) given $S(t_0) = S_i$. Further, let $RT_{i,j} = \sum_{k=i}^{j-1} WT_{i,k}$ be the total time to restore the building's functionality to S_j from its initial state S_i. Accordingly, $e_{i,j}(t)$, defined as the probability that $S(t)$ is equal to or exceeds S_j, $j = 1, \ldots, 5,$ at any time t given the initial functionality state S_i at t_0, can be expressed as:

$$
\begin{aligned}
e_{i,j}(t) &= \text{Prob}\left[S(t) \geq S_j \middle| S(t_0) = S_i\right] \\
&= \text{Prob}\left[RT_{i,j} \leq t\right] \\
&= \text{Prob}\left[\sum_{k=i}^{j-1} WT_{i,k} \leq t\right] \\
&= \int \dots \int_{\sum_{k=i}^{j-1} wt_{i,k} \leq t} \prod_{k=1}^{j-1} f_{WT_{i,k}}\, d\left(wt_{i,k}\right), \quad j = 1, \dots, 5
\end{aligned}
\tag{5-4}
$$

where $f_{WT_{ij}}$ denotes the PDF of $WT_{i,j}$. For a given initial state S_i, $WT_{i,j}$ are treated as independent random variables in Eq. (5-4) because each $WT_{i,j}$ is determined only by a set of unique restoration activities that take place during that specific timeframe. The detailed discussion and probabilistic estimation of $WT_{i,j}$ will be presented in Section 5.2.2.

Denote the exceedance probability $e_{i,j}(t)$ as the *conditional building restoration function (CBRF)*, representing the probability of a building achieving or exceeding a predefined functionality state S_j at any post-event time t conditional on its initial (pre-restoration) functionality state S_i immediately following hazard occurrence at t_0. Accordingly, the elements of the $\boldsymbol{TPM}(t)$ become:

$$
\begin{aligned}
p_{i,j}(t) &= \text{Prob}\left[S(t) = S_j \middle| S(t_0) = S_i\right] \\
&= \text{Prob}\left[S(t) \geq S_j \middle| S(t_0) = S_i\right] - \text{Prob}\left[S(t) \geq S_{j+1} \middle| S(t_0) = S_i\right] \\
&= e_{i,j}(t) - e_{i,j+1}(t), \qquad j = 1, \dots, 4
\end{aligned}
\tag{5-5}
$$

$$
p_{i,j}(t) = e_{i,j}(t), \qquad j = 5 \tag{5-6}
$$

Finally, the restoration state probability vector $\boldsymbol{\pi}(t)$ at any time t is:

$$
\boldsymbol{\pi}(t) = [\pi_1(t), \dots, \pi_5(t)\,] = \boldsymbol{\pi}(t_0) * \boldsymbol{TPM}(t) \tag{5-7}
$$

Define $e_j(t)$ as the *building restoration function (BRF)*, representing the total probability of a building achieving or exceeding a predefined functionality state S_j at any post-event time t regardless of its initial functionality state. The *BRF* can be estimated quantitatively as:

$$e_j(t) = \text{Prob}\left[S(t) \geq S_j\right] = \sum_{k=j}^{5} \pi_k(t) \tag{5-8}$$

Figure 5-4 presents an illustration of *BRF* of a building for $j = 2 \ldots 5$, respectively; when $j = 1$, $e_j(t) \equiv 1$, meaning the probability that a building is in, or exceeds, the worst functionality state S_1 (i.e. *RE*) is always 100%. In particular, $e_j(t_0)$, determined from $\boldsymbol{\pi}(t_0)$, represents the probability of the building at or exceeding functionality state S_j at time t_0 before any restoration activity takes place.

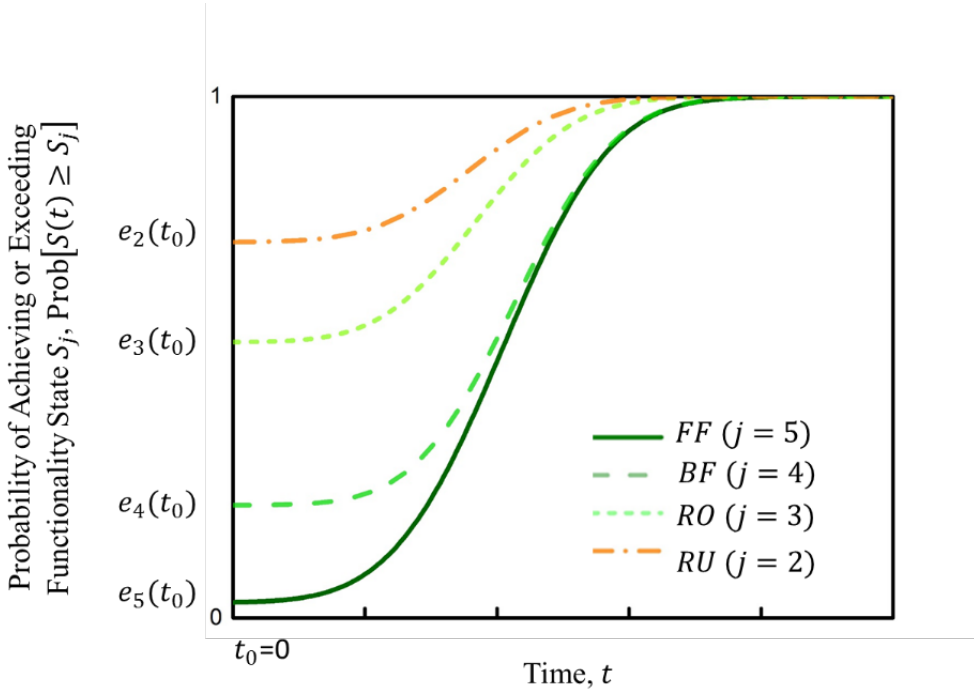


Figure 5-4. Illustration of building restoration function (*BRF*) of an individual building

*5.1.2 Determination of Transition Probability Matrix (**TPM**)*

The key element of the CTMC building-level restoration model is the transition probability matrix, ***TPM***, defined in Eq. (5-3). The elements of ***TPM***, i.e. $p_{i,j}(t)$, estimated by Eqs. (5-4)-(5-6), ultimately are functions of waiting time $WT_{i,j}$. The $WT_{i,j}$ vary from building to building, are highly uncertain and are strongly influenced by the social-economic status of building owners as well as the post-disaster construction market within the community. Quantification of $WT_{i,j}$ has been challenged by the lack of systematically documented data on *delay* and *repair* time regarding building restoration and inadequate understanding of the uncertain factors involved in the restoration process, which often are outside of the domain of engineering (Comerio, 2006). In this study the engineering process of building-level restoration is examined and mapped to the theoretical continuous-time Markov Chain model introduced in Section 5.2.1, and a simulation-based method supported by empirical data is used to obtain the probabilistic distributions of $WT_{i,j}$ which are critical input for estimating the ***TPM***.

Examining the engineering process of building reconstruction, the waiting times are functions of the delay time (T_{Delay}), repair time (T_{Repair}), and the time to regain utility service ($T_{Utility}$), i.e.,

$$WT_{i,j}^{n} = fcn\left(T_{Delay}^{n}, T_{Repair}^{n}, T_{Utility}^{n} | \boldsymbol{x}^{n}, \boldsymbol{X}^{c}\right) \quad (5\text{-}9)$$

in which the superscript n represents a specific building in a community building portfolio; $\boldsymbol{x}^{n}$ represents a vector of building-specific attributes that affect the three components of the waiting time, e.g., occupancy type, construction material, post-

disaster damage and functionality loss of the building; and $\boldsymbol{X}^c$ represents community-specific characteristics that have an impact on the three components of the waiting time, such as strength of regional economy, local regulations or policies [e.g., changes to planning, zoning, or construction regulations by a local jurisdiction after an extreme event], financing mechanisms for repair [i.e. private funding from personal savings, private loans, insurance, etc. public assistance from federal and state governments or non-profit organizations, such as the Federal Emergency Management Agency (FEMA), the Small Business Administration (SBA), and the Department of Housing and Urban Development (HUD), etc.], human resources [such as available workforce, construction contractors, and engineers for inspection, design and construction], and relevant pre- and post-event risk mitigation activities.

The *delay time* (T^n_{Delay}), the time takes to initiate repair for building n, includes three specific phases, as represented by the double-dashed lines in Figure 5-5: 1) time to inspect the building ($T^n_{INSP,i}$); 2) time to secure funding for repair ($T^n_{FINA,i}$), to commission architects and engineers ($T^n_{CONM,i}$), and to design and prepare construction drawings ($T^n_{ENGM,i}$), all of which can occur simultaneously; and finally 3) time to obtain permits, and hire contractors and construction crews ($T^n_{PERM,i}$). The subscript *i* indicates that these delay time segments are conditional on a building's initial functionality state $S_i,\ i = 1,2,3,4$. Accordingly, the *delay phase* T^n_{Delay} can be further expressed as [denoted downtime assessment methodology in the REDi™ framework (Almufti & Willford, 2013)]:

$$T^n_{Delay,i} = T^n_{INSP,i} + \max\left\{T^n_{FINA,i},\ T^n_{CONM,i}, T^n_{ENGM,i}\right\} + T^n_{PERM,i} \tag{5-10}$$

These time segments of the delay phase are uncertain and conditional on the building-specific ($\boldsymbol{x}^n$) and community-specific attributes ($\boldsymbol{X}^c$) expressed in Eq. (5-9); as a result, these time segments are difficult to formulate from first principles, but can be efficiently represented statistically using data collected from reconnaissance efforts following previous major disasters in the U.S. and supported by opinions from experts, including engineers, building owners, contractors, cost estimators, and bankers. The first such restoration-focused statistical database can be found in REDi™ (Almufti & Willford, 2013), which is expected to be further refined and expanded as additional post-disaster field investigations and data collection efforts are completed (e.g. multiple post-event field investigations are included in the work plan of the NIST-funded Center of Excellence for Risk-based Community Resilience Planning).

The *repair time* (T^n_{Repair}) is the duration to complete all repair classes (*RC*s) necessary to restore the full functionality of building *n,* as represented by the solid dark lines in Figure 5-5. The four *RC*s and the mapping between these *RC*s and the five predefined functionality states are presented in Figure 3-1. For example, the repair phase for a red-tagged building, i.e. *RE*, will need to include *RC*s 1-4, while a building with a pre-repair functionality state of *RO* only needs to undergo *RC*3 and *RC*4 to achieve *FF*. Denote repair class i as RCi, representing the repair effort required to upgrade building functionality from S_i to an intermediate state S_{i+1}, and $T^n_{Repair,RCi}$ as the time takes to complete the RCi. In general, once a repair construction initiates it will continue until the building regains its full structural and non-structural integrity. Accordingly, it is assumed that there are no arbitrary time breaks between RCs,

although the structural and non-structural components being repaired in those *RC*s are different.

FEMA P-58 (FEMA, 2012) presented a methodology to estimate the repair time of a building, in which the time to repair all damaged structural and non-structural components was estimated by dividing the total workload per floor by the number of workers allocated to each floor for an assumed repair sequence (which is basically consistent with the sequence of RCs shown in Figure 3-1). This method is only practical when detailed information is available for an individual building and a probabilistic damage estimate can be obtained for every structural and non-structural component within the building. To achieve the ultimate goal of community-level building portfolio recovery modeling, such a detailed estimate of repair time is impractical and perhaps unnecessary; instead, a statistical approach to determine $T^{n}_{Repair,RCi}$ based on relevant analytical studies and empirical data is more appealing, such as those presented in HAZUS (FEMA/NIBS, 2003) and MAEViz (Steelman et al., 2007).

Utilities availability must be considered when a building's restoration process moves beyond the Re-Occupancy (*RO*) state, as shown in Figure 5-5. Analytically, the time ($T^{n}_{Utility}$) to bring utility service to building *n* in a community can be estimated by coupling probabilistic damage assessment and restoration decision optimization regarding resource allocation and repair sequencing within an overarching framework of interdependency modeling of utility networks (e.g. González et al., 2015; Zhang et al., 2018). This approach requires comprehensive input information regarding functional and topological attributes of utility systems (water, power, gas, etc.), structural properties of network components (water and gas pipelines, water pumping

stations, power generation stations or substations, etc.), service areas of the demand nodes in each utility, and the available resources and characteristics of the decision process that leads to the restoration of utilities; such information often is not available. Alternatively, in a holistic manner, the $T^{n}_{Utility}$ can again be represented statistically using data collected from utility restoration efforts from past disaster recovery experiences in conjunction with observations from analytical studies reported in the literature. For example, RADi^{TM} (Almufti & Willford, 2013) provides typical utility disruption curves for electric, water and gas systems, giving the likelihood of utility availability at a building site as a function of time elapsed from the occurrence of a hazard.

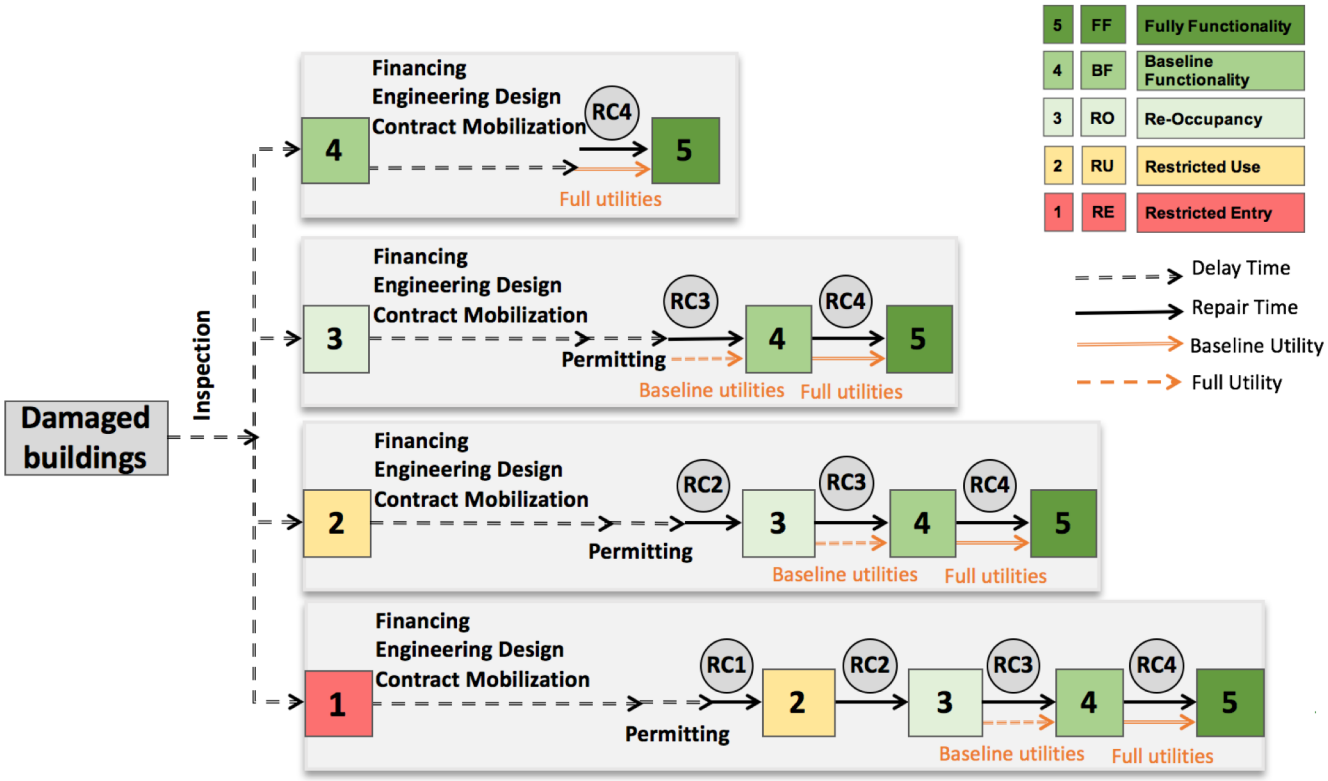


Figure 5-5. An illustration of the general restoration process of individual buildings

Figure 5-6(a)-(d) illustrate the mapping between the waiting time (WT^n) in CTMC and the three major time segments (T^n_{Delay} , T^n_{Repair}, $T^n_{Utility}$) of the building-level restoration process, for building with initial functionality states *RE*, *RU*, *RO* and *BF*, respectively. It's noteworthy that the T^n_{Delay}, T^n_{Repair}, $T^n_{Utility}$ are essentially conditional on the pre-recovery damage state of a building, as well as the operability status of utility at the building site. Considering the definition of building functionality presented in Figure 3-1, in the present study a building' physical damage is categorized into five states, from worst to the best, ds_1, ds_2, ds_3, ds_4, ds_5, with each including certain levels of structural and nonstructural damages listed in Figure 3-1; the availability status of utility at the building site is categorized into three states: ua_1 (not available), ua_2 (partially available), and ua_3 (fully available), as also shown in Figure 3-1. Temporally, the building damage restoration and utility operability restoration occur in parallel, as depicted in Figure 5-7. Further, let $T^n_{Utility,1}$ be the time takes for utility at the site of building *n* to recover utility status from state ua_1 to state ua_2, and $T^n_{Utility,2}$ be the time to recover from ua_2 to ua_3 (cf. Figure 5-7).

Regarding waiting time of the CTMC, the first waiting time ($WT^n_{i,i}$) includes two segments: the time to prepare for repair, T^n_{Delay}, and the time to upgrade the building to the next functional level, T^n_{Repair}. In addition, if the initial functionality state is *RO* or *BF*, the waiting time $WT^n_{i,i}$ also depends on the availability of utility service, i.e., *BF* or *FF* cannot be achieved unless utility service has been partially or fully restored (as defined in Figure 3-1 and illustrated in Figure 5-5 and Figure 5-6). The T^n_{Delay}, T^n_{Repair},

$T^n_{Utility}$ are conditional on building's damage state $ds_p,\ p = 1,2,3,4,5$ and utility's availability state $ua_q, q = 1,2,3$. Accordingly, the $WT^n_{i,i}$ is:

$$WT^n_{i,i} = T^n_{Delay,i} + T^n_{Repair,RCi}\,, \qquad i = 1,2 \tag{5-11a}$$

$$WT^n_{i,i}|ds^n_p, ua^n_q = \begin{cases} \max\left(T^n_{Delay,p} + T^n_{Repair,p}, T^n_{Utility,q}\right), & i = p;\ (p,q) = \{(3,1),(4,2)\} \\ T^n_{Delay,p} + T^n_{Repair,p}, & i = p;\ (p,q) = \{(3,2),(3,3),(4,3)\} \\ T^n_{Utility,q}, & p > i;\ i = 3,4 \end{cases} \tag{5-11b}$$

Similarly, the subsequent waiting time segments, $WT_{i,j},\ j > i$, are:

$$WT^n_{i,j} = T^n_{Repair,RCj}, \qquad j = 2;\ j > i \tag{5-12a}$$

$$WT^n_{i,j}\left|ds^n_p, ua^n_q\right. \tag{5-12b}$$

$$= \max\left(T^n_{Delay,p} + \sum\nolimits_{k=p}^{j} T^n_{Repair,RCk}\,, \sum\nolimits_{l=q}^{j-2} T^n_{Utility,l}\right) - \sum\nolimits_{h=i}^{j-1} WT^n_{i,h}\left|ds^n_p, ua^n_q\right., \qquad j = 3,4; j > i$$

Table 5-1 lists all the conditional waiting times given different pre-recovery building damage condition $ds_p, p = 1,2,\ldots,5$ and utility availability $ua_q, q = 1,2,3$ (superscript *n* is not written for simplification). Taking into account all the possibilities of combination of building damage and utility disruption (which affects the functionality states *BF* and *FF*), the waiting time $WT^n_{i,j}$ is obtained using total probability theorem, i.e.,

$$WT_{i,j}^{n} = \frac{\sum_{(p,q)\in A_i} WT_{i,j}^{n}|ds_p^n, ua_q^n \cdot \text{Prob}\left[DS(t_0) = ds_p^n, UA(t_0) = ua_q^n\right]}{\text{Prob}[S(t_0) = S_i]} \quad (5\text{-}13)$$

where $DS(t_0)$ and $UA(t_0)$ represent the initial damage status of buildings and availability status of utility at the building site, respectively. A_i denote the collections of the index of building and utility damage scenarios leading to functionality state S_i. More specifically, $A_{RE} = \{(1,1),(1,2),(1,3)\}$; $A_{RU} = \{(2,1),(2,2),(2,3)\}$; $A_{RO} = \{(3,1),(3,2),(3,3),(4,1),(5,1)\}$; and $A_{BF} = \{(4,3),(4,2),(5,2)\}$, as indicated in Table 5-1. The conditional waiting time $WT_{i,j}^{n}|ds_p^n, ua_q^n$ is summarized in Table 5-1, while the $\text{Prob}\left[DS(t_0) = ds_p^n, UA(t_0) = ua_q^n\right]$ is calculated from the initial damage evaluation of buildings and performance assessment of the utility networks.

Using the Eqs. (5-11)-(5-13) for calculating waiting time and the statistical or analytical estimation of the time segments involved in these equations, the PDFs of the waiting time $WT_{i,j}^{n}$ can be obtained. When substituting these PDFs into Eqs. (5-4) - (5-6), the ***TPM*** and *BRFs* can be obtained for all different building types in a community building portfolio.

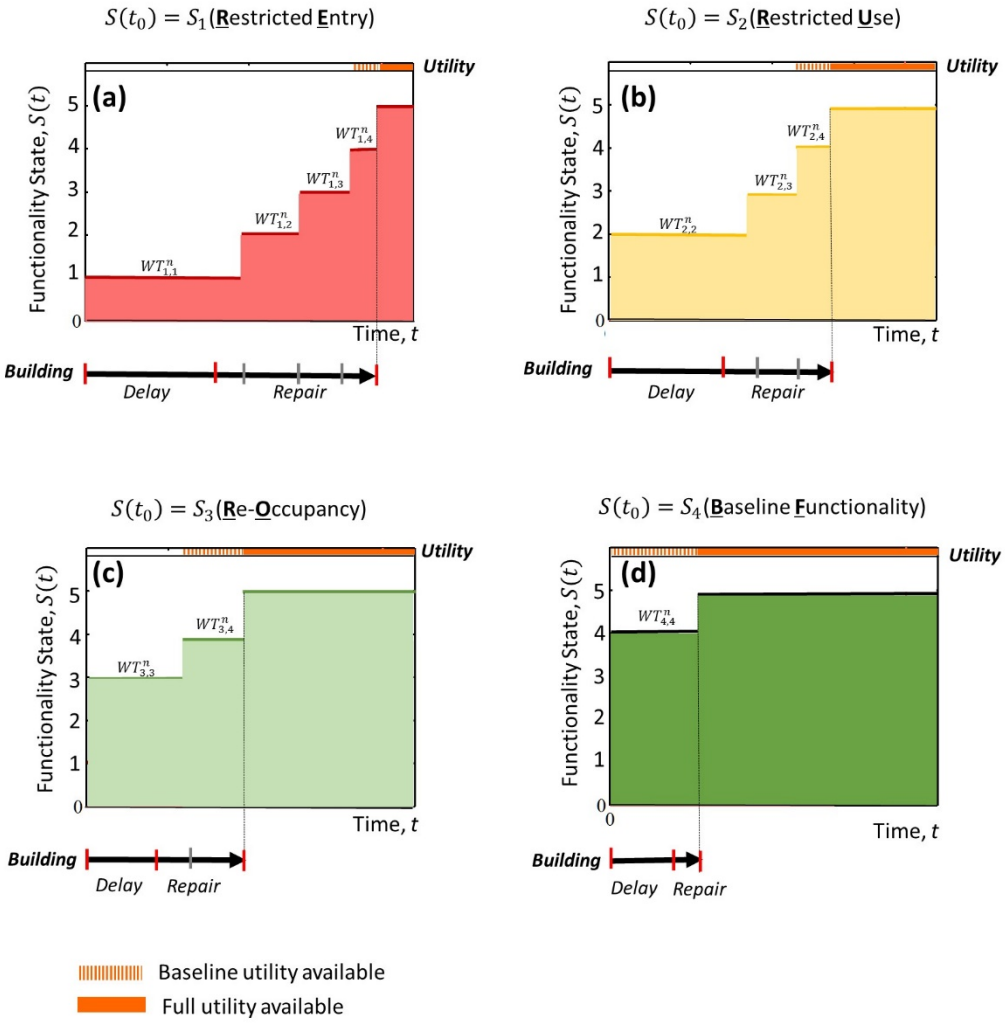


Figure 5-6. General restoration paths for individual buildings with initial pre-repair functionality states of a) RE, b) RU, c) RO, and d) BF.

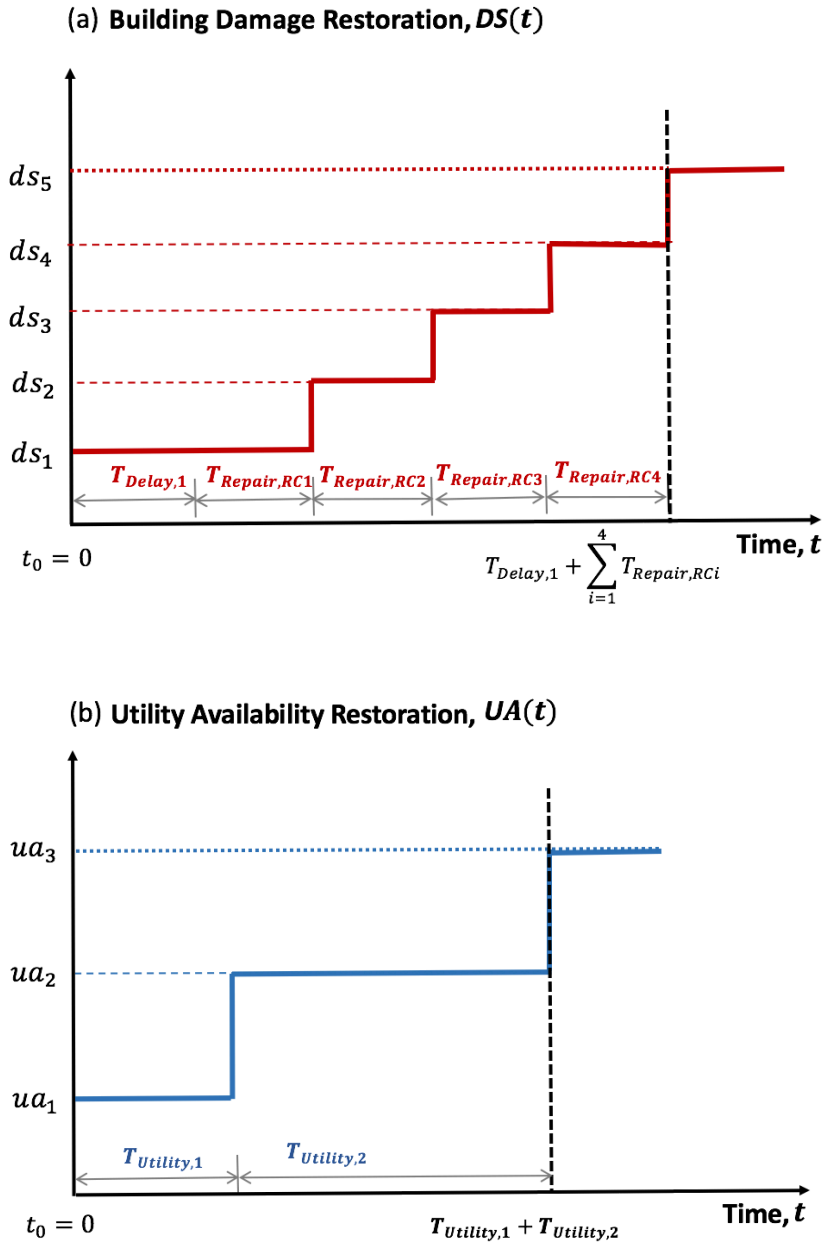


Figure 5-7. Illustration of the (a) building damage restoration and (b) utility availability restoration

Table 5-1. Waiting time conditional on initial damage condition and utility availability, $WT_{i,j}^{n}|ds_p, ua_q$

Functionality State, $S(t_0)$	**Damage State, $DS(t_0)$**	**Utility Availability, $UA(t_0)$**	**Waiting Time, $WT_{i,i}$**	**Waiting Time, $WT_{i,j}, j > i$**
RE	ds_1	N/A	$T_{Delay,1} + T_{Repair,RC1}$	$Max(T_{Repair,RCj}, T_{Utility} - T_{Delay,i} - \sum_{k=i}^{j-1} T_{Repair,RCk})^*$
RU	ds_2	N/A	$T_{Delay,2} + T_{Repair,RC2}$	$Max(T_{Repair,RCj}, T_{Utility} - T_{Delay,i} - \sum_{k=i}^{j-1} T_{Repair,RCk})^*$
RO	ds_3	ua_3	$T_{Delay,3} + T_{Repair,RC3}$	$T_{Repair,RCj}$
RO	ds_3	ua_2	$T_{Delay,3} + T_{Repair,RC3}$	$\text{Max}(T_{Repair,RC4}, T_{Utility,2} - WT_{3,3})$
RO	ds_3	ua_1	$\text{Max}(T_{Delay,3} + T_{Repair,RC3}, T_{Utility,1})$	$\text{Max}(T_{Delay,3} + T_{Repair,RC3} + T_{Repair,RC4} - WT_{3,3}, T_{Utility,1} + T_{Utility,2} - WT_{3,3})$
RO	ds_4	ua_1	$T_{Utility,1}$	$\text{Max}(T_{Repair,RC4} + T_{Repair,RC4} - T_{Utility,1}, T_{Utility,2})$
RO	ds_5	ua_1	$T_{Utility,1}$	$T_{Utility,2}$
BF	ds_4	ua_3	$T_{Delay,4} + T_{Repair,RC4}$	0
BF	ds_5	ua_2	$T_{Utility,2}$	0
BF	ds_4	ua_2	$\text{Max}(T_{Delay,4} + T_{Repair,RC4}, T_{Utility,2})$	0
FF	ds_5	ua_3	0	0

$^*T_{Utility} = 0$ if $UA(t_0) = ua_3$; $T_{Utility} = \begin{cases} 0, & j = 3 \\ T_{Utility,2}, & j = 4 \end{cases}$ if $UA(t_0) = ua_2$; $T_{Utility} = \begin{cases} T_{Utility,2}, & j = 3 \\ T_{Utility,1} + T_{Utility,2}, & j = 4 \end{cases}$ if $UA(t_0) = ua_1$

5.2 Step 2: Portfolio-Level Recovery

5.2.1 Portfolio Recovery Trajectory (PRI)

The second step of the BPRM is portfolio-level recovery in which the CTMC restoration processes of individual buildings are aggregated across the geographic domain of the community and over the entire recovery time horizon. A community building portfolio includes numerous buildings of different occupancies and construction types that collectively support different community functions (e.g. housing, business, education, healthcare, government, etc.). In order to track the recovery time and trajectory of a building portfolio as a whole, a building *portfolio recovery index*, $PRI_j(t)$ (which is the BPFM introduced in Chapter 3, as well as the vertical axis of the Figure 5-1) is proposed and defined as the percentage of buildings in a community that are in the functionality state S_j at any given time t, i.e.:

$$PRI_j(t) = \frac{\sum_{n=1}^{N} I_j^n(t)}{N}\ , \qquad j \in 1 \dots 5 \tag{5-14}$$

where N is the total number of buildings in a community, and $I_j^n(t)$ is the functionality state indicator of building n, i.e.:

$$I_j^n(t) = \begin{cases} 0 & S^n(t) \neq S_j \\ 1 & S^n(t) = S_j \end{cases},\ n \in 1, 2, \cdots, N \tag{5-15}$$

Accordingly, the Probability Mass Function (PMF) of $I_j^n(t)$ is:

$$P_{I_j^n}(t) = \begin{cases} 1 - \pi_j^n\ (t) & I_j^n(t)\ = 0 \\ \pi_j^n(t) & I_j^n(t) = 1 \end{cases}, \qquad n \in 1, 2, \dots, N \tag{5-16}$$

where $\pi_j^n(t)$ is the probability of $S^n(t) = S_j$ at any time t for building n, as defined in Eq. (5-1) and estimated by Eq. (5-7). Moreover, the time-dependent expected value and variance of $PRI_j(t)$ are:

$$E\left[PRI_j(t)\right] = \frac{1}{N}\sum_{n=1}^{N} \pi_j^n\,(t), \qquad n \in 1,\ 2, \ldots, \mathrm{N} \tag{5-17}$$

$$\sigma^2_{PRI_j}(t) = \frac{1}{N^2}\sum_{n=1}^{N}\sum_{m=1}^{N} \rho_j^{mn}(t)\sigma_j^n(t)\sigma_j^m(t)\,, \quad n, m \in 1, 2, \ldots, N \tag{5-18}$$

in which, $\sigma_j^n(t) = \sqrt{\pi_j^n(t)\left[1 - \pi_j^n(t)\right]}$ is the standard deviation of $I_j^n(t)$ and $\rho_j^{mn}(t)$ is the correlation matrix describing correlations between functionality states of building *n*, $I_j^n(t)$, and that of building *m*, $I_j^m(t)$, at any time t. Such correlations are introduced by the correlated initial functionality states between building pairs at t_0 resulting from correlated damage states (which, in turn, are introduced by the similarities in design and construction of buildings in the same community and the correlated hazard demands, e.g., earthquake ground motion intensities from the same hazard event). These correlations are propagated through the building restoration process; temporally, these correlations are strongest at t_0 and decrease monotonically with t as the buildings' restorations progress, and spatially, these correlations depend on the geographical locations of individual buildings and other attributes that affect building's damage state due to the hazard events. A detailed approach to estimate this correlation will be presented subsequently in Section 5.3.

The mean values of $PRI_j(t)$ represented by Eq. (5-17) are illustrated in Figure 5-8, for $j = RE, RU, RO, BF\ and\ FF$, respectively, tracking the temporal evolution of the percentage of buildings falling into each of the five functionality states.

The uncertainties associated with these curves are given by Eq. (5-18). Further, define the curve associated with the FF state, i.e. $PRI_{FF}(t)$, as the *portfolio recovery trajectory*, which represents the percentage of the buildings in the *FF* state at any given elapsed time t from the hazard occurrence, and is monotonically increasing with time. In contrast, the curve that tracks the percentage of buildings at the lowest functionality state (*RE*), i.e. $PRI_{RE}(t)$, is always decreasing with time because buildings that are initially red-tagged (with a *RE* state) will be gradually restored to higher functionality states as the portfolio recovery proceeds. The portfolio recovery trajectory $PRI_{FF}(t)$ may not always converge to 100% and the $PRI_{RE}(t)$ may not always diminish to 0, as shown in Figure 5-8, which could be due to the population in- and out-migration following an extreme hazard. The trajectories of intermediate functionality states *RU*, *RO* and *BF* can be either increasing or decreasing at early stages of portfolio recovery, but all will ultimately decrease and approach to zero as most buildings in a portfolio are ultimately restored to the *FF* state. The summation of the five mean trajectories at any given time is approximately 100%.

5.2.2 Portfolio Recovery Time (PRT)

The portfolio recovery time, $PRT_{j,a\%}$, as already defined in Section 3.1, is the time takes for a% (e.g. 95%) of community buildings to regain a predetermined functionality state j (e.g. *FF*). Then, the CDF of $PRT_{j,a\%}$ can be derived as:

$$F_{PRT_{j,a\%}}(t) = Prob\left[PRT_{j,a\%} \le t\right] = Prob\left[PRI_j(t) \ge a\%\right] = \int_{a\%}^{1} f_{PRI_j}(x,t)\,dx \tag{5-19}$$

where $f_{PRI_j}(x,t)$ is the PDF of PRI_j at time *t*, which can be obtained through multiple layers of MCS, propagating uncertainties throughout the portfolio recovery process, from spatially correlated hazard intensity, to spatially correlated structural and nonstructural building damage, and waiting time estimates. Such MCS, however, can quickly become computationally unmanageable as the size of the building portfolio (*N*) increases. Alternatively, since $PRI_j(t)$ at any given time, as defined in Eq. (5-14), is the summation of I_j^n, $n = 1, \dots, N$ (which become uncorrelated random variables as time elapses because the correlations in I_j^n , ρ_j^{mn}, diminish with time, as discussed previously), the $PRI_j(t)$ is approximated by a normal distribution when t approaches to full recovery time, with mean and variance expressed in Eq. (5-17) and Eq. (5-18), as the building portfolio approaches its full recovery. The normal distribution need to be truncated at 1.0 because PRI_j cannot exceed 100%. Accordingly, the distribution of portfolio recovery time, $PRT_{FF,95\%}$, estimated using Eq. (5-19) is also illustrated in Figure 5-8.

A community building portfolio is a spatially distributed system in the geographic domain of the community. This spatial distribution of buildings reflects the community's development pattern, zoning, demographics and social disparities. Therefore, the spatial variation of the portfolio recovery is also of great interest to community decision makers in considering, e.g. the recovery resource allocation. The two-step BPRM developed in this study, when applied to a real community, can provide insights regarding the temporal evolution of the spatial variation in recovery speed in different zones of the community, as conceptually illustrated in Figure 5-9.

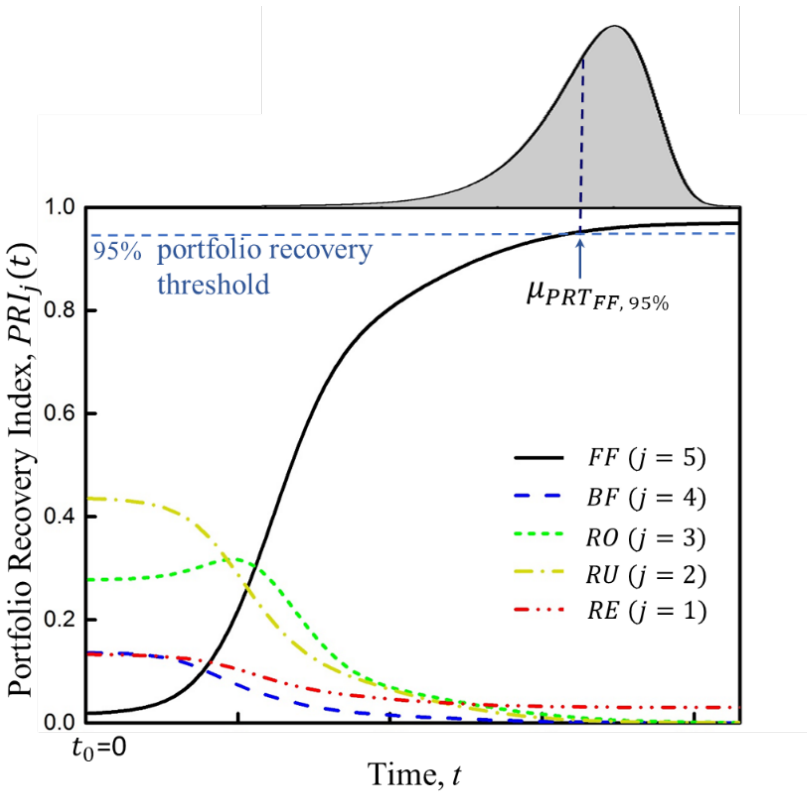


Figure 5-8. Illustration of the mean trajectory of the building portfolio recovery

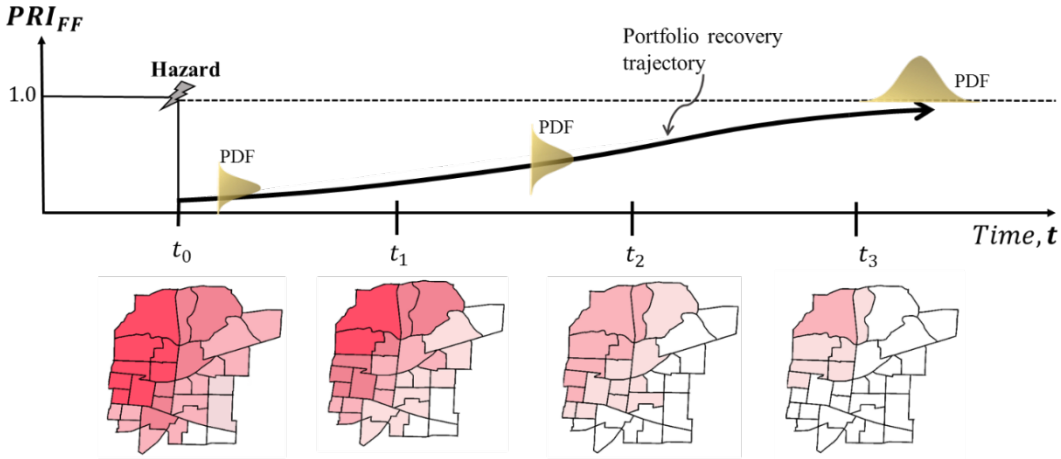


Figure 5-9. Expected outcome of the two-step BPRM - spatial and temporal evolution of portfolio recovery (areas are shaded to indicate level of functionality; darker means lower functionality state)

5.3 Uncertainty Propagation and Correlation Quantification

The quantification of uncertainty in portfolio functionality metric $PRI_j(t)$, as indicated in Eq. (5-18), requires the calculation of correlation matrix $\rho_j^{mn}(t)$, the information of which can be captured during uncertainty propagation from spatial damage states of buildings (***DS***) to time-variant spatial functionality states $S(t)$.

As discussed in Section 4.1.4, the correlation among damage states of building pairs within a building portfolio will be carried over, through the damage-to-functionality mapping, to the initial functionality states of buildings $S(t_0)$. This correlation contributes to the uncertainty in probable portfolio functionality metric at t_0, $PRI_j(t_0)$. Because the correlation in hazard demand and building response invariably is positive, neglecting such spatial correlation results in an unconservative estimate of uncertainty in $PRI_j(t_0)$ and quantification of risk (Jayaram & Baker, 2009; Vitoontus & Ellingwood, 2013). Further, as time goes on, the correlation among functionality states of buildings at t_0 will continue to propagate all the way through the building portfolio recovery process until it diminishes to zero.

To quantify the correlation among functionality states of buildings, the mean restoration process of building *n*, $S^n(t)$, either conditional on its initial functionality state $S^n(t_0)$, or unconditional, is:

$$E[S^n(t)|S^n(t_0) = S_i] = \sum_{j=i}^{5} S_j \cdot p_{i,j}^n(t) \tag{5-20a}$$

$$E[S^n(t)] = \sum_{j=1}^{5} S_j \cdot \pi_j^n(t) \tag{5-20b}$$

in which $p_{i,j}^n(t)$ is the element of ***TPM*** of building *n* as defined in Eq. (5-3).

Accordingly, the covariance of functionality states $S^m(t)$ and $S^n(t)$ at any time $t > t_0$ for any building pair (m, n) is calculated as:

$$Covar[S^m(t)S^n(t)] = E[S^m(t)S^n(t)] - E[S^m(t)] \cdot E[S^n(t)] \tag{5-21}$$

in which:

$$E[S^m(t)S^n(t)] = \sum_{k=1}^{5}\sum_{i=1}^{5} E[S^m(t)|S^m(t_0) = S_k] \cdot E[S^n(t)|S^n(t_0) = S_i] \cdot P[S^m(t_0) = S_k, S^n(t_0) = S_i] \tag{5-22}$$

The joint PMF of initial functionality states $P[S^m(t_0) = S_k, S^n(t_0) = S_i]$ can be captured in the spatially-correlated initial functionality states obtained from the damage-to-functionality mapping in Figure 4-2.

Eqs. (5-20)-(5-22) calculates the correlation in time-variant functionality states of building pairs within a building portfolio. Further, to obtain the uncertainty associated with the recovery trajectory $PRI_j(t)$ [cf. Eq. (5-18)], it requires the estimate of correlation $\rho_j^{mn}(t)$ in functionality state indicators of any building pair (m, n) at any time t, $I^m(t)$ and $I^n(t)$, by:

$$\rho_j^{mn}(t) = \frac{E\left[I_j^m(t)I_j^n(t)\right] - E\left[I_j^m(t)\right] \cdot E\left[I_j^n(t)\right]}{\sigma_j^m(t)\sigma_j^n(t)} = \frac{P\left[S^m(t) = S^n(t) = S_j\right] - \pi_j^m(t) \cdot \pi_j^n(t)}{\sigma_j^m(t)\sigma_j^n(t)} \tag{5-23}$$

where the probabilities $P\left[S^m(t) = S^n(t) = S_j\right]$ are the diagonal terms of the joint PMF of (spatially correlated) functionality states of all buildings at time t, which is described collectively by its marginal distributions [i.e., $\boldsymbol{\pi}^m(t)$ and $\boldsymbol{\pi}^n(t)$ obtained in Section 5.2] and the covariance matrix quantified by Eqs. (5-21)-(5-22). Accordingly, the mean and variance of $PRI_{FF}(t)$ representing the portfolio recovery trajectory can be determined using Eqs. (5-17)-(5-18), and the portfolio recovery time can further be derived by Eq.

(5-19). The probabilistic outcomes of the BPRM quantified herein can further support future work on risk-based community resilience planning and hazard mitigation.

5.4 Closure

In this chapter, a novel simulation-based, stochastic building portfolio recovery model, BPRM, is formulated to estimate portfolio recovery time and recovery trajectory following a natural disaster. The BPRM includes two steps of modeling: building-level restoration and portfolio-level recovery. The major contributions are the following:

(1) Individual building-level restoration is modeled as a discrete-state, continuous-time Markov Chain (CTMC), using the five building functionality states - *RE*, *RU*, *RO*, *BF*, and *FF* – introduced in Chapter 3 as the discrete building functionality metric. The realistic process of building-level restoration is investigated (cf. Figure 5-5) and mapped onto the theoretical CTMC restoration model (cf. Figure 5-3), from which the ***TPM*** is obtained. The CTMC restoration model results in the building restoration functions (*BRF*) for a building, defining the functionality state probabilities for the building at any elapsed time *t* following the occurrence of the hazard event.

(2) Stochastic building portfolio recovery is modeled in both spatial and temporal dimensions. Two portfolio-level recovery metrics are investigated: 1) the portfolio recovery index, $PRI_{FF}(t)$, indicating the percentage of buildings that are in the *FF* state at any *t*; and 2) the portfolio recovery time, $PRT_{FF,a\%}$, representing the time required to restore $a\%$ of portfolio buildings to the *FF* state. Both metrics are

quantified probabilistically by integrating the building-level CTMC restoration processes across the community and over the entire recovery time horizon.

(3) The two-step BPRM is calibrated through a review of existing recovery-related databases and variables known to be essential for building portfolio recovery analysis. Uncertainties in these variables are propagated, and the time-variant spatial correlations in buildings' functionality states are quantified throughout the BPRM in the estimation of the portfolio recovery trajectory and recovery time.

Chapter 6 Assessment of Building Portfolios in Two Testbed Communities

In this chapter, the BPLE and BPRM developed in Chapters 4 and 5 are applied to two testbed communities: a hypothetical community – Centerville, and a real community − Shelby County, TN. The case studies are targeted to assess the practical feasibility of the BPLE and BPRM in supporting community resilience assessment and in facilitating resilience-based risk mitigation.

Section 6.1 focuses on Centerville, which includes an introduction of Centerville building portfolio in Section 6.1.1; portfolio demand and damage assessment in Section 6.1.2; portfolio DLR and HDR estimation in Section 6.1.3; portfolio functionality loss and functionality recovery assessment, in Sections 6.1.4 and 6.1.5, respectively; and finally, a sensitivity study to illustrate the feasibility of BPLE and BPRM in supporting risk-mitigation decisions as illustrated in Section 6.1.6. The Shelby building portfolio resilience assessment is presented in Section 6.2, with Shelby portfolio characteristics, spatial seismic demand and portfolio recovery prediction presented in 6.2.1, 6.2.2, and 6.2.3, respectively.

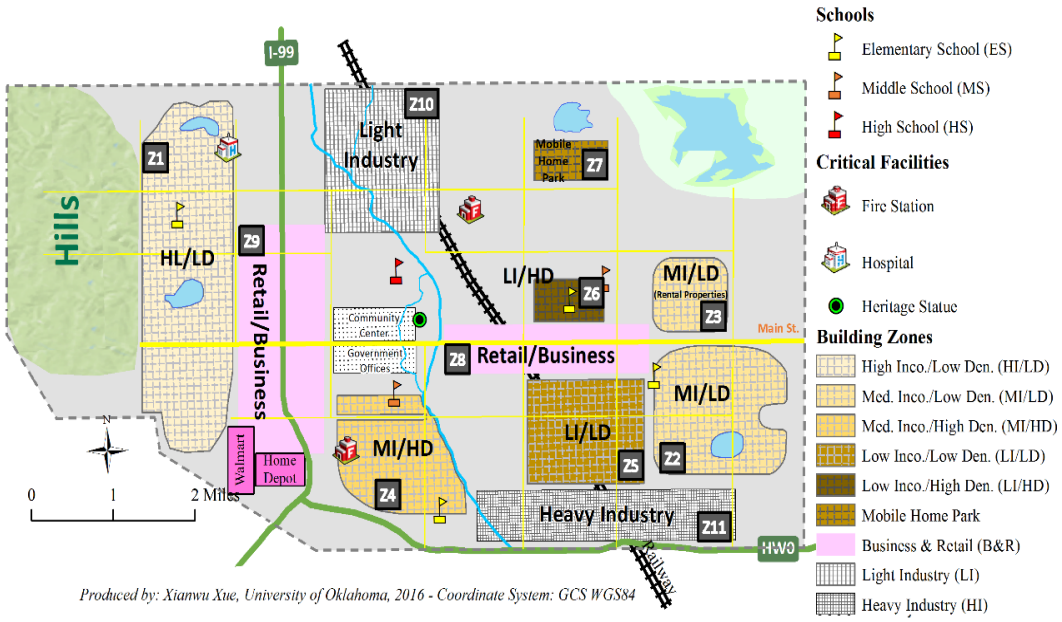
6.1 Centerville Building Portfolio Analysis

6.1.1 Centerville Building Portfolio Characteristics

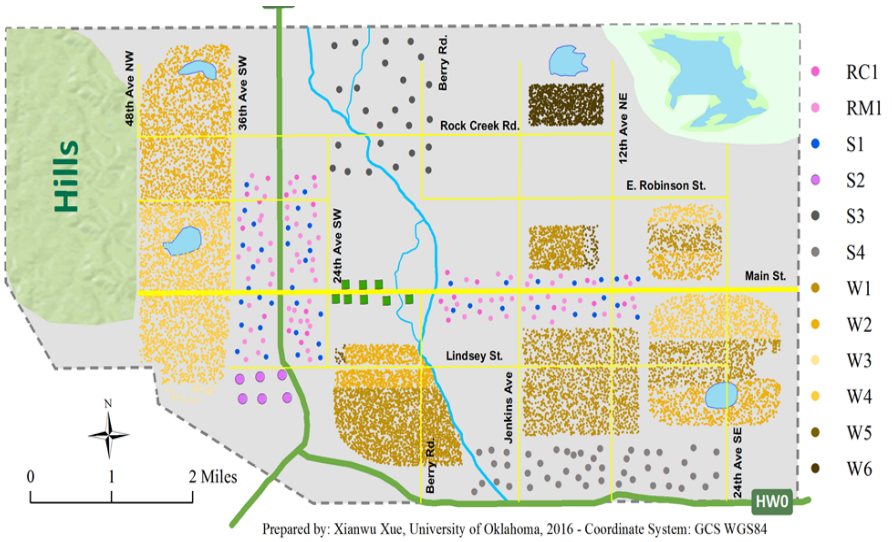
Centerville is a hypothetical community utilized by the NIST-Funded Center for Risk-Based Community Resilience Planning (CRCRP) to embody all typical features of a community and to allow and facilitate research teams to perform various resilience-related analyses of physical, social and economic infrastructure systems (Ellingwood et

al., 2016). Centerville is designed as a typical mid-size community, with a population of approximately 50,000, situated in a Midwestern State in the US, and is approximately 8km by 13km (5 miles by 8 miles) in size. As shown in Figure 6-1(a) (Lin & Wang, 2017b), Centerville includes 7 residential zones (Z1-Z7) which are categorized and distributed by the income level of the residents, 2 commercial zones (Z8-Z9), 2 industrial zones – one light industry (Z10) and one heavy industry (Z11). Specifically, Z1 is a high income/low density (HI/LD) development abutting the western hills, Z2-Z4 are mixture of middle income (MI) zones, Z5-Z6 are low-income (LI) residential areas around and east of the Interstate I-99, which runs north-south, and a sizeable mobile home park (Z7) is adjacent to one of the industrial facilities. The 2 commercial zones are located along major roadways. The light industrial zone (Z10) is located at the north of the community while the heavy industrial zone (Z11) is located at the south east of the community, both along a railway for easy cargo transportation.

The Centerville building portfolio as introduced in Lin &Wang (2017b) of approximately 15,000 buildings consists of 16 building archetypes, including residential, commercial, industrial occupancies, as well as critical facilities such as hospitals, fire stations, schools and government offices, as tabulated in Table 6-1. The spatial distribution of all buildings within Centerville is shown in Figure 6-1(b). Particularly, the residential building portfolio accounts for nearly 98% of the Centerville building portfolio. All residential buildings, located in Z1-Z7, are wood frame structures with different occupancy types, stories, and year built (denoted as W1 – W6 in Table 6-1). The number of buildings and the household (HH) income range in each of the residential zones are summarized in Table 6-2.



(a) Zoning map



(b) Building portfolio

Figure 6-1. Centerville (a) zoning map, and (b) building portfolio

Table 6-1. Summary of Centerville building types [data source: Lin &Wang (2017b)]

Type ID	Construction	Occupancy Class	Story	Year Built	Area (ft2)
W1	Wood	Residential, SF*	1	1945-1970	1,400
W2	Wood	Residential, SF	1	1985-2000	2,400
W3	Wood	Residential, SF	2	1985-2000	3,200
W4	Wood	Residential, SF	1	1970-1985	2,400
W5	Wood	Residential, MF*	3	1985	36,000
W6	Wood	Mobile Home	NA	NA	NA
S1	Steel braced frame	Commercial	1	1980	50,000
RC1	RC frame	Commercial	2	1980	50,000
RM1	Reinforced masonry	Commercial	2	1960	25,000
S2	Mix of steel and OWSJ* roof	Commercial	1	NA	125,000
S3	Steel braced frame	Industrial	2	1975	100,000
S4	Steel braced frame	Industrial	1	1995	500,000
RC2	RC frame	Hospital	4	1980	120,000
RM2	Reinforced masonry	Fire Station	2	1985	10,000
RC3	RC frame	School	3	1990	100,000
RM3	Light reinforced masonry	School	1	NA	100,000

*SF – single family
*MF – multiple family
*OWSJ – open web steel joist

Table 6-2. Household characteristics of residential zones (Zone 1- Zone 7) [Data source: Lin &Wang (2017b)]

Zone ID		Residential Zones						
		Zone1 (Z1)	Zone2 (Z2)	Zone3 (Z3)	Zone4 (Z4)	Zone5 (Z5)	Zone6 (Z6)	Zone7 (Z7)
Description		High income/ Low density (HI/LD)	Medium income/ Low density (MI/LD)	Medium income/ Low density (MI/LD)	Medium income/ Low density (MI/HD)	Low income/ Low density (LI/LD)	Low income High density (LI/HD)	Mobile Homes
Household ID		HH1	HH2	HH3	HH4	HH5	HH6	HH7
Avg. Household Income		≥$100k	$70k-$100k	$70k-$100k	$40k-$70k	$20k-$40k	≤ $20k	≤ $10k
No. of Household		4,246	2,267	800	4,767	1,856	4,396	1,352
No. of Buildings	W1	0	767	300	2,567	1,856	700	0
	W2	2,000	700	300	1,000	0	0	0
	W3	50	0	0	0	0	0	0
	W4	2,196	800	200	0	0	0	0
	W5	0	0	0	1,200	0	3,696	0
	W6	0	0	0	0	0	0	1,352

6.1.2 Seismic Demands and Building Damages

The determination of seismic demands propagated from earthquake source to the building sites requires modeling of ground motion attenuation relation, local soil amplification, and spatial ground motion correlation. Regarding scenario earthquake analysis, a hypothetical scenario earthquake with M_w 7.8 and an epicenter located approximately 40 km southwest of Centerville is considered for illustration. The ground motion attenuation model by Campbell (2003) is adopted with mean value of the logarithm of seismic intensity,

$$\ln(IM) = c_1 + c_2 \cdot M_w + c_3 \cdot (8.5 - M_w)^2 + c_4 \cdot \ln R + (c_5 + c_6 \cdot M_w) \cdot r + f \tag{6-1a}$$

$$R = \sqrt{r^2 + [c_7 \cdot \exp(c_8 \cdot M_w)]^2} \tag{6-1b}$$

$$f = \begin{cases} 0; & r \le 70km \\ c_7 \left[\ln\left(\frac{r}{70}\right)\right]; & 70km \le r \le 130km \\ c_7 \left[\ln\left(\frac{r}{70}\right)\right] + c_8 \left[\ln\left(\frac{R}{130}\right)\right]; & r > 130km \end{cases} \tag{6-1c}$$

and standard deviation of the $\ln(IM)$

$$\sigma_{\ln(IM)} = \begin{cases} c_{11} + c_{12} \cdot M_w; & M_w < 7.16 \\ c_{13}; & M_w > 7.16 \end{cases} \tag{6-1d}$$

in which r is the epicenter distance; c_1 through c_{13} are period-dependent regression coefficients of the attenuation model, as listed in Table 6 in Campbell's paper (2003).

The ground motion intensity may be amplified depending on the soil condition of a building site. *The ASCE Standard 7-10* (ASCE, 2010) has classified six categories

of site classes (symbolized as A, B, C, D, E, F) and defined a site coefficient to amplify ground motion intensities at different site classes (using rock site, which is Site Class B, as the baseline). The ground motion intensities calculated from the ground motion attenuation models in the literature are for Site Class A. In this study, Centerville is assumed, for simplicity, to be situated on Site Class A soils.

The capacity spectral method is used to determine the spectral displacement S_d for determining damage of structural and drift-sensitive nonstructural components, and spectral acceleration S_a for acceleration-sensitive nonstructural components and building contents (FEMA/NIBS, 2003). Seismic fragility functions for the three types of building components are mapped from the HAZUS-MH database (FEMA/NIBS, 2003), based on building characteristics such as occupancy, structural type, construction material, number of stories, square footage area and year built, as tabulated in Table 6-1, to support the analysis herein. The fragility parameters with respect to structural component, nonstructural drift-sensitive component, and nonstructural acceleration-sensitive component of each of the 16 building types are listed in Table 6-3, Table 6-4, and Table 6-5, respectively.

Both site-to-site and structure-to-structure spatial correlations are modeled in the probabilistic building portfolio analysis. The spatial correlation in seismic intensities of different building sites is estimated by Eq. (4-4) assuming the correlation distance $R = 10\ km$. This correlation distance value has been assumed to be in the range of 20-40km (Wang & Takada, 2005), and it is scaled down herein since Centerville is a relatively small community. The standard deviation of intra-event error term τ in Eq. (4-3) is computed using Eq. (6-1d). The spatial correlations between *DV*s of any two buildings

are determined from Eq. (4-9), assuming that $\rho_{Y_i.Y_j} = 0.35$ when buildings *i* and *j* are of different building types, and $\rho_{Y_i.Y_j} = 0.9$ if otherwise. Ideally, for a "real" community, these correlation coefficients should be determined based on collected building portfolio data coupled with professional judgement. The noise term σ_ε in Eq. (4-5) is neglected due to a lack of empirical data.

Table 6-3. Structural fragility curve parameters (unit: inch) [data source: HAZUS-MH (FEMA/NIBS, 2003)]

TypeID	FragilityID (HAZUS)	Slight		Moderate		Extensive		Complete	
		Median	Beta	Median	Beta	Median	Beta	Median	Beta
W1	pre-code W2	0.4	1.01	1	1.05	3.09	1.07	7.56	1.06
W2	low-code W1	0.5	0.93	1.25	0.98	3.86	1.02	9.45	0.99
W3	moderate-code W1	0.86	0.97	2.14	0.9	6.62	0.89	16.2	0.99
W4	pre-code W1	0.4	1.01	1	1.05	3.09	1.07	7.56	1.06
W5	low-code W2	0.69	1.04	1.71	0.97	5.29	0.9	12.96	0.99
W6	low-code MH	0.48	0.91	0.96	1	2.88	1.03	8.4	0.92
S1	low-code S2L	0.86	1.01	1.38	0.96	3.46	0.88	8.64	0.95
RC1	low-code C1L	0.72	0.98	1.15	0.94	2.88	0.9	7.2	0.97
RM1	pre-code RM1L	0.58	1.2	0.92	1.1	2.31	1.17	6.3	0.93
S2	low-code S3	0.54	0.98	0.87	0.99	2.17	1.01	5.91	0.9
S3	pre-code S2L	0.86	1.01	1.38	0.96	3.46	0.88	8.64	0.95
S4	moderate-code S2L	1.3	0.77	2.07	0.78	4.38	0.78	10.8	0.96
RC2	low-code C1M	0.72	0.98	1.15	0.94	2.88	0.9	7.2	0.97
RM2	low-code RM1L	0.58	1.2	0.92	1.1	2.31	1.17	6.3	0.93
RC3	moderate-code C1L	0.9	0.95	1.44	0.91	3.6	0.85	9	0.97
RM3	moderate-code RM1L	0.58	1.2	0.92	1.1	2.31	1.17	6.3	0.93

Table 6-4. Nonstructural drift-sensitive fragility curve parameters (unit: inch) [data source: HAZUS-MH (FEMA/NIBS, 2003)]

TypeID	FragilityID (HAZUS)	Slight		Moderate		Extensive		Complete	
		Median	Beta	Median	Beta	Median	Beta	Median	Beta
W1	pre-code W2	0.5	1.07	1.01	1.11	3.15	1.11	6.3	1.14
W2	low-code W1	0.5	0.98	1.01	0.99	3.15	1.02	6.3	1.09
W3	moderate-code W1	0.86	1.01	1.73	0.97	5.4	0.93	10.8	1.03
W4	pre-code W1	0.5	1.07	1.01	1.11	3.15	1.11	6.3	1.14
W5	low-code W2	0.86	1.06	1.73	1	5.4	0.93	10.8	1.01
W6	low-code MH	0.48	0.96	0.96	1.05	3	1.07	6	0.93
S1	low-code S2L	0.86	1.06	1.73	0.97	5.4	0.96	10.8	1.04
RC1	low-code C1L	0.72	1.02	1.44	0.98	4.5	0.93	9	1.03
RM1	pre-code RM1L	0.72	1.22	1.44	1.12	4.5	1.01	9	0.99
S2	low-code S3	0.54	1.03	1.08	1.02	3.38	0.96	6.75	0.99
S3	pre-code S2L	0.86	1.06	1.73	0.97	5.4	0.96	10.8	1.04
S4	moderate-code S2L	0.86	1.01	1.73	0.94	5.4	0.94	10.8	1.03
RC2	low-code C1M	0.72	1.02	1.44	0.98	4.5	0.93	9	1.03
RM2	low-code RM1L	0.72	1.22	1.44	1.12	4.5	1.01	9	0.99
RC3	moderate-code C1L	0.72	0.99	1.44	0.96	4.5	0.9	9	1.01
RM3	moderate-code RM1L	0.72	1.22	1.44	1.12	4.5	1.01	9	0.99

Table 6-5. Nonstructural acceleration-sensitive fragility curve parameters (unit: g) [data source: HAZUS-MH (FEMA/NIBS, 2003)]

TypeID	FragilityID (HAZUS)	Slight		Moderate		Extensive		Complete	
		Median	Beta	Median	Beta	Median	Beta	Median	Beta
W1	pre-code W2	0.2	0.72	0.4	0.7	0.8	0.67	1.6	0.67
W2	low-code W1	0.2	0.71	0.4	0.68	0.8	0.66	1.6	0.66
W3	moderate-code W1	0.2	0.67	0.4	0.67	0.8	0.7	1.6	0.7
W4	pre-code W1	0.2	0.72	0.4	0.7	0.8	0.67	1.6	0.67
W5	low-code W2	0.2	0.66	0.4	0.67	0.8	0.65	1.6	0.65
W6	low-code MH	0.2	0.65	0.4	0.67	0.8	0.67	1.6	0.67
S1	low-code S2L	0.2	0.65	0.4	0.68	0.8	0.68	1.6	0.68
RC1	low-code C1L	0.2	0.66	0.4	0.68	0.8	0.68	1.6	0.68
RM1	pre-code RM1L	0.2	0.66	0.4	0.67	0.8	0.66	1.6	0.66
S2	low-code S3	0.2	0.65	0.4	0.68	0.8	0.68	1.6	0.68
S3	pre-code S2L	0.2	0.65	0.4	0.68	0.8	0.68	1.6	0.68
S4	moderate-code S2L	0.2	0.65	0.4	0.68	0.8	0.68	1.6	0.68
RC2	low-code C1M	0.2	0.66	0.4	0.68	0.8	0.68	1.6	0.68
RM2	low-code RM1L	0.2	0.66	0.4	0.67	0.8	0.66	1.6	0.66
RC3	moderate-code C1L	0.2	0.65	0.4	0.68	0.8	0.68	1.6	0.68
RM3	moderate-code RM1L	0.2	0.66	0.4	0.67	0.8	0.66	1.6	0.66

6.1.3 Building Portfolio DLR and HDR

To illustrate the application of the BPLE, two building portfolio performance metrics commonly used in literature, as reviewed in Section 2.2, are examined: direct economic loss (economic-based metric) and household dislocation (social-based metric). The state-of-the-art methodologies from existing literature are adopted for quantifying these two metrics.

Direct loss ratio (DLR): Monetary loss to a building portfolio due to its physical damage, referred as the direct loss herein, is one of the most commonly studied building portfolio metrics. The direct loss ratio, DLR, defined as the ratio of total direct loss to total assessed value (including building contents) of a building portfolio, is often used for community-level policy making and insurance underwriting.

The direct loss of a portfolio can be computed as (Steelman et al., 2007):

$$Z_{Loss} = \sum_{i=1}^{N} Loss_i \quad = \sum_{i=1}^{N} M_i \cdot (\alpha_i^{SD} DV_i^{SD} + \alpha_i^{ND} DV_i^{ND} + \alpha_i^{NA} DV_i^{NA} + \alpha_i^{CL} DV_i^{CL}) \tag{6-2}$$

where $Loss_i$ is the direct loss of the building i; M_i is the replacement cost of the building i; α_i^{SD}, α_i^{ND}, α_i^{NA} are the fractions of the values of structural components, and non-structural acceleration-sensitive and drift-sensitive components, respectively; and α_i^{CL} is the ratio of the contents value to the replacement cost. These values of α are usually determined from historical or empirical data collected by construction companies. In this study, these values are taken from the HAZUS-MH MR2 Technical Manual (FEMA/NIBS, 2003). $DV_i^{SD}, DV_i^{ND}, DV_i^{NA}$ and DV_i^{CL} are the damage values in building i of the above-mentioned components, which are random variables and can be assessed from damage analysis. DLR can then be calculated as:

$$\text{DLR} = \frac{Z_{Loss}}{\sum_{i=1}^{N} M_i} \tag{6-3}$$

Household dislocation ratio (HDR): Significant household dislocation is one of the most undesirable outcomes to a community following an extreme hazard event; it may be caused by a variety of reasons, with one of the major contributors being lack of habitable residential buildings. Household dislocation ratio, HDR, is defined as the percentage of households in a community that are displaced due to loss of housing habitability and short-term shelter needs (FEMA/NIBS, 2003). The HDR is an important metric of community social vulnerability to natural hazard. In this study, the ordinary least squares (OLS) regression model (Peacock et al., 2008) is adopted to estimate the HDR:

$$\text{HDR} = \delta_{VLOSS} \times [b_1 + b_2 \cdot \delta_{Minorities} + b_3 \cdot \delta_{VAC} + b_4 \cdot \delta_{MHHIK} + b_5 \cdot \delta_{SFDET}] \tag{6-4}$$

where $\delta_{Minorities}$ is the percentage of minorities in the community; δ_{VAC} is the percentage of vacant housing units; δ_{MHHIK} is the median housing income in the community (in \$K); δ_{SFDET} is the percentage of detached single family houses; and b_i ($i = 1,2,\ldots,5$) are regression coefficients obtained using building portfolio data, population demographics, post-event damage and social survey data from past hazard events (Girard & Peacock, 1997; Peacock et al, 2008; Lin, 2009). δ_{VLOSS} is the fraction of direct losses (structural and non-structural components) of all buildings within a portfolio to the total portfolio replacement cost, which is a key parameter for determining the portfolio HDR and can be estimated from DV_i presented in Section 4.1.

The two social and economic-base resilience metrics, DLR and HDR, are investigated for Centerville building portfolio loss estimation. The coefficients required for estimating these metrics are obtained from the original references of their formulation (such as HAZUS, MAEViz), which were mostly based on readily available data, either from collected databases or expert opinions. For example, for assessing total direct loss ratio, DLR, Table 6-6 lists building appraised values M_i, as well as the fraction of value of structural component α_i^{SD}, nonstructural drift-sensitive component α_i^{ND}, and nonstructural acceleration-sensitive components α_i^{NA}, and the ratio of building contents to the replacement cost α_i^{CL}, which are the parameters in Eq. (6-2) in order to calculate DLR. The mean and standard deviation of repair cost ratio, defined as the fraction of repair cost to the building's appraised value, are listed in Table 6-7 and Table 6-8. For calculating HDR, Table 6-9 lists several social characteristics of the 7 residential zones in Centerville, namely, percentage of minorities ($\delta_{Minorities}$), percentage of vacant housing units (δ_{VAC}), median housing income (δ_{MHHIK}), percentage of detached single family housing (δ_{SFDET}) used in Eq. (6-4). Moreover, the coefficients of the OLS regression model for the HDR are: $b_1 = 0.995$, $b_2 = -0.00255$, $b_3 = -0.01397$, $b_4 = 0.01114$, $b_5 = -0.00297$, determined by the social science team of the CRCRP.

Table 6-6. Building appraised value and fractions of values of structural, nonstructural acceleration-sensitive, nonstructural drift-sensitive components, and building contents [data source: HAZUS-MH (FEMA/NIBS, 2003)]

TypeID	Mean Cost /Sq Feet ($)	Appraised Value ($), M_i	Component Value Percent (%)			Contents Percent (%)
			α_i^{SD}	α_i^{ND}	α_i^{NA}	α_i^{CL}
W1	99.59	139,426	23.4	26.6	50	50
W2	99.59	239,016	23.4	26.6	50	50
W3	99.63	318,816	23.4	26.6	50	50
W4	99.59	239,016	23.4	26.6	50	50
W5	108.86	3,918,960	13.8	43.7	42.5	50
W6	30.9	61,800	24.4	37.8	37.8	50
S1	102.69	5,134,500	16.2	50	33.8	100
RC1	98.96	4,948,000	16.2	50	33.8	100
RM1	88.21	2,205,250	16.2	50	33.8	100
S2	61.91	7,738,750	29.4	43.1	27.5	100
S3	73.82	7,382,000	15.7	72.5	11.8	150
S4	78.61	39,305,000	15.7	72.5	11.8	150
RC2	144.6	17,352,000	15.7	72.5	11.8	150
RM2	110.34	1,103,400	15.3	50.5	34.2	150
RC3	90.22	9,022,000	18.9	32.4	48.7	100
RM3	95.21	9,521,000	18.9	32.4	48.7	100

Table 6-7. Mean structural, nonstructural drift-sensitive, nonstructural acceleration sensitive repair cost ratio, $\mu_{DV_i|DS_i}$ for DLR (unit: %) [Data sources: HAZUS-MH (FEMA/NIBS, 2003)]

Zone	Structural damage state (SD)				Nonstructural drift-sensitive damage damage state (ND)				Nonstructural acceleration-sensitive damage state (NA)			
	slight	moderate	extensive	complete	slight	moderate	extensive	complete	slight	moderate	extensive	complete
Z1	0.5	2.3	11.7	23.4	1	5	25	50	0.5	2.7	8	26.6
Z2	0.5	2.3	11.7	23.4	1	5	25	50	0.5	2.7	8	26.6
Z3	0.5	2.3	11.7	23.4	1	5	25	50	0.5	2.7	8	26.6
Z4	0.5	2.3	11.7	23.4	1	5	25	50	0.5	2.7	8	26.6
Z5	0.5	2.3	11.7	23.4	1	5	25	50	0.5	2.7	8	26.6
Z6	0.5	2.3	11.7	23.4	1	5	25	50	0.5	2.7	8	26.6
Z7	0.4	2.4	7.3	24.4	0.8	3.8	18.9	37.8	0.8	3.8	11.3	37.8
Z8	0.4	1.9	9.6	19.2	0.7	3.4	16.9	33.8	0.9	4.8	14.4	47.9
Z9	0.6	2.9	14.7	29.4	0.6	2.7	13.8	27.5	0.8	4.4	12.9	43.1
Z10	0.4	1.6	7.8	15.7	0.2	1.2	5.9	11.8	1.4	7.2	21.8	72.5
Z11	0.4	1.6	7.8	15.7	0.2	1.2	5.9	11.8	1.4	7.2	21.8	72.5
ES1	0.4	1.9	9.5	18.9	0.9	4.9	24.3	48.7	0.7	3.2	9.7	32.4
ES2	0.4	1.9	9.5	18.9	0.9	4.9	24.3	48.7	0.7	3.2	9.7	32.4
ES3	0.4	1.9	9.5	18.9	0.9	4.9	24.3	48.7	0.7	3.2	9.7	32.4
ES4	0.4	1.9	9.5	18.9	0.9	4.9	24.3	48.7	0.7	3.2	9.7	32.4
MS1	0.4	1.9	9.5	18.9	0.9	4.9	24.3	48.7	0.7	3.2	9.7	32.4
MS2	0.4	1.9	9.5	18.9	0.9	4.9	24.3	48.7	0.7	3.2	9.7	32.4
HS	0.4	1.9	9.5	18.9	0.9	4.9	24.3	48.7	0.7	3.2	9.7	32.4
Fire1	0.3	1.5	7.7	15.3	0.7	3.4	17.1	34.2	1	5.1	15.1	50.5
Fire2	0.3	1.8	9	17.9	0.7	3.3	16.4	32.8	1	4.9	14.8	49.3
Hospital	0.2	1.4	7	14	0.8	3.5	17.4	34.7	1	5.1	15.4	51.3
Govt	0.3	1.8	9	17.9	0.7	3.3	16.4	32.8	1	4.9	14.8	49.3

Table 6-8. Standard deviation of repair cost ratio with respect to structural (SD), nonstructural drift-sensitive (ND), nonstructural acceleration-sensitive (NA) components, and building contents (CL), $\boldsymbol{\sigma_{DV_i|DS_i}}$ for DLR (unit: %) [Data source: MAEViz (Steelman et al., 2007)]

Component	slight	moderate	extensive	complete
Structural	0.333	9.67	16.7	6.67
Nonstructural drift-sensitive	2	8	15	8.33
Nonstructural accel.-sensitive	2	4.67	15	11.7
Contents	1	4	7.5	4.17

Table 6-9. Social characteristics of residential zones [Data source: Ellingwood et al. (2016); Lin & Wang (2016)]

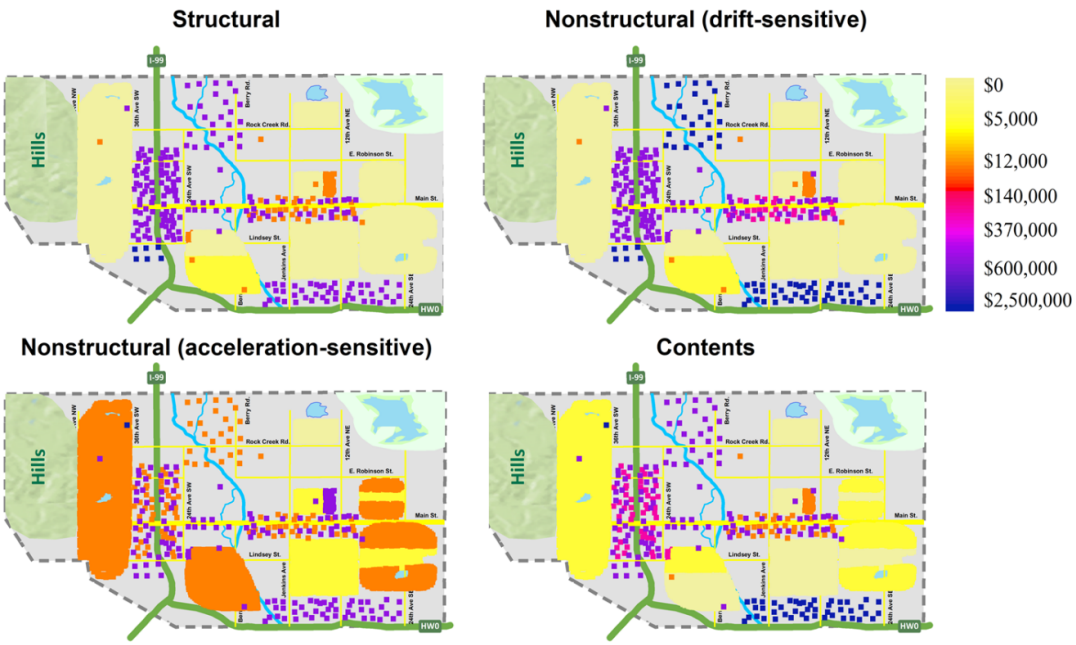
Parameters	Residential Zones						
	Zone1 (Z1)	Zone2 (Z2)	Zone3 (Z3)	Zone4 (Z4)	Zone5 (Z5)	Zone6 (Z6)	Zone7 (Z7)
$\delta_{Minorities}$	1.0%	16.0%	10.0%	15.0%	19.0%	37.0%	20.0%
δ_{VAC}	0.0%	0.0%	0.0%	0.0%	0.0%	0.0%	0.0%
δ_{MHHIK} ($K)	100	85	60	45	30	15	10
δ_{SFDET}	100%	100%	100%	52%	100%	51%	0%

The mean loss distribution within the Centerville building portfolio is illustrated in Figure 6-2. The heaviest losses, in terms of dollar losses, tend to occur in commercial/retail and industrial areas as shown in Figure 6-2(a), while in terms of DLR, they tend to occur in multi-family and high income residential zones. Aggregating these distributed losses within each zone, Figure 6-3 compares the mean direct dollar losses and the mean DLR between building zones. While Zone 11 (heavy industrial) represents the highest dollar losses, Zone 9 (retail/commercial) represents the highest economic impact in terms of DLR. Note in particular that Zone 7 (mobile home park) indicates a relatively low dollar value, but is among the highest in terms of DLR.

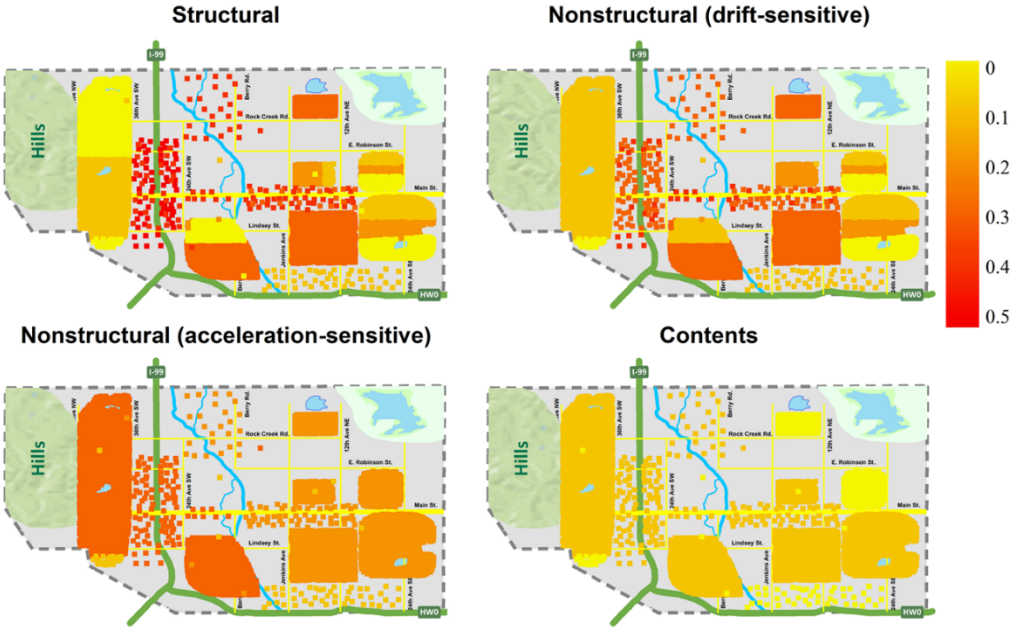
In general, for all buildings, dollar losses due to the damage to structural components are much less than the losses due to non-structural components and building contents.

Figure 6-4 (a), (b) and (c) plot the complementary cumulative distribution functions of DLR and HDR, respectively, for Zone 1 (Z1), Zone 3 (Z3) and Zone 7 (Z7), representing high-, medium-, and low-income household zones, respectively, for the considered scenario event. The performance of Z7 with respect to DLR is much less favorable than that of Z1 and Z3, as shown in Figure 6-4(a). This is easily explained by the fact that mobile homes in Z7 generally experience more severe damage than the typical wood residential buildings in the other two zones; moreover, buildings in Z1, which are occupied by high-income households, are usually better constructed and likely to have better structural performance. The complementary cumulative distributions of DLR indicate that the median loss for Z1, Z3 and Z7 is 8.4%, 6.9%, 10%, respectively. Such information is most informative for insurance underwriting and government subsidies policy-making.

Even with lower DLR, Figure 6-4(b) indicates, somewhat counter-intuitively, that the high-income Z1 exhibits a higher HDR, reflecting the fact that wealthy households are more apt to dislocate because they are less tolerant to building damages and are more likely to have the necessary resources for relocation (Peacock et al., 2008).

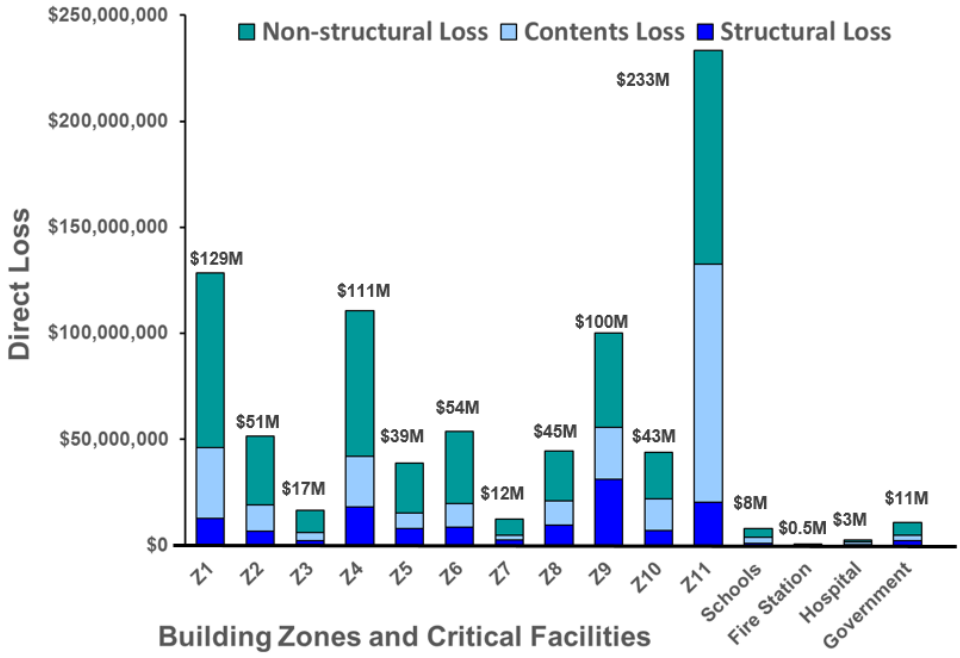


(a) Expected direct loss

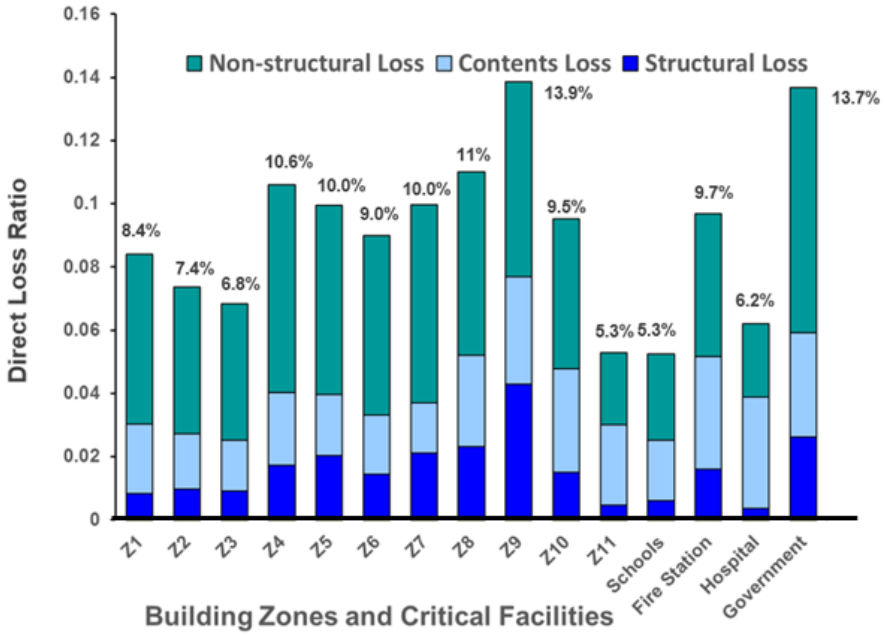


(b) Expected direct loss ratio

Figure 6-2. (a) Expected direct loss and (b) expected direct loss ratio for each building in Centerville

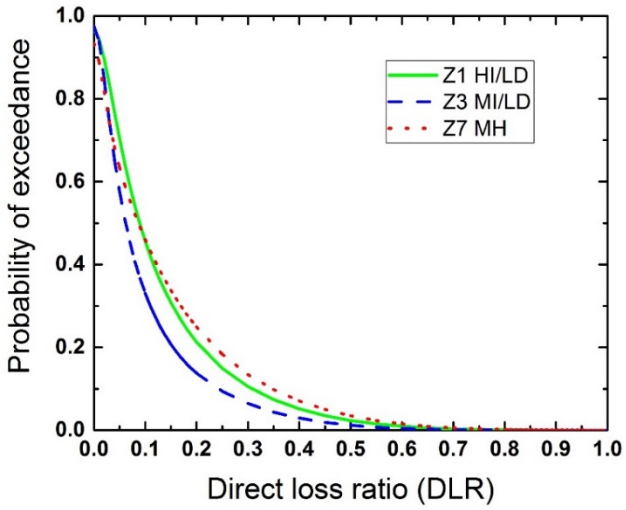


(a) Expected direct loss

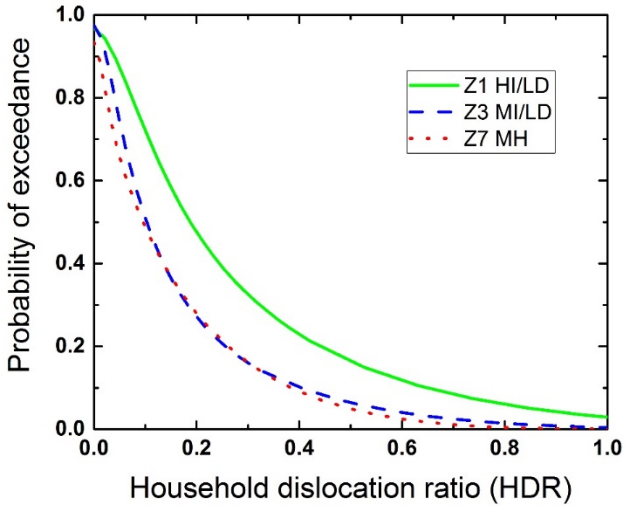


(b) Expected direct loss ratio (DLR)

Figure 6-3. (a) Expected direct loss and (b) expected loss ratio for each building zone and critical facility in Centerville



(a) Direct loss ratio (DLR)



(b) Household dislocation ratio (HDR)

Figure 6-4. Probability of exceeding (a) Direct Loss Ratio (DLR) and (b) Household Dislocation Ratio (HDR), for Centerville Zones 1, 3 and 7 for the Mw7.8 earthquake

6.1.4 Building-Level and Portfolio-Level Functionality Loss

The functionality recovery of residential building portfolio in Centerville is investigated following a M_w 7.8 earthquake with an epicenter located 45 kilometers northeast of Centerville[5]. Due to the lack of utility data for lifeline system performance assessment, it's assumed, for simplicity, that 30% residential buildings in Centerville have no access to full utility service (i.e. $FU^{0,n} = 0$), and of which 20% are provided with baseline utility to support temporary housing function (i.e. $BU^{0,n} = 1$). This assumption implies that the correlation between building damage and utility disruption, originated from the common hazard source they subject to, is neglected. The pre-recovery functionality states of individual buildings within the residential building portfolio are probabilistic due to the many sources of uncertainties associated with hazard demand and structural response; accordingly, each building's initial functionality state probability vector, $\boldsymbol{\pi}(t_0)$, is estimated using a damage-to-functionality mapping approach proposed in Section 4.1.4.1and quantified through employing a multi-layer MCS (one layer for modeling hazard intensity $\boldsymbol{IM}$ and the other for modeling building damage $\boldsymbol{DS}$ conditional on $\boldsymbol{IM}$) .

The spatial variations with respect to the mean damage states of structural components, nonstructural drift-sensitive and nonstructural acceleration-sensitive components are shown Figure 6-5(a), (b) and (c). In the figures, it is evident that buildings in the northeast area of the Centerville community (which are mostly medium-income and low-income zones) in average suffer more damage than that of the

[5] The scenario earthquake is different from the one examined in the loss estimation in Section 6.2. This scenario earthquake is chosen such that the recovery patterns of the Centerville building portfolio is closer to the cases in reality.

southwest area (which are high-income zones). The spatial variation in buildings' initial functionality states at t_0 is shown in Figure 6-5(d). The PMF of the initial functionality state for each individual building, obtained by Eqs. (4-10)-(4-11), is illustrated in Figure 6-6(a), using W2 in Zone 4 as an example. Further, by aggregating the individual buildings' initial functionality states to the portfolio level, the Centerville portfolio recovery index at time t_0, i.e., $PRI(t_0)$, defined as the percentage of buildings in the portfolio that falls in each of the five functionality states prior to restoration in Eq. (5-14), is derived and shown in Figure 6-6(b).

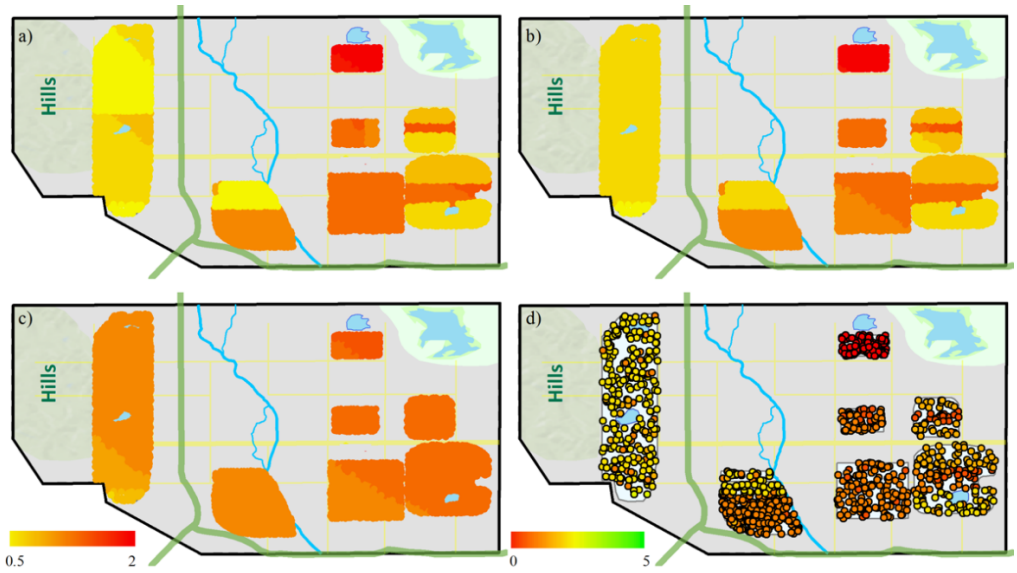


Figure 6-5. Spatial variation in the mean damage state of (a) structural components (SD), (b) non-structural drift-sensitive (ND), (c) acceleration-sensitive components (NA), and (d) the mean initial functionality state at $\boldsymbol{t_0}$.

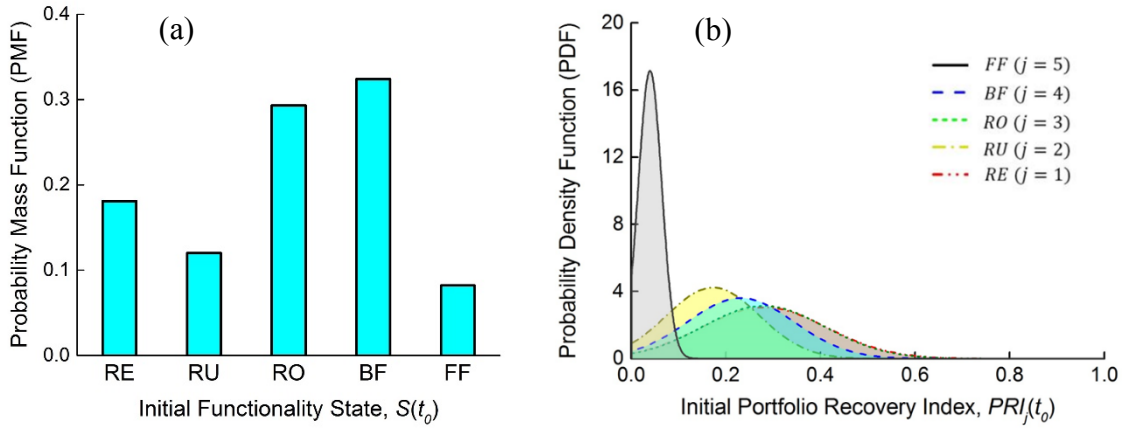


Figure 6-6. Probability assessment of (a) building-level pre-repair functionality state PMF, $\boldsymbol{\pi^n(t_0)}$, (illustrated using W2 in Zone 4); and (b) portfolio-level pre-recovery functionality index, $\boldsymbol{PRI_j(t_0)}$.

6.1.5 Building-Level and Portfolio-Level Functionality Recovery

6.1.5.1 Building-level Restoration

The discrete-state CTMC, $S^n(t)$, representing the restoration process of an individual building n, is characterized by the five building functionality states, the building's initial functionality state probabilities $\boldsymbol{\pi}^n(t_0)$ and its transition probability matrix $\boldsymbol{TPM}^n(t)$. The mathematical formulation of $S^n(t)$ presented in Section 5.2.1 requires the determination of $\boldsymbol{TPM}^n(t)$; the elements of $\boldsymbol{TPM}^n(t)$, $p_{i,j}^n(t)$, are calculated using the statistics of delay time (T_{Delay}^n) , repair time (T_{Repair}^n) and the time to resume utility supplies ($T_{Utility}^n$). In the Centerville analysis, data in Table 6-10 and Table 6-11 is synthesized from the information provided in Almufti & Willford (2013) and HAZUS-MH (FEMA/NIBS, 2003), for T_{Delay}^n and T_{Repair}^n, respectively. For $T_{Utility}^n$, it is assumed that it takes buildings having no utility service at t_0 (i. e. $BU^{0,n} = 0$; $FU^{0,n} = 0$) 3 weeks on average to regain baseline utility service (i. e. $BU^{t>3weeks,n} = 1$)

and 15 weeks to regain full utility service (i. e. $FU^{t>15weeks,n} = 1$); the coefficient of variation (C.O.V) of $T^n_{Utility}$ is assumed 0.7 (Almufti & Willford, 2013).

It is noteworthy such databases are community-specific, and should be collected and maintained by communities themselves to support their own resilience planning activities. The social-economic characteristics of a community that affect its building portfolio recovery are reflected and categorized in the 2nd column of Table 6-10, as well as in Table 6-12, which was constructed with the assistance of the social science team of the CRCRP. In particular, the time required to secure finance, $T^n_{FINA,i}$, (Table 6-10) is dependent on the financing resources available to homeowners (Table 6-12). In the United States, private insurance is the primary source for post-hazard event building repair and reconstruction (Comerio, 1998; Peacock, 1997), which may be included in a homeowner's policy, often with an additional premium. However, the percentage of residential recovery financed by private insurance varies considerably from one community to another and across different hazard types. Public funding from federal and state governments, as well as from non-profit organizations, is another major resource for community recovery, including assistance from the Federal Emergency Management Agency, low-interest loans from the Small Business Administration, funding from the Department of Housing and Urban Development. However, certain populations, often low-income and racial/ethnic minority homeowners, have limited access to such public aid programs due to their inability to repay even subsidized loans, leading to delays in repair or reconstruction of their damaged properties (Quarantelli, 1982; Bolin, 1985). For those groups, selling belongings, reconstructing household budgets or shrinking discretionary expenses, and loans from friends or relatives may

become the only options for financing repair (Bolin & Bolton, 1986). For Centerville analysis, it is assumed that 3% (0.6%, 0.3%, 0.9% and 1.2%, respectively, in zones Z3, Z5, Z6, and Z7) of damaged buildings will not be restored at all due to population outmigration following the earthquake event. The CRCRP is in the process of collecting data such as that appearing in Table 6-10, Table 6-11, and Table 6-12 through post-disaster field investigations to support future community resilience-related research. As risk-informed community resilience planning takes hold across the nation, many communities will start to collect and maintain such databases to support their own planning activities and day-to-day risk management decisions.

Figure 6-7 illustrates (a) the conditional mean restoration process as well as (b) the *BRF* [presenting the probability of a building achieving or exceeding a predefined functionality state S_j at any post-event time t as defined in Eq. (5-8)] of any building type in Centerville, using W2 buildings in Zone 4 as an example.

Table 6-10. Statistics of Delay Time [Data source: REDi™ framework (Almufti & Willford, 2013)]

Delay Phases , $T^n_{Delay,i}$ ~ Lognormal(θ, β) (Unit: weeks)				
Sequence	**Delay Time Components**	**Building specific conditions**	**Median (θ)**	**C.O.V (β)**
Delay Phase 1	Inspection ($T^n_{INSP,i}$)	slight	0	0
		above slight	5	0.54
Delay Phase 2	Engineering mobilization & Review/Re-design ($T^n_{ENGM,i}$)	slight	6	0.4
		moderate/extensive	12	0.4
		complete	50	0.32
	Financing ($T^n_{FINA,i}$)	insurance	6	1.11
		private loans	15	0.68
		SBA-backed loans	48	0.57
		Not cover	48	0.65
	Contractor mobilization and Bid process ($T^n_{CONM,i}$)	slight	7	0.6
		above slight	19	0.38
Delay Phase 3	Permitting ($T^n_{PERM,i}$)	slight	1	0.86
		above slight	8	0.32

Table 6-11. Statistics of building Repair Time with respect to repair classes (RCs) [synthesized from HAZUS-MH (FEMA/NIBS, 2003) database]

Repair time $T^n_{Repair,RCi}$ ~Lognormal $((\theta, \beta))$ (Unit: weeks)				
Sequence	**Item**	**Occupancy**	**Median (θ)**	**C.O.V (β)**
Repair class1 ($T^n_{Repair,RC1}$)	Heavily damaged structural and nonstructural components threaten life-safety	Single family	6	0.4
		Multiple family	8	0.4
		Mobile homes	2	0.4
Repair class2 ($T^n_{Repair,RC2}$)	Moderately to heavily damaged nonstructural components not threaten life-safety	Single family	6	0.4
		Multiple family	8	0.4
		Mobile homes	2	0.4
Repair class3 ($T^n_{Repair,RC3}$)	minor damage to structural components; minor to moderate damage to nonstructural components	Single family	11	0.4
		Multiple family	15	0.4
		Mobile homes	3.5	0.4
Repair class4 $T^n_{Repair,RC4}$	Minor cosmetic damage to structural and non-structural component	Single family	0.5	0.4
		Multiple family	0.5	0.4
		Mobile homes	0.5	0.4

Table 6-12. Financing resources for Centerville buildings restoration

Zone	Insurance	SBA-backed Loans	Private loan	Savings (personal resources)	Others
Z1(HI)	60%	5%	10%	25%	0%
Z2(MI)	50%	10%	30%	10%	0%
Z3(MI)	10%	10%	10%	5%	65%
Z4(MI)	30%	15%	30%	0	25%
Z5 (LI)	25%	30%	10%	0	35%
Z6 (LI)	25%	30%	10%	0	35%
Z7 (MH)	5%	5%	0	0	90%

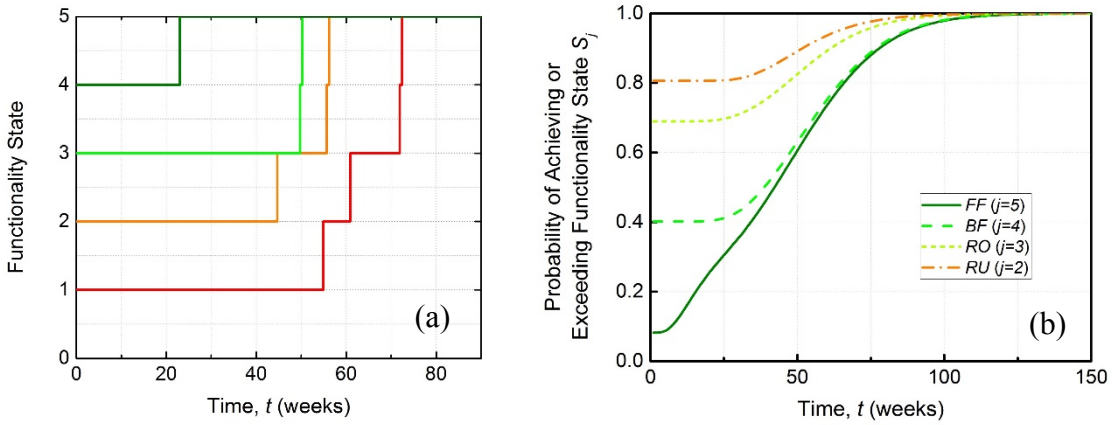


Figure 6-7. Illustration of building-level restoration: (a) conditional mean restoration process and (b) the building restoration function, BRF (both illustrated using W2 building in Zone 4 as an example).

6.1.5.2 Portfolio-level Recovery

The building-level restoration processes, $S^n(t)$, are aggregated, temporally and spatially, to obtain the portfolio-level recovery trajectory $PRI_j(t)$, and the portfolio recovery time $PRT_{FF,95\%}$, as defined in Section 5.2.2.

The mean values of $PRI_j(t), j$ = *RE, RU, RO, BF, FF*, are shown in Figure 6-8; the curve associated with *FF*, i.e. $PRI_{FF}(t)$, is the mean portfolio recovery trajectory. The time required for 95% of the building portfolio to achieve the *FF* state (i.e. $PRI_{FF}(t) = 95\%$) is defined as the portfolio recovery time and is denoted as $PRT_{FF,95\%}$; the PDF of $PRT_{FF,95\%}$ is also illustrated in this figure. Figure 6-8 indicates that the mean portfolio recovery time for Centerville is approximately 160 weeks (approximately 3 years). The reason that the mean portfolio recovery trajectory PRI_{FF} does not converge to 1.0 is that we assumed 3% housing units in Centerville are not restored due to possible population outmigration as discussed previously.

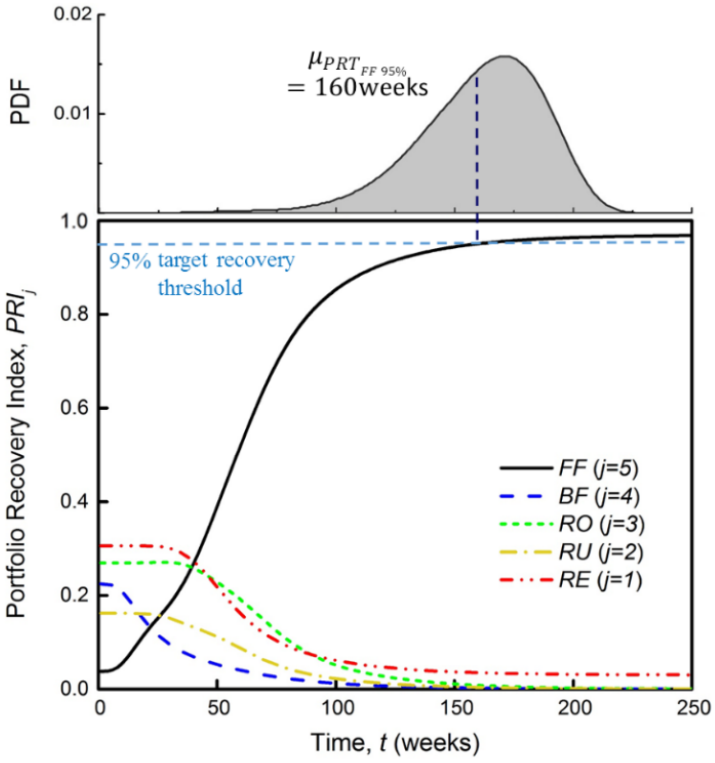


Figure 6-8. Mean portfolio recovery trajectory and recovery time

Furthermore, the uncertainty associated with the mean recovery trajectory is shown in Figure 6-9(a), indicating significant variation in portfolio recovery, especially in the early phase, which is due to the uncertainties and spatial correlations in initial functionality states mapped from the community-wide hazard-induced damages and uncertainties in delay time and reconstruction time during building restorations. The mean recovery trajectories for each of the residential zones (Z1-Z7) in Centerville, shown in Figure 6-9 (b), depict the different recovery patterns for different population groups: high income residential zones (Z1 and Z2) recover much faster than low income zones (Z6, and Z7). Houses in Z1 and Z2 are better constructed and experience less damage; moreover, higher-income households in Z1 and Z2 are likely to secure the funding for housing repair more quickly than the households in other zones.

Figure 6-10 depicts the spatial variation in mean building functionality states in Centerville at four different points in time during recovery. Notable disparities are observed, reflecting differences in hazard-induced damages and recovery capacities, both underlined by the social and economic disparities among different residential zones.

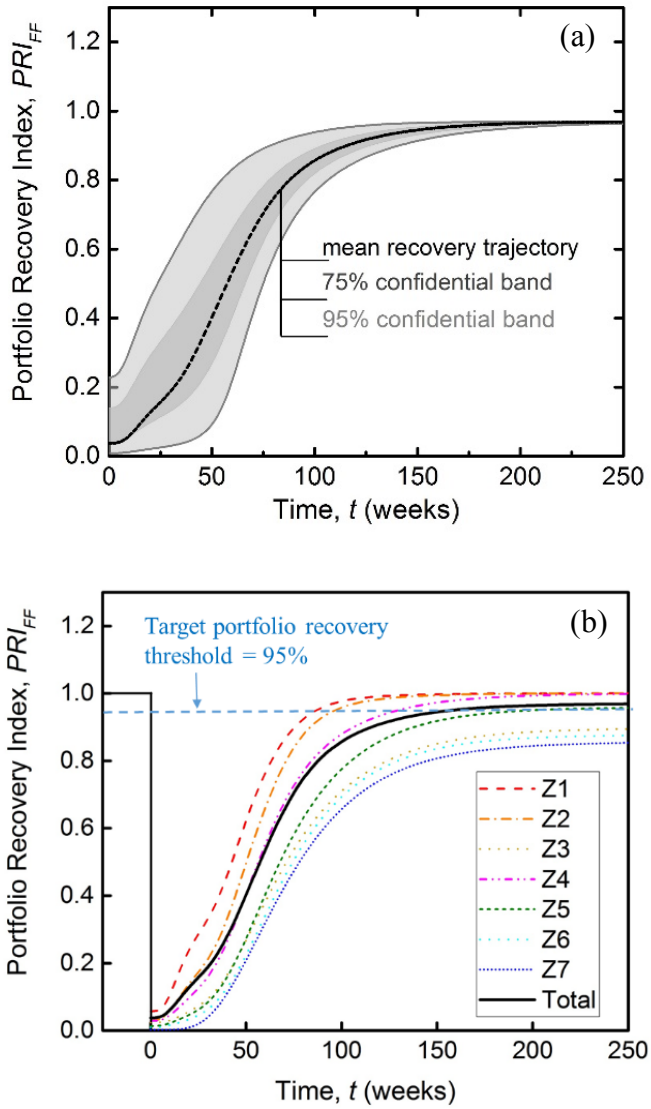


Figure 6-9. An illustration of (a) uncertainty in the portfolio recovery trajectory; and (b) the mean recovery trajectory for each of the seven residential zones (Zone1-Zone7)



Figure 6-10. Spatial variation of functionality recovery at a) $\boldsymbol{t_0 = 0}$; b) 30 weeks; c) 60 weeks; and d) 90 weeks following the hazard occurrence.

6.1.6 Sensitivity Study

The "What-if" scenario analysis is performed to the pre-disaster mitigation of Centerville residential building portfolio, to look at how the projected recovery trajectory and time might change if pre-hazard mitigation actions had taken place. Building retrofit has long been regarded as one of the most cost-effective engineering mitigation strategies to improve community resilience against natural hazards. In addition, well-designed policy incentives that stimulate builders, developers, or property owners to engage in practices that are consistent with community-level objectives with respect to hazard mitigation are often regarded as effective non-engineering risk mitigation strategies (Holmes, 2016). Accordingly, two pre-hazard mitigation scenarios are considered below, to investigate how these scenarios will affect the BPRM-projected Centerville recovery.

- Case 1- A community-wide *residential building retrofit program* was conducted prior to the M_w 7.8 earthquake to upgrade all buildings in Centerville that were built prior to 1980 (Table 6-1) to a current seismic design level, represented by shifting the fragilities of these buildings to a target level that represents current seismic design practice (Bruneau & Reinhorn, 2007).
- Case 2 – Community-wide *insurance incentives* were introduced in Centerville prior to the M_w7.8 earthquake, which caused more homeowners to purchase earthquake insurance and led to the updated financing resources for post-earthquake recovery. The redistribution of financing resources for Centerville building repair/reconstruction after applying the insurance incentives is demonstrated in Table 6-13. A comparison between the past and updated recovery resources is shown in Figure 6-11, indicating 50% of housing reconstruction funds now coming from insurances as opposed to 38% in the past.

Figure 6-12 plots the Centerville portfolio recovery trajectories when the above pre-hazard mitigation scenarios are implemented. There are two major observations: (1) retrofitting buildings (Case 1) results in less damage and therefore less functionality loss at the pre-recovery stage ($t = 0$), leading to smaller delays and repair/reconstruction times during building restoration. Consequently, the overall mean portfolio recovery time for Case 1 is reduced significantly to 97 weeks from the 160 weeks without pre-hazard retrofitting. (2) The Centerville portfolio with the updated makeup of recovery resources stimulated by insurance incentives recovers 51 weeks faster (with a mean of 109 weeks) than the original recovery path without the pre-hazard insurance incentives,

indicating that community recovery can be influenced significantly and positively by implementing non-engineering strategies.

Table 6-13. Financing resources for Centerville buildings restoration after applying insurance incentives

Zone	Issuance	SBA-backed Loans	Private loan	Savings (personal resources)	Others
Z1(HI)	70%	0%	5%	25%	0%
Z2(MI)	65%	10%	15%	10%	0%
Z3(MI Rental)	30%	10%	10%	5%	45%
Z4(MI)	45%	15%	30%	0	10%
Z5 (LI)	35%	30%	10%	0	25%
Z6 (LI)	35%	30%	10%	0	25%
Z7 (MH)	15%	5%	0	0	80%

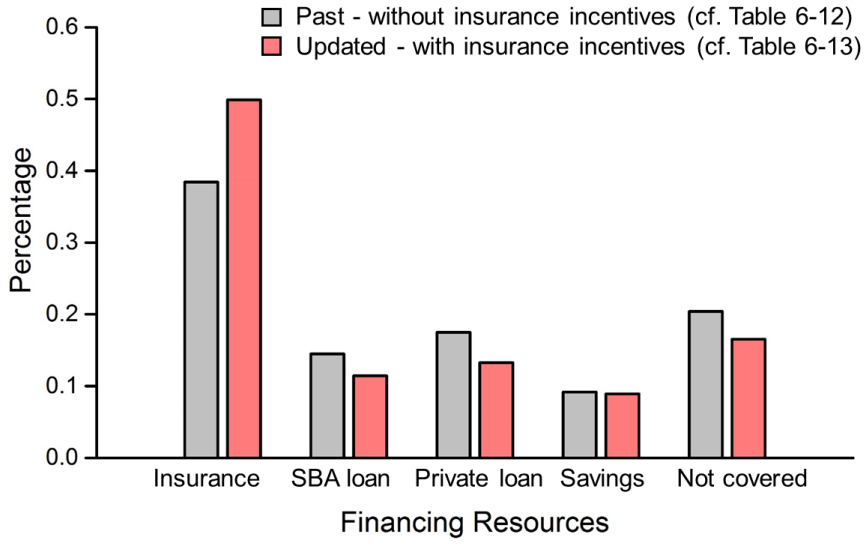


Figure 6-11. Comparison between recovery resources with and without insurance incentive

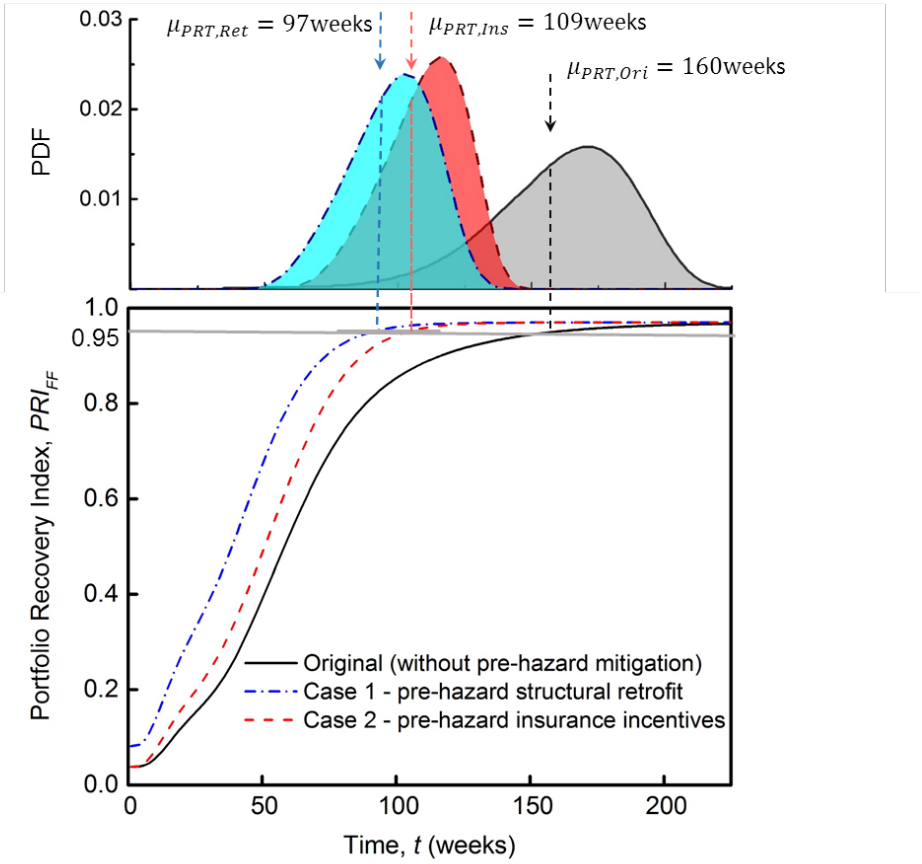


Figure 6-12. Updated Centerville portfolio recovery trajectory and recovery time respectively for Case 1 and Case 2

6.2 Shelby County Building Portfolio Analysis

6.2.1 Shelby Building Portfolio Characteristics

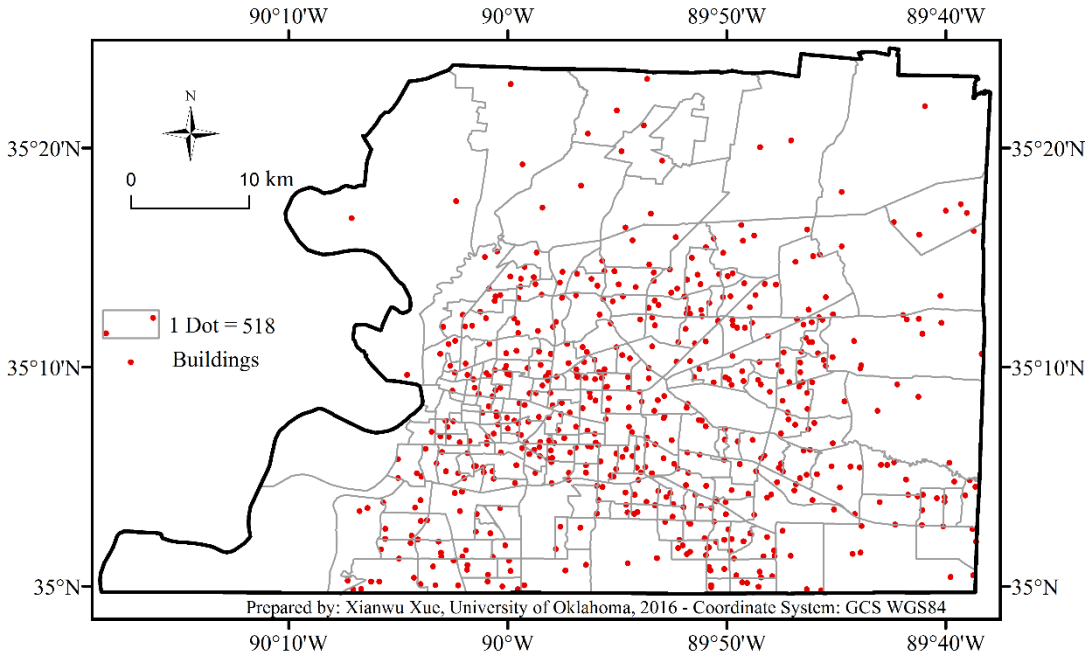
In this section, the proposed BPRM is further applied to a real world case study − the residential building portfolio (RBP) in Shelby County, TN for a likely scenario earthquake. The RBP accounts for approximately 90% of the Shelby building inventory (which consists of nearly 300,000 buildings) and is distributed spatially across 221 census tracts. Similar to most small and midsized communities in the U.S., the RBP in Shelby consists mainly of wood frames. Table 6-14 summarizes the Shelby RBP by structural types and seismic design code levels, which are consistent with those defined

in HAZUS (FEMA/NIBS, 2003). In particular, the W1 Type wood buildings designed by "low" seismic code (FEMA/NIBS, 2003) account for 93% of the RBP in Shelby. Fragility functions of these building types are adopted from HAZUS-MH for the damage evaluation. Figure 6-13(a) shows the 221 census tracts and the associated RBP spatial distribution.

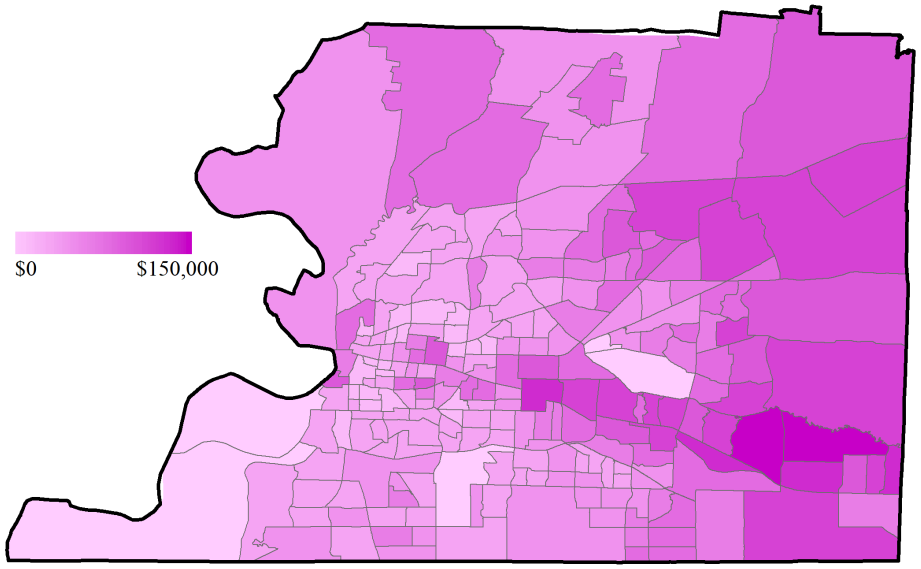
Table 6-14. Residential building portfolio by structural type and seismic design code [Data Source: MAEViz (Steelman et al., 2007)]

Str_ type*	Pre code	Low code	Moderate code	High code	Total
C1L	6	21	2	0	29
C1M	4	1	1	0	6
C2H	4	17	8	0	29
C2L	1	1	0	0	2
C2M	0	1	2	0	3
MH	4	32	6	1	43
PC1	0	13	0	1	14
RM1L	0	0	1	0	1
S1H	7	12	6	1	26
S1L	3	286	80	54	423
S1M	0	11	38	25	74
S3	1	4	6	23	34
URML	4,042	3,338	0	0	7,380
URMM	5	0	0	0	5
W1	0	267,958	0	0	267,958
W2	185	4719	7,166	0	12,070
Total	4,262	276,414	7,316	105	288,097

*Description of the structural type: C1—concrete moment frame; C2—concrete shear walls; MH—mobile homes; PC1—precast concrete tilt-Up walls; RM1—reinforced masonry bearing walls with wood or metal deck diaphragms; S1—steel moment frame; S3—steel light frame; URM—unreinforced masonry bearing walls; W1—wood, light frame; W2—wood, greater than 5,000 Square Feet. The character following the abbreviation describing structural type, if present, represents building height class: L—low, M—medium, or H—high.



(a) Residential building portfolio (RBP) in Shelby



(b) Annual household income in Shelby

Figure 6-13. Distribution of (a) the residential buildings in census tracts of Shelby County (Data source: MAEViz, Steelman et al., 2007); (b) annual household income in 2015 inflation-adjusted dollars (Data source: https://censusreporter.org/profiles/05000 US47157-shelby-county-tn/)

6.2.2 Seismic Demands

Significant earthquakes in Shelby are likely to initiate from the New Madrid seismic zone (NMSZ), which consists of three fault segments (New Madrid North, Reelfoot, and Cottonwood Grove). The buildings in Shelby are subjected to a scenario earthquake with M_w=7.7 and an epicenter located at 35.3N and 90.3W, which is one of the most probable extreme level scenarios with a 2475-year return period based on the disaggregation analysis by United States Geological Survey (USGS: https://earthquake.usgs.gov/hazards/hazmaps/). Detailed information on soil condition at building sites is unavailable, and the soil is assumed to be Category D over the entire region (Building Seismic Safety Council, 2003). The Atkinson and Boore (1995) attenuation relationship is used to calculate the ground motion intensity (in terms of spectral acceleration) at the building site, as well as the ground motion intensity (in terms of PGA shown in Figure 6-14 and PGV) for both engineered facilities and distributed line segments. The standard deviation used for seismic intensity is 0.32. The spatial correlation in ground motion intensity is simulated using Wang and Takada (2005)'s model, in which the correlation distance equals to 30km.

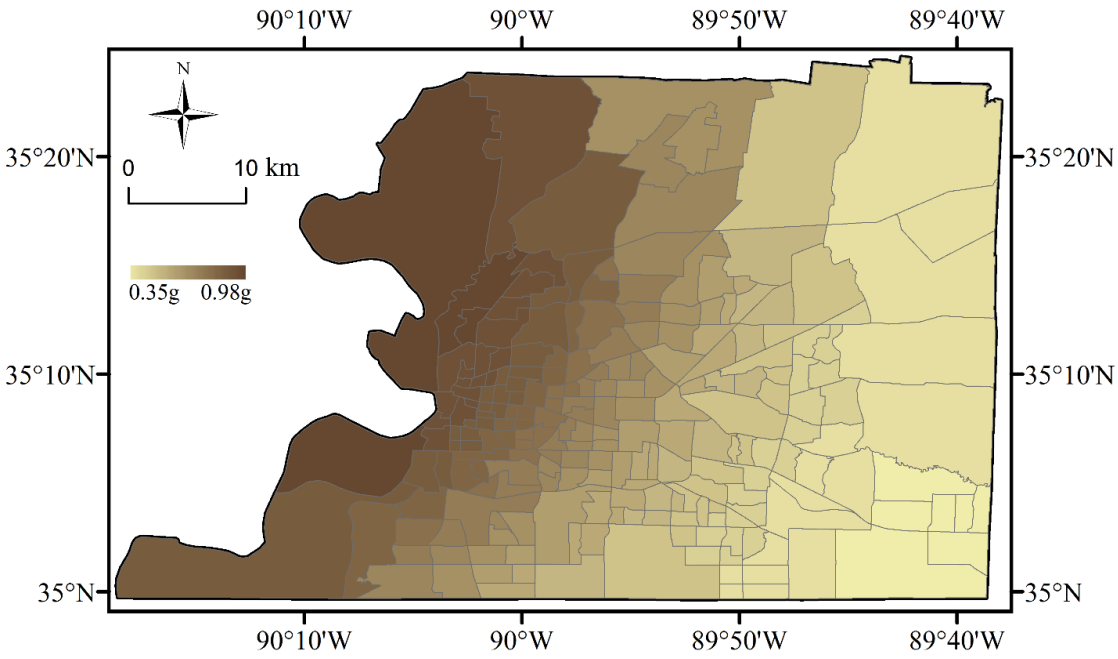


Figure 6-14. Median peak ground acceleration (PGA) with soil amplification

6.2.3 Building Portfolio Recovery

The spatial distribution of annual household income in Shelby is plotted in Figure 6-13(b). Since specific social-economic characteristics of the community required to determine building delay time, repair time and financing resources for building reconstruction are not available, we constructed Table 6-15, Table 6-16, and Table 6-17, for illustration, to support the Shelby RBP recovery simulation performed herein. The percentage of each financing resource for the Shelby RBP reconstruction is shown in Figure 6-15.

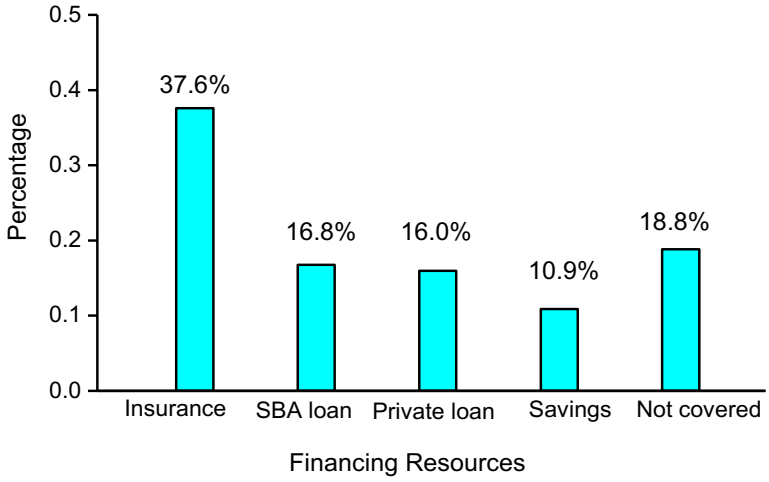


Figure 6-15. Financing resources percentage in Shelby RBP

Table 6-15. Statistics of delay time used in Shelby RBP recovery

Delay Phases, $T^n_{Delay,i}$ ~ Lognormal(θ,β) (Unit: weeks)					
Sequence	Item		Building condition	Median	c.o.v
Phase 1	**Inspection ($T^n_{INSP,i}$)**		Slight	0	0
			Moderate	1	0.54
			Extensive/Complete	4	0.54
Phase 2	**Engineering mobilization& Review/Re-Design ($T^n_{ENGM,i}$)**		Slight	0.5	0.4
			Moderate	3	0.4
			Extensive/Complete	15	0.32
	Financing ($T^n_{FINA,i}$)	Insurance	Slight	3	1.11
			Above slight	6	1.11
		private loans	slight	7	0.68
			Above slight	15	0.68
		SBA-backed loans	slight	10	0.57
			Above slight	30	0.57
		Not covered	slight	15	0.65
			Above slight	40	0.65
	Contractor Mobilization and Bid Process ($T^n_{CONM,i}$)		Slight	3	0.6
			Moderate	6	0.6
			Extensive/Complete	12	0.38
Phase 3	**Permitting ($T^n_{PERM,i}$)**		sight/moderate	0	0
			Extensive/Complete	6	0.32

Table 6-16. Statistics of repair time used in Shelby RBP recovery

Repair time, $T^n_{Repair,RCi}$ ~Lognormal $((\theta,\beta))$ (Unit: weeks)				
Sequence	**Item**	**Occupancy**	**Median (θ)**	**C.O.V (β)**
Repair class1 ($T^n_{Repair,RC1}$)	Heavily damaged structural and nonstructural components threaten life-safety	Single family	8	0.4
		Multiple family	11	0.4
		Mobile homes	3	0.4
Repair class2 ($T^n_{Repair,RC2}$)	Moderately to heavily damaged nonstructural components not threaten life-safety	Single family	13.5	0.4
		Multiple family	17	0.4
		Mobile homes	3.5	0.4
Repair class3 ($T^n_{Repair,RC3}$)	minor damage to structural components; minor to moderate damage to nonstructural components	Single family	1.5	0.4
		Multiple family	3	0.4
		Mobile homes	1	0.4
Repair class4 $T^n_{Repair,RC4}$	Minor cosmetic damage to structural and non-structural component	Single family	0.5	0.4
		Multiple family	1	0.4
		Mobile homes	0.5	0.4

Table 6-17. Distribution of financing resources in different income levels in Shelby

Income level	**Number of Buildings**	**Issuance**	**SBA-backed Loans**	**Private loan**	**Savings**	**Not covered**
>$150,000	24733	70%	0%	0%	30%	0%
$100,000-$150,000	32502	60%	10%	0%	30%	0%
$60,000-$100,000	56597	50%	10%	10%	25%	5%
$40,000-$60,000	46510	40%	25%	30%	0	5%
$20,000-$40,000	63909	25%	30%	30%	0	15%
$10,000-20,000	35919	20%	20%	20%	0	40%
<$10,000	27904	5%	5%	0	0	90%

The utility disruption at the initial pre-recovery stage ($FU^{0,n}$, $BU^{0,n}$) and the time required to restore utility services ($T^n_{Utility}$) are derived from an interdependent lifeline network recovery model developed by Zhang, et al. (2018), which is one of the

modules of the IN-CORE being developed in CRCRP. The recovery analysis of the utility networks from the same earthquake scenario provided the water and power availability across Shelby as a function of time following the earthquake event. Figure 6-16 shows the spatial variations of expected recovery in terms of power service, water service, and functionality of RBP in Shelby, respectively, for the first 50 days following the event. It can be visualized that at the initial pre-recovery stage (Day-0) almost all buildings in Shelby are rendered non-functional due to the lack of either water or power supplies in those regions. This phenomenon reflects the fact that the cascading effect of utility network disruption on the functionality of building portfolio can be devastating, and therefore considering dependence of buildings and utility networks during recovery modeling is significant for quantifying community resilience and implementing hazard mitigation plans. Moreover, Figure 6-16 reveals the temporal evolution of the three systems' recovery patterns at the short-term recovery phase (from Day-0 to Day-50). It is found that, at the early stage of community recovery, building's functionality is governed by the restoration of lifelines since most severely damaged buildings in this period are in the process of inspection, securing funding for repair, and obtaining permit, thus the vitalization of building functionality, despite slow, is aligned with the restoration of water and power networks.

Figure 6-17(a) shows the spatial variation and temporal evolution of the RBP functionality during a longer phase of recovery (until week-70) from the same event. After the first 50 days of recovery, utility networks have fully recovered and the functionality of RBP is now governed by the buildings' own reconstruction progress, which is in turn determined by the resourcefulness and social economic characteristics

of the community, relies on the governmental recovery programs and plans, as well as various decisions made by different public or private building owners. It can be observed that the long-term recovery pattern of the RBP in Shelby is consistent with the hazard intensity pattern as shown in Figure 6-14, as well as the distribution of annual household income displayed in Figure 6-13(b). This spatial variation in recovery speed in different income groups indeed reflects the disparities in resourcefulness and recoverability of homeowners with different social and economic status. Further, the recovery process of the RBP subjected to a less intense scenario earthquake (correspond to a 475-year return period) with M_w=7.76 and an epicenter located at 35.9N and 90.8W is shown in Figure 6-17(b), indicating less functionality losses and more speedy recovery when compared with the damage and recovery in Figure 6-17(a) due to a more intense event. Figure 6-18 shows the overall mean recovery trajectory of RBP in Shelby and it is concluded that the RBP takes around 2 years (96 weeks) to regain full functionality.

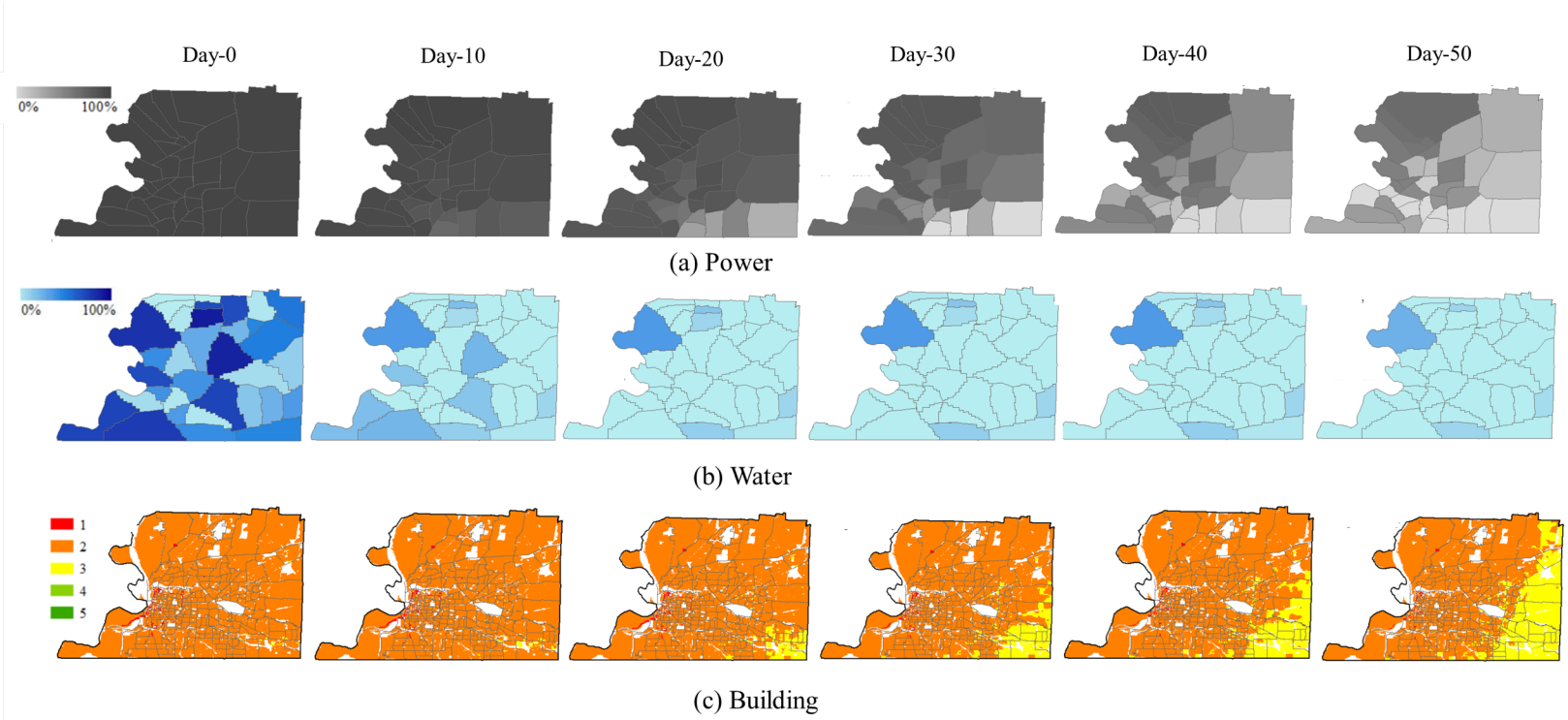
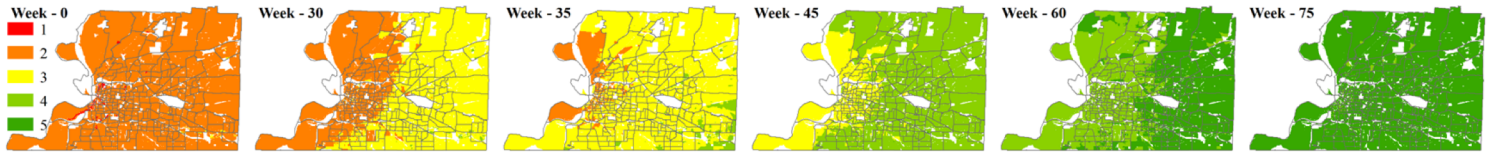
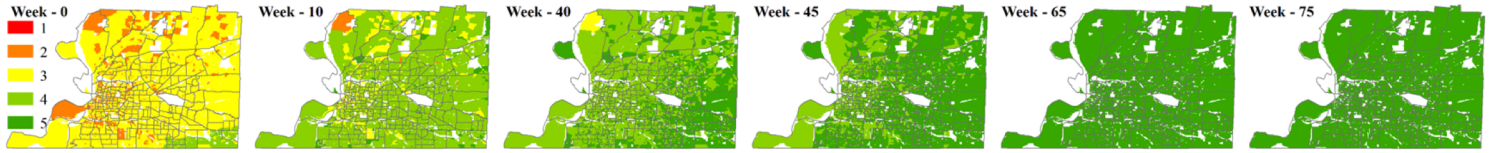


Figure 6-16. Spatial variation and temporal evolution of recovery to (a) power service (0-fully available; 100%-not available); (b) water service (0-fully available; 100%-not available); (c) building functionality (1-RE; 2-RU; 3-RO; 4-BF; 5-FF)



(a) Extreme level scenario earthquake (2475-year return period)



(b) Expected level scenario earthquake (475-year return period)

Figure 6-17. Recovery trajectory of Shelby RBP under (a) extreme level scenario earthquake; (b) expected level scenario earthquake (1-RE; 2-RU; 3-RO; 4-BF; 5-FF)

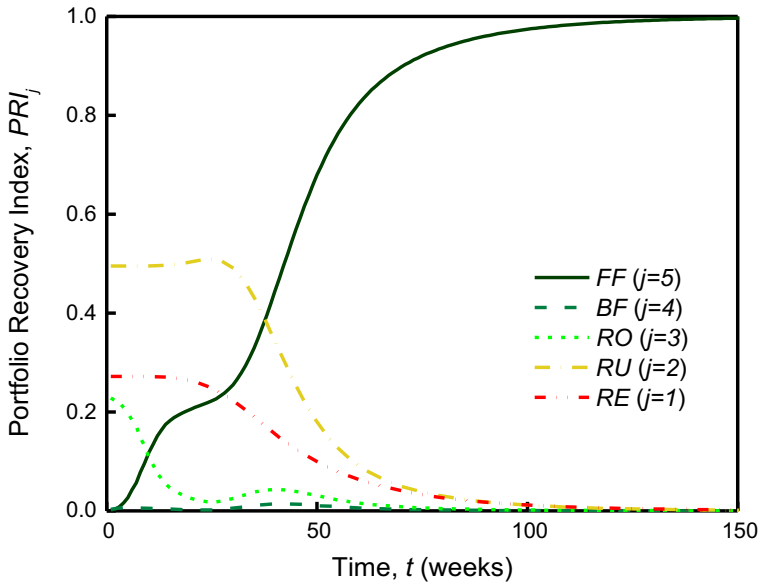


Figure 6-18. Mean recovery trajectory of RBP in Shelby

6.3 Closure

In this chapter, the BPLE and BPRM have been applied to two testbed communities – Centerville and Shelby County, TN.

First, two typical social and economic-based resilience metrics, DLR and HDR, are examined for Centerville building portfolio by utilizing the BPLE framework developed in Chapter 4. Spatial variation in the disaster losses of buildings located in different building zones is examined in the analysis, as shown in Figure 6-2. The DLR indicates that monetary loss due to nonstructural damage and content damage in the building portfolio on average is much greater than that of the structural damage in different building zones, as shown in Figure 6-3. Nevertheless, vulnerability of nonstructural components is much less understood and investigated than that of structural components.

Second, using the BPRM, the spatial variation in the recovery rapidity of different residential zones in the Centerville is projected, which reflects the disparities in resourcefulness and recoverability of homeowners with different social and economic status. Furthermore, there are significant uncertainties associated with the building portfolio recovery trajectories [as shown in Figure 6-9(a)], the neglect of which can lead to unconservative characterization of recovery for risk-informed decisions.

Third, two "what-if" scenario analyses are performed on the Centerville building portfolio to demonstrate the effectiveness of the BPRM in quantifying the impact of the pre-hazard mitigation strategies on the overall portfolio recovery outcome (trajectory and time). Such analysis can facilitate the comparison between alternative risk mitigation strategies and support risk-informed community resilience planning.

Fourth, the recovery prediction of Shelby residential building portfolio reveals that 1) the restoration of utility networks governs the short-term portfolio functionality recovery; neglecting the impact of utility on the functionality of buildings will lead to underestimation of portfolio recovery time. 2) in the long-term recovery phase, the portfolio functionality recovery process is mainly determined by the resourcefulness and social economic characteristics of the community.

Lastly, implementing BPLE and BPRM framework requires a core collection of data, as those presented in in Table 6-10, Table 6-11, and Table 6-12. As communities start to implement risk-based resilience planning, they must maintain their own databases to support resilience-related decisions regarding hazard mitigation and recovery. The case studies have provided insight for establishing community-specific databases to support their own community-specific resilience planning.

Chapter 7 Building Portfolio Decision Support (BPDS)

The ultimate purpose of developing quantitative, physics-based resilience assessment models, such as the BPLE and BPRM developed in previous chapters, is to guide and support community planning decisions toward achieving community-specific resilience goals. In this chapter, a preliminary formulation of building portfolio decision support (BPDS) is presented. The research hypotheses are that the BPLE and BPRM can indeed support the quantitative decision formulation regarding building portfolio risk mitigation and recovery strategies, and that such decisions can be optimized to enable community resilience planning efforts to be conducted in a risk-informed and cost-effective manner.

In Section 7.1, an array of possible pre-hazard community actions is identified that can effectively mitigate the risk and enhance the resilience of community building portfolios. Then with a special focus on building portfolio retrofit as one of the most effective and commonly used mitigation actions, in Section 7.2 the BPDS is formulated as a multi-objective optimization problem to support the decisions involved in designing a building portfolio retrofit plan. In Section 7.3, a case study in presented to illustrate the potential implementation of the BPDS.

7.1 Pre-Event Risk Mitigation Strategies for Building Portfolios

Effective community resilience planning should include both pre-event risk mitigation strategies aimed at enhancing community resilience and preparing community for the future hazards, and post-event response and recovery plans aimed at limiting hazard impact in a most time and resource-efficient manner. Decisions (of

building owners, policy makers and other stakeholders) regarding effective resilience planning often are desired to achieve multiple objectives and goals and, at the same time, constrained by limited time, human, and financial resources. Resilience planning for community building portfolio might include pre-event risk reduction measures (e.g. building portfolio retrofit strategies, land use regulations, etc.) and risk spreading control mechanisms (e.g. housing insurance policies, government subsidies, etc.), as well as post-event recovery actions (e.g. resource allocation, recovery prioritization and scheduling, etc.).

Pre-event hazard mitigation strategies refer to those activities and actions take place before an extreme event strikes a community with the objective of providing protections to the community if an extreme event actually occurs (Lindell et al, 2006). In the predominant literature, mitigation strategies have been classified into engineering and non-engineering solutions (Godschalk et al., 1999; Lindell et al., 2006; Peacock et al., 2011; Baxte, 2013). Engineering mitigation involves the use of engineered safety features to provide disaster protection, such as structural retrofit, and construction of levees and dams. Non-engineering mitigation refers to a broad set of mitigation s trategies, such as real estate development regulation, land use management, incentive policies, public risk awareness and risk communication. The FEMA (FEMA Training, Chapter 3: mitigation) enumerates several types of hazard mitigation strategies, as summarized in Table 7-1.

Table 7-1. Community disaster mitigation tools

Mitigation tools	Example
Hazard identification and mapping	Detailed flood maps by FEMA's National Flood Insurance Program (NFIP); earthquake maps by the U.S. Geological Survey (USGS)
Design and construction application	building codes, architecture and design criteria, and soils and landscaping considerations
Land use planning	Acquisition, easements, storm water management, annexation, environmental review, and floodplain management plans
Financial incentives	Insurance incentives; creation of special tax assessments; passage of tax increases or bonds to pay for mitigation; relocation assistance and targeting of Federal community development or renewal grant funds for mitigation
Structural controls	Levees, sea walls, bulkheads, breakwaters, groins and jetties

Mitigation strategies that are directly relevant to community building portfolio include: structural retrofit, financing incentives, land use planning, and many other alternative actions taken to reduce the building restoration time. The REDi downtime assessment methodology (Almufti & Willford, 2013) has provided several actions that private building owners can take to reduce building recovery time. For example, the building owners can either pre-arrange for a qualified professional to inspect their buildings or sign up for programs such as the Building Occupancy Resumption Program (BORP) or other equivalents to reduce time delay due to inspection (Almufti & Willford, 2013). To reduce delay time due to engineering or contract mobilization, building owners can arrange contractual agreements with engineers immediately following the hazard. A possible mitigation for reducing time to financing is to obtain a secured credit line as a contingency plan such that funds will be readily available in the event of a disaster.

Besides decisions made by private building owners, planners for community development can improve the disaster resilience of building portfolios by establishing and implementing resilience-based building design criteria; by retrofitting an existing building portfolio to enhance its robustness; or even indirectly by reducing the vulnerability of the lifeline systems in the community, the disruption of which can disable functionality of buildings and produce cascading effect throughout a building's restoration phase.

While extensive studies on disaster research and risk management have examined past disaster events as case studies, effective and intelligent decision framework to guide and inform decision makers of a community toward achieving disaster resilience is scarcely explored. The reason is twofold: (1) many quantitative assessment models that underline risk-informed decision for community resilience planning are yet to be developed. For instance, the post-disaster recovery of a community is complex and highly uncertain; yet a simulation-based recovery model capable of incorporating different types of hazard mitigation strategies is rare; (2) Both the process in which such decisions (mitigation strategies) are made and implemented and the regulatory and resource constrains that community decision-makers must consider are poorly understood by researchers. The situation is exacerbated by the lack of data of various kinds, ranging from physical system inventory and topology, social and economic characteristics of a community, regional human and construction resources, to regulations and policies regarding disaster mitigation.

In Section 7.2, a risk-informed decision framework is developed to obtain the optimal resilience-driven decisions in terms of building retrofit (more specifically, an

optimal portfolio retrofit plan). This study is expected to articulate the concept of risk-informed decision making in supporting community resilience planning and risk mitigation, as well as the need to develop multi-objective optimization algorithms for obtaining optimal decisions with an ultimate goal of achieve community disaster resilience.

7.2 Decision Support for Building Portfolio Retrofit Planning

7.2.1 Problem Description and Assumptions

Ideally, resilience-driven decisions should achieve targeted community-level resilience goals that reflect the preferences and risk tolerance of the community as a whole, and at the same time produce desired outcomes (or minimize undesired outcomes) pursuit by different stakeholders of the community, which is often fulfilled by solving a multi-objective decision problem.

To formulate the multi-objective decision problem, the decision makers should first identify possible mitigation strategies that can be fulfilled pre- and post-disaster, depending on the hazard event of interest, geographic location and topology of the community, resource accessibility, regional economy, local regulations or policies, etc. Structural retrofit, acknowledged as one of the most effective means to address risk, is chosen herein as a preliminary study for developing risk-informed decision framework[6]. Although building retrofit decisions usually are made by individual building owners,

[6] In reality, multiple hazard mitigation strategies are often taken into account and the tradeoff among alternative risk mitigation strategies can be investigated through "what-if" scenario analysis (as demonstrated in Section 6.1.6), cost-benefit analysis, or more advanced multi-objective optimization algorithms.

government agencies and the insurance industry have a significant role to play in designing and employing incentives and effective risk mitigation policies such as government subsidies, tax incentives or insurance products, to stimulate stakeholder actions towards achieving the desired level of community resilience. For example, the Mandatory Soft Story Retrofit Program (MSSP) in San Francisco, CA was created in 2013 as a multi-year community-based effort by the Earthquake Safety Implementation Program and enforced by the Department of Building Inspection to ensure the safety and resilience of San Francisco's housing stock through the retrofit of older, wood-framed, multi-family buildings (Porter & Cobeen, 2012). An effective community resilience-based portfolio retrofit plan should specify: 1) the overall portfolio resilience objective that the retrofit plan is trying to achieve; 2) the minimum number of buildings that must be retrofitted; 3) the target building performance level for retrofitting; and 4) the overall cost associated with the retrofit plan. These four aspects are necessary for government agencies to design effective community risk mitigation policies.

A community building portfolio can be modeled as a series of development areas or "zones" that are related to the structural characteristics of the dominant buildings found in each zone (Mahsuli & Haukaas, 2013), as those in Centerville Community (cf. Figure 6-1). It is defined that a community has m zones, $I = \{n_1, n_2, \dots, n_m\}$, where n_i is the total number of buildings in zone $i \in [1, m]$ and $\sum_{i=1}^{m} n_i = N$. For buildings in each of the *m* zones, the building's pre-retrofit design code level is $\beta_i, i \in [1, m]$. Further, define a building portfolio retrofit plan decision variable $(\boldsymbol{z}, \boldsymbol{\beta^T}) = \{(z_1, \beta_1^T), (z_2, \beta_2^T), \dots, (z_m, \beta_m^T)\}$, where z_i is the number of buildings to be retrofitted in zone $i \in [1, m]$; β_i^T is the target pre-event retrofit level

(which is discrete and may use those existing code levels in the standard or a new designed code level) for zone $i \in [1, m]$. Under these assumptions, the pre-disaster building portfolio retrofit plan can be formulated as a multi-objective optimization problem, in which a set of near-optimal retrofit plans ($\boldsymbol{z}, \boldsymbol{\beta^T}$) is determinated, which achieves a prescribed target *building portfolio performance goal* (detailed in section 7.2.2) with minimum *portfolio retrofit cost* (PRC) and fastest expected *portfolio recovery time* (PRT) given the occurrence of the considered hazard scenario.

7.2.2 Building Portfolio Performance Goal

Fulfilling building portfolio performance goals serves as one of the constraints of the current risk-informed decision framework. Community planning for resilience has identified a set of community-level goals to instruct stakeholders of the community in terms of developing and prioritizing strategies in order to achieve the stipulated goals, such as minimizing functionality losses and recovery time (NIST, 2015). Such community goals are usually high levels of performance that community is desired to achieve; the gap between the desired community performance and anticipated community performance needs to be identified while effective risk mitigation strategies and optimal mitigation plans or policies are expected to fill this gap.

Considering the uncertainties associated with the performance of an earthquake-stricken building portfolio of interest, the *building portfolio performance goal* to be achieved by planners responsible for community development can be expressed in the following form:

$$Prob\left(Z < G|S_{EQ}\right) = \alpha \tag{7-1}$$

in which Z is the portfolio functionality metric of interest; G is the stipulated building portfolio performance goal while α is the confidence level for the probable event. The value of G and α are set in pairs to represent the building portfolio performance goal, which reflects the preferences and risk tolerance of the community.

For building retrofit plan, we use *portfolio robustness goal* (i.e., an acceptable level of functionality loss due to immediate impact of a hazard) as the performance goal, as it is the most direct and sensitive measure of the collective performance of individual buildings, and is not complicated by any social-economic characteristics of the community. For example, considering a M_w 7.5 earthquake, a portfolio robustness goal for the residential building portfolio can be "less than 10% of housing units are in the functionality states of *RE* and *RU* immediately following the hazard with a 90% confidence level". This objective to be achieved, in turn, needs the individual dwellings within the community to meet certain strength requirements, which can be fulfilled through designing optimal building portfolio retrofit plans to be formulated in the following section.

7.2.3 Formulation of Portfolio Retrofit Plan Optimization

The optimal pre-disaster portfolio retrofit plan is obtained by minimizing the total *PRC* and the expected *PRT* (as estimated by BPRM in Chapter 5) subject to the constraint imposed by the stipulated portfolio robustness goal (G, α) (as discussed in 7.2.2). The complete optimization problem formulation is summarized in Table 7-2. Local constraints 1 and 2 are dictated by the resources available to the

community and its building portfolio configuration. Multi-objective optimization problems can be solved by a number of different algorithms, including exhaustive enumeration, exact solution approaches (e.g. branching and bound), or metaheuristic techniques (e.g. genetic algorithm), depending on the characteristics of the problem (Bocchini & Frangopol, 2011; Zhang & Wang, 2016).

Table 7-2. Summary of the optimization formulation

Description	Notation
Input Parameters	Portfolio topology: $I = \{n_1, n_2, \dots, n_m\}$ Pre-retrofit building design code level: β_i, for $i \in [1, \mathrm{m}]$
Decision Variables The number of retrofitted buildings in each zone and the retrofit target	$(\boldsymbol{z}, \boldsymbol{\beta^T}) = \{(z_1, \beta_1^T), (z_2, \beta_2^T), \dots, (z_m, \beta_m^T)\}$
Global Objective 1 Minimize total retrofit cost	$\min PRC$
Global Objective 2 Minimize expected portfolio recovery time	$\min PRT$ (estimated by BPRM)
Global Constraint 1 Portfolio system reliability (resilience goal)	$Prob(Z < G \mid S_{EQ}) = \alpha$
Local Constraint 2 The number of retrofitted buildings in each zone cannot exceed the total number of buildings in the zone	$z_i \leq n_i$, $i \in [1, m]$

7.3 Case Study

The risk-informed decision framework developed in Section 7.2 is applied to a small existing community with two residential zones, in which community resilience under an earthquake scenario event is considered. Zone I contains 50 non-seismically designed one-story wood frames developed mainly in the 1950s, while Zone II consists of 50 seismically designed one-story wood single family dwellings developed during the 1970-1980s. For illustration, consider these 100 houses as being uniformly scattered in Zones I and II. It is further assumed that the correlations among performance of buildings (more specifically, correlation in functionality states) in the same zone is described by Eq. (4-4). For buildings located in different zones, the correlation due to common code and construction practices is weak, but the portion of the correlation that results from common hazard demand may still exist unless the considered building zones are very further apart. In this illustration, performances of buildings located in different zones are assumed to be uncorrelated, for simplicity; this assumption can be easily relaxed when analyzing realistic building portfolios. A scenario earthquake with a magnitude M_w of 7.5 and epicenter of 25 km from the center of the community is considered for this study. The ground motion attenuation proposed by Campbell (2003) is used to simulate the seismic intensity measure for each individual building within the community. Seismic fragility functions and appraised values for buildings in both Zone I and Zone II are adopted from HAZUS-MH (i.e., FEMA/NIBS, 2003 for building type W1): Zone I buildings are "pre-code" according to the HAZUS definitions ($\beta_1 = 1$), while Zone II buildings are "low-code" ($\beta_2 = 2$). The total appraised value of the 100 buildings is approximately \$15 million.

The portfolio robustness goal is defined as "the probability that less than 10% buildings in the community become unoccupiable (corresponds to *RU* and *RE*) after a particular hazard is 90%", namely:

$$Prob[PRI_1(t_0) + PRI_2(t_0) < 10\%] = 90\% \quad (7\text{-}2)$$

In Eq. (7-2), the distribution of $PRI_1(t_0) + PRI_2(t_0)$ is calculated using the PBLE, which essentially defines the relation between building portfolio performance *PRI* and individual building performance [denoted by building's code level $\beta \in (1,2,3,4)$, representing pre-code, low-code, moderate-code, and high-code level, respectively].

For simplicity, this case study has made several assumptions for the portfolio retrofit plan optimization: (1) because the portfolio investigated is hypothetical, and there is no detailed information regarding building's nonstructural components and utility availability (cf. Figure 4-2), the building performance is quantified solely by its structural capacities when calculating *PRI* using BPLE; (2) there is no information regarding the social- economic characteristics and political response of the community, the delay time is neglected and the building restoration time is equal to its repair/reconstruction time when calculating expected *PRT* using BPRM.

To investigate the gap between current performance of the building portfolio and the anticipated performance to be achieved, we define *portfolio system reliability* (*PSR*) as $PSR = Prob[PRI_1(t_0) + PRI_2(t_0) < 10\%]$. The building portfolio functionality losses calculated using BPLE reveal that the probability that no more than 10% of buildings will become unoccupiable (*RE* and *RU*) after the scenario event is

79%, i.e., $PSR = 79\%$, which is lower that the desired confidence level associated with the prescribed portfolio robustness goal ($\alpha = 90\%$). Identifying this gap is the first step in considering alternative hazard mitigation strategies (code improvements, targeting investments on rehabilitation, etc.) to meet prescribed resilience goals. Based on this assessment, a decision to seismically retrofit certain residential building structures to a higher seismic code level is implemented; the optimization process leading to the optimal seismic retrofit plan is described below.

Since both Zone I (pre-code) and Zone II (low-code) buildings can be retrofitted to either moderate-code level or high-code level, three alternative retrofit schemes[7] (RS) are considered, as summarized in Table 7-3 together with the mean retrofit cost [based on empirical recommendations from Yoshikawa and Goda (2013)] associated with each RS. The damage state probabilities with respect to the considered scenario hazard event are summarized in Table 7-4 for pre-, low-, moderate- and high code-compliant levels, respectively. Moreover, based on the mean restoration time of 2, 64, 270 and 360 days, corresponding, respectively, to slight, moderate, extensive and complete damage levels (FEMA/NIBS, 2003), the expected building restoration time with each code-compliance level is tabulated in Table 7-4.

[7] Since Zone II buildings are more vulnerable than Zone I buildings, the option of retrofitting type I building to high-code level and retrofitting type II building to moderate-code level is not considered. Therefore, the following results only consider three alternatives.

Table 7-3. Alternative portfolio retrofit schemes (RS) for Zone I and Zone II buildings

Retrofit scheme, RS (β_1^T, β_2^T)	**Target retrofit level β_1^T for Zone I (pre-code) buildings (associated mean cost/bldg.)**	**Target retrofit level β_2^T for Zone II (low-code) buildings (associated mean cost/bldg.)**
RS 1	Moderate-code ($5,500)	High-code ($6,500)
RS 2	High-code ($8,000)	High-code ($6,500)
RS 3	Moderate-code ($5,500)	Moderate-code ($4,000)

Table 7-4. Damage state probabilities for residential buildings (building type: W1) (FEMA/NIBS, 2003)

		Performance levels of existing buildings		**Candidate target levels for retrofit**	
		Zone I (Pre-code)	**Zone II (Low-code)**	**Moderate-code**	**High-code**
Damage state probability	None	0.3018	0.373	0.5301	0.5316
	slight	0.3437	0.3619	0.3426	0.3939
	moderate	0.2768	0.2213	0.1184	0.0719
	extensive	0.0663	0.0399	0.007	0.0023
	complete	0.0114	0.0039	0.0019	0.0003
Mean restoration time		**40 days**	**27 days**	**11 days**	**6 days**

Consistent with the decision framework presented in Section 7.2, a portfolio retrofit plan is sought that should fulfill the prescribed portfolio robustness goal, and at the same time minimize the total *PRC* and expected *PRT*. Because the solution space for this particular problem is limited, a naïve exhaustive enumeration method can be used to identify the optimal solutions. While both *PRC* and *PRT* can be modeled as random variables if the uncertainties in the retrofit cost and restoration time for each building are known, the optimal solution in this example is obtained by minimizing the mean of the objective functions. Figure 7-1(a), (b) and (c) illustrate the solution space for the three retrofit schemes RS1, RS2 and RS3 (Table 7-3), respectively, when the

portfolio robustness goal $PSR < \alpha$ is not yet considered as a constraint. Figure 7-1(d) displays the comparison of the optimal solution sets with respect to the three different retrofit schemes when minimizing *PRC* is considered as the dominant objective. From Figure 7-1, it is clear that: (1) larger *PRC* usually results in higher PSR and shorter expected *PRT*; and (2) with the same level of *PRC*, RS3 on average achieves higher *PSR* than the other two retrofit schemes due to the fact that, with a fixed amount of resources, the total number of buildings that can be retrofitted under RS3 is greater than that of the other two retrofit schemes. This observation reveals that for the portfolio robustness goal defined in this study, when the financial resources for seismic retrofitting are limited, retrofitting more buildings to a relatively lower performance target level is more effective than retrofitting fewer buildings to a relatively higher performance level.

Figure 7-2 shows the number of buildings that must be retrofitted in Zone I and Zone II to achieve the targeted portfolio robustness goal $\alpha = 90\%$. Note that z_1 and z_2 are negatively correlated. Moreover, considering the total number of buildings required for retrofit (i.e. z_1+z_2), RS2 requires fewer buildings on average than the other two RSs because the target performance levels for individual buildings in both Zones I and II are the highest in RS2. Figure 7-3 shows the range and median of the total number of buildings required for retrofit to achieve the target portfolio robustness goal with the three retrofit schemes. The minimum numbers of buildings required for retrofit are 43, 39 and 43 for RS1, RS2 and RS3, respectively. Such information would be useful for public policy makers who might prefer a mitigation policy in which fewer buildings are retrofitted to achieve the same resilience goal.

Figure 7-4 shows the tradeoff between the competing objectives *PRT* and *PRC* when the target portfolio robustness goal $\alpha = 90\%$ is achieved. It is obvious that the *PRT* and *PRC* are negatively correlated for all three retrofit schemes. RS3 generally is associated with lower *PRC* but longer *PRT*, while RS2 often results in higher *PRC* but shorter *PRT*. This observation is also reflected in the histograms of *PRT* and *PRC* for the three retrofit schemes. The optimal solutions (described by the Pareto front) under the competing objectives are presented with solid markers, which reveals the minimum *PRC* required to achieve the community resilience objective for a given expected *PRT*, and vice versa. For example, if the portfolio recovery time is targeted to be within 250 days, then the minimum portfolio retrofit cost is $ 0.34 million.

Table 7-5 and Table 7-6 tabulate the optimal solutions that achieve the target portfolio robustness goal $\alpha = 90\%$ with minimized *PRC* and minimized *PRT*, respectively. The following observations can be made: (1) the optimal solutions associated with minimum *PRC* as shown in Table 7-5 all require that the focus of retrofit should be buildings in Zone I regardless of the RS; (2) the optimal solutions associated with minimum *PRT* as shown in Table 7-6 all imply that the number of retrofitted buildings in Zones I and II need be balanced almost equally in order to ensure fastest post-disaster recovery.

In summary, if the targeted portfolio robustness goal is to be satisfied, the optimal portfolio retrofit plan depends on the objective of interest, which reflects the preferences of policy-makers and other stakeholder within the community. If the retrofit cost is of a compelling preference, then the optimal policy is to retrofit most of the buildings in Zone I to moderate-code level ($z_1 = 43, z_2 = 0,$ RS1 or RS3). On the

other hand, if the portfolio recovery time is of most concern, then the optimal retrofit plan is to retrofit a nearly identical number of buildings in Zones I and II to high-code level ($z_1 = z_2 = 29, \mathrm{RS2}$).

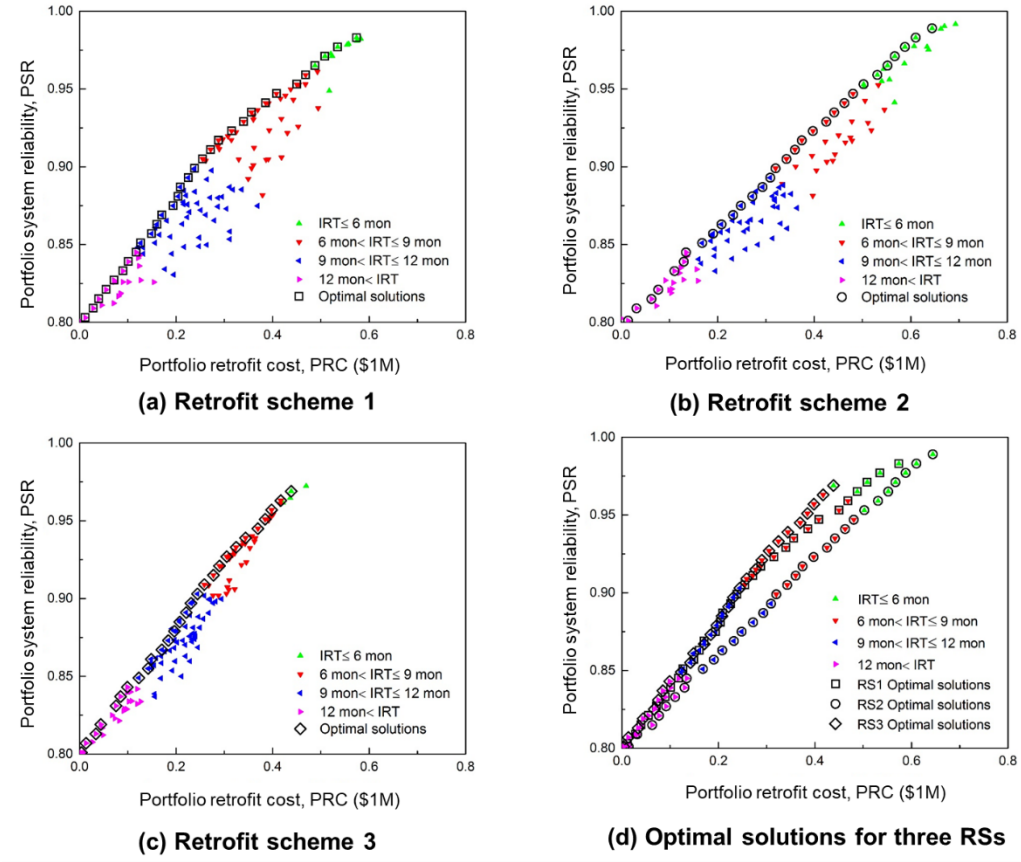


Figure 7-1. Portfolio system reliability (*PSR*) versus portfolio retrofit cost (*PRC*)

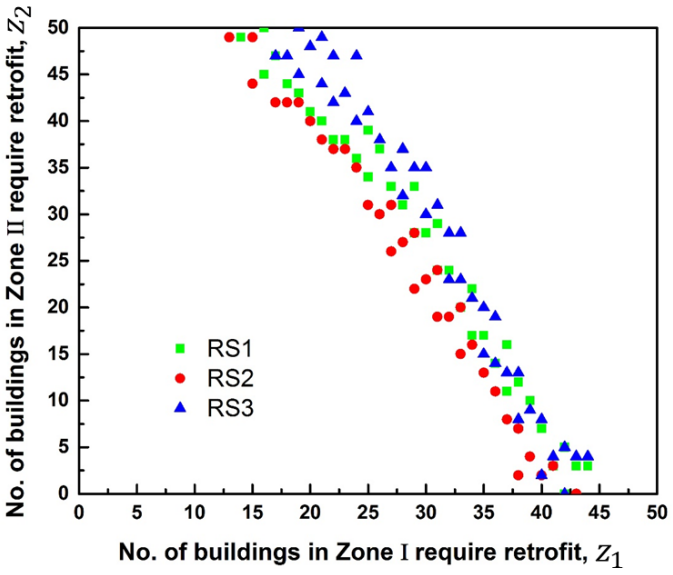


Figure 7-2. Number of buildings in Zones I (z_1) and II (z_2) that require retrofit (for target portfolio robustness goal $\boldsymbol{\alpha = 90\%}$)

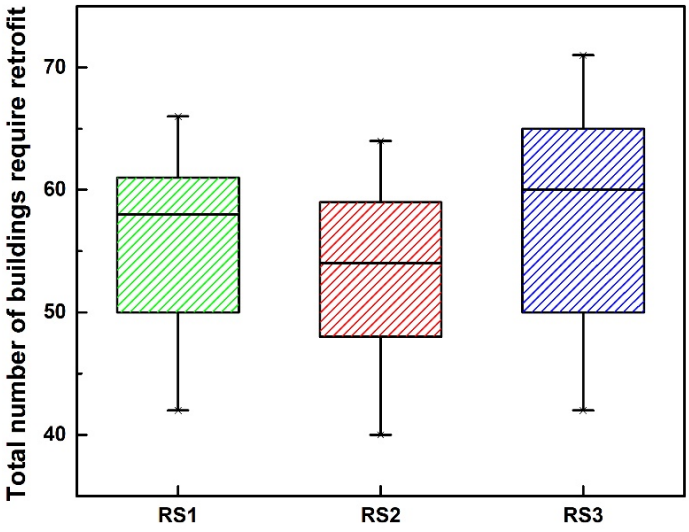


Figure 7-3. Boxplot of total number of buildings require retrofit (for target portfolio robustness goal $\boldsymbol{\alpha = 90\%}$)

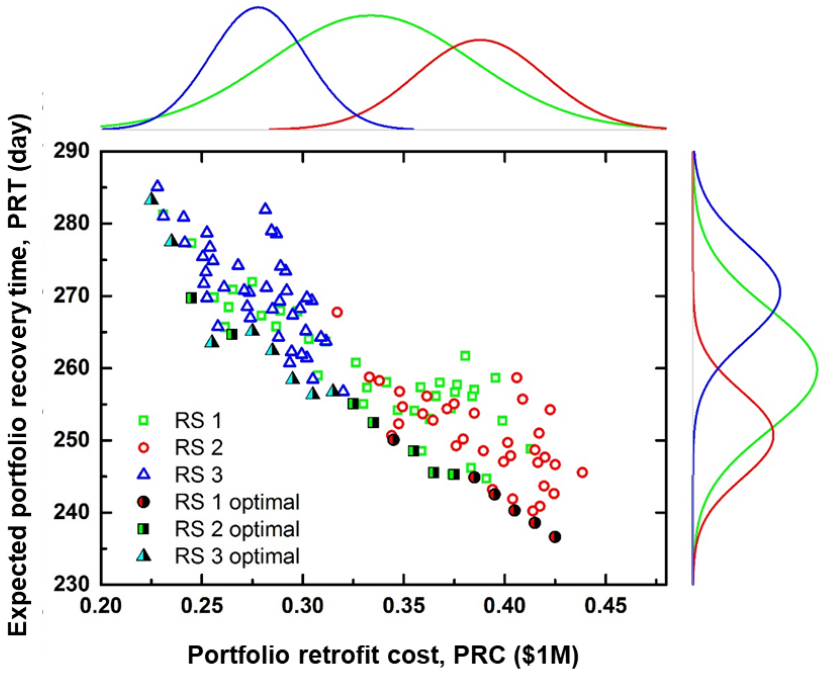


Figure 7-4. Portfolio recovery time (*PRT*) versus portfolio retrofit cost (*PRC*) (for target portfolio robustness goal $\boldsymbol{\alpha = 90\%}$)

Table 7-5. Optimal solutions to achieve the target portfolio robustness goal ($\boldsymbol{\alpha = 90\%}$) with minimized *PRC*

Retrofit scheme (Table 7-3)	No. of buildings to be retrofitted in Zone I, z_1	No. of buildings to be retrofitted in Zone II, z_2	**Minimized portfolio retrofit cost (PRC)**	Corresponding portfolio recovery time (PRT)
RS 1	43	0	**$237,000**	278 days
RS 2	40	2	**$333,000**	259 days
RS 3	43	0	**$237,000**	278 days

Table 7-6. Optimal solutions to achieve the target portfolio robustness goal ($\boldsymbol{\alpha = 90\%}$) with minimized *PRT*

Retrofit scheme (Table 7-3)	No. of buildings to be retrofitted in Zone I, z_1	No. of buildings to be retrofitted in Zone II, z_2	**Minimized portfolio recovery time (PRT)**	Corresponding portfolio retrofit cost (PRC)
RS 1	29	33	**245 days**	$374,000
RS 2	29	29	**238 days**	$421,000
RS 3	33	31	**258 days**	$303,000

7.4 Closure

In this chapter, a preliminary BPDS is presented. The purpose of this study is not yet set to develop a comprehensive decision tool for hazard mitigation and resilience planning, rather, we explore a feasibility path forward by proving the following hypotheses: 1) the BPLE and BPRM can indeed support the quantitative decision formulation regarding building portfolio risk mitigation and recovery strategies, and 2) such decisions can be optimized to enable community resilience planning efforts to be conducted in a risk-informed and cost-effective manner.

Community-scale hazard mitigation strategies for building portfolios can be largely categorized into engineering measures (such as building retrofit, elevating a building, basement protection, etc.) and non-engineering measures (financial incentives, zoning, etc.). The BPDS is formulated in this chapter for designing an effective building portfolio retrofit plan for illustration, in which the number of buildings to be retrofitted as well as the design code level for retrofitting are specified in a way to ensure the target portfolio robustness goal is achieved, and at the same time the total *PRC* and the expected *PRT* are minimized.

In the BPDS, the robustness (the constraint) and recovery (the objective) of the building portfolio under investigation are quantified using BPLE and BPRM, respectively. The BPLE and BPRM are highly quantitative, which enable the BPDS to be modeled as a rigorous multi-objective optimization problem; the BPLE and BPRM both include a comprehensive uncertainty propagation, which enables the resilience goals in the BPDS to be specified probabilistically in a risk-informed manner; and the

BPLE and BPRM are both physics-based models with a building-level modeling resolution, which enables the BPDS to support engineering mitigation decisions at building scales. It is the characteristics of the assessment models underlying a decision that ultimately determine the key characteristics of a decision model. In another word, what resilience planning decisions one trying to support determine the approach, the resolution, and the simplifications of the supporting resilience assessment models.

Chapter 8 Conclusions and Future Work

8.1 Summary

Resilience is often regarded as an attribute of communities rather than a property of individual civil infrastructure facilities. Conventional quantitative tools for building portfolio analysis have treated topologically discrete buildings independently, without considering the functional dependences among buildings of different occupancies as well as dependencies between the building portfolio as a whole and other infrastructure systems that together contribute to the social-economic stability of a community. To facilitate community resilience planning, the current engineering practice of design, assessment, and risk management of buildings should move beyond the individual building-level to a comprehensive portfolio-level approach. This portfolio-level approach must be developed through investigation and modeling of the functionality losses and recovery process of spatially distributed buildings within a community as a whole, as an integrated system, to enable pre-disaster mitigation decisions and post-disaster recovery planning strategies to be optimized under various resources and regulatory constraints in a risk-informed manner.

Toward that goal, this research has been conducted in four steps: 1) a new building portfolio functionality metric (BPFM) was proposed as an effective indicator of a building portfolio's capacity to respond and recover from a hazard; 2) a building portfolio functionality loss estimation (BPLE) framework was developed to estimate the spatial functionality loss across a community building portfolio immediately following a hazard event; 3) a novel stochastic post-disaster building portfolio recovery model (BPRM) was formulated to characterize the spatial and temporal evolution of a building

portfolio's recovery following a hazard event; and 4) a building portfolio decision support (BPDS) framework was constructed to facilitate communities to achieve risk-informed resilience goals through optimized mitigation strategies and recovery planning activities at a community scale.

8.2 Conclusions

The risk-based framework for resilience assessment of community building portfolios developed in this dissertation has made several distinct contributions, as compared with approaches that appear in the recent literature:

First, the newly introduced BPFM includes a building-level functionality metric (*RE*, *RU*, *RO*, *BF*, and *FF*) and a portfolio-level functionality metric (*PRI*, defined as the percentage of buildings in a portfolio that are in any of the five pre-defined functionality states). The BPFM explicitly reflects the dependency of the building portfolio on other community infrastructure systems in maintaining its desired functionality level, which is not reflected in other typical building-related metrics in the literature. Furthermore, it enables the performance of a building portfolio to be assessed on a consistent measure at various spatial scales (e.g. parcel, block, census, zone or community) and to be tracked throughout the time domain of resilience assessment (including pre-event planning, immediate post-disaster response, and long-term recovery).

Second, the BPLE framework provides a probabilistic and spatial depiction of functionality losses across a community building portfolio. The major contributions of the BPLE are manifested in the following aspects. The uncertainties associated with

hazard demands and building vulnerabilities as well as the spatial correlations among demands and within building responses due to common design and construction practices are propagated through the analysis through multiple-layers of Monte Carlo Simulation of conditional events coupled with proposed sample techniques. In contrast to widely-used existing loss estimation platforms (e.g. HAZUS-HM and MAEViz), this rigorous and consistent uncertainty modeling scheme enables the uncertainty in the spatial loss of distributed building portfolios to be estimated realistically. Furthermore, a damage-to-functionality mapping is proposed to relate the building functionality states to the joint status of building's physical damage and utility disruption of a building; this mapping, distinguished from some existing building-level functionality assessments supported by detailed building-specific information, effectively facilitates the portfolio functionality loss estimation at regional or community scale. The outcomes of BPLE characterize the initial functionality state for recovery modeling, which is the starting point of the BPRM.

Third, the novel BPRM is constructed in two critical steps: i) modeling individual building restoration as a discrete state, continuous time Markov Chain (CTMC); and ii) modeling building portfolio recovery through aggregating the CTMC restoration processes of individual buildings across the domain of the community and over the entire recovery time horizon. The two-step BPRM was calibrated through a review of existing recovery-related databases and variables known to be essential for building portfolio recovery analysis. Uncertainties in these variables were propagated, and the time-variant spatial correlations in buildings' functionality states were quantified throughout the BPRM in the estimation of the portfolio recovery trajectory

and recovery time. The BPRM is capable of quantifying the impact of different pre-hazard mitigation strategies on the overall portfolio recovery process, and as a result can facilitate community recovery planning. The coupled BPLE and BPRM framework together can be used to quantify both the robustness and recovery of community building portfolios in a rigorous, probabilistic and consistent manner, as illustrated through the testbed communities assessed – Centerville and Shelby County, TN.

Finally, the BPDS framework can guide and support community planning decisions. The BPDS is formulated for designing an effective building portfolio retrofit plan. As an illustration, the number of buildings to be retrofitted as well as the design code level for retrofitting can be specified to ensure that the target portfolio robustness goal is achieved and, at the same time, the total *portfolio retrofit cost* and the expected *portfolio recovery time* are minimized. The BPDS framework has proven that the BPLE and BPRM can indeed support the quantitative decision formulation regarding building portfolio risk mitigation and recovery strategies, and that such decisions can be optimized to enable community resilience planning efforts to be conducted in a risk-informed and cost-effective manner.

8.3 Future Work

The present work has identified some issues that should be addressed and improved in the future research:

Conceptually, the resilience assessment framework proposed in this study can be applied to different natural hazards. For illustration purpose, the developed methodologies are applied to scenario earthquakes. Nevertheless, its application to other

types of hazards needs to be completed, which will require hazard-specific adjustments in the framework in both loss estimation and recovery modeling. Moreover, efforts need to be devoted to the validation of the proposed methodologies, preferably using observed data from historical events.

In this study, a random sampling technique to increase computational efficiency of the BPLE was implemented at the expense of computational accuracy. The practical implementation of the method, however, depends on the size and topology of the building portfolio, as well as the level of the site-to-site and structure-to-structure correlations in hazard demand and structural response. Additional sensitivity studies should be performed to explore the efficiency of the sampling technique when applied to building portfolios of different sizes and topologies. Moreover, advanced sampling techniques aimed at reducing the computational efforts of MCS should be explored, to quantify the uncertainties of all spatially correlated intermediate random variables associated with building functionality loss and recovery analysis and to minimize computational effort for large size community building portfolios.

Community building portfolios, by nature, interconnect with other infrastructure systems within a community. On the one hand, the functionality of buildings relies on lifeline systems to provide services (say, power, water). On the other hand, the building portfolios of different occupancies provide functionality to support social and economic activities of a community. The BPLE and BPRM have considered the effect of utility disruption resulting from cascading failures of the community's utility networks. Nevertheless, the effect of other infrastructure systems (e.g., transportation) and the effect of social-economic recovery on building functionality recovery have not been

adequately explored. Future work should include "re-couple" social science into the building portfolio recovery model, for example, capturing the effect of social vulnerability during recovery of building portfolios. To be specific, future research should develop a community recovery model that integrates the recovery models of the community built environment and socioeconomic systems through well-designed information flow among these models at appropriate spatial and temporal resolutions throughout the time horizon of community recovery process.

A well-defined risk-informed decision framework should be formulated to facilitate multiple hazard mitigation strategies, identify optimal resource allocation plans, reflect the values and risk tolerance of the community, and balance needs and interest of different community stakeholders. Such studies will require advance multi-objective optimization algorithms and a collection of data to support framework modeling. Future studies should identify effective disaster mitigation strategies and develop comprehensive risk-informed decision tools to guide stakeholder of the community in terms of hazard mitigation and community resilience planning.

References

Adachi, T. & Ellingwood, B.R. (2008). Serviceability of earthquake-damaged water systems: Effects of electrical power availability and power backup systems on system vulnerability. *Reliability Engrg. and System Safety 93*(1):78-88.

Almufti, I., & Wilford, M. (2013). REDi™ Rating System: Resilience based Earthquake Design Initiative for the Next Generation of Buildings, Version 1.0. October, Arup.

Arup (2014). City Resilience Framework. *The Rockefeller Foundation, Arup*.

ASCE Standard 7 (2010). Minimum design loads for buildings and other structures (ASCE Standard 7-10). *Am. Soc. of Civil Engr., Reston, VA*.

ASCE/SEI (ASCE/Structural Engineering Institute). (2016). Minimum design loads for buildings and other structures. ASCE/SEI 7-16, *Am. Soc. of Civil Engr., Reston, VA*.

Atkinson, G. M., & Boore, D. M. (1995). Ground-motion relations for eastern North America. *Bulletin of the Seismological Society of America*, *85*(1), 17-30.

Baxter, J. (2013). Mitigation Ideas: A Resource for Reducing Risk to Natural Hazards. *US Department of Homeland Security*. FEMA.

Berke, P., Jack, K., & Dennis, W. (1993). Recovery after Disaster: Achieving Sustainable, Development, Mitigation and Equity. *Disasters 17*(2), 93-109.

Bocchini, P & Frangopol, D.M. (2011). Resilience-driven disaster management of civil infrastructure. *ECCOMAS Thematic Conference on Computational Methods in Structural Dynamics and Earthquake Engineering*, Corfu, Greece, 25-28 May 2011.

Bolin, R. (1985). Disasters and Long-Term Recovery Policy: A Focus on Housing and Families. *Review of Policy Research*, 4(4), 709-715.

Bolin, R. C., & Bolton, P. A. (1986). Race, religion, and ethnicity in disaster recovery.

Bolin, R., & Stanford, L. (1991). Shelter, housing and recovery: a comparison of US disasters. *Disasters*, 15(1), 24-34.

Bonstrom, H., & Corotis, R.B. (2014). Building portfolio seismic loss assessment using the First-Order Reliability Method. *Structural Safety*, doi:10.1016/j.strusafe.2014.09.005.

Bruneau, M., Chang, S., Eguchi, R., Lee, G., O'Rourke, T., Reinhorn, A.M., Shinozuka, M., Tierney, K., Wallace, W., & Winterfelt, D.V. (2003). A framework to quantitatively assess and enhance the seismic resilience of communities. *Earthquake Spectra, 19* (4), 733–752.

Bruneau, M. (2006). Enhancing the resilience of communities against extreme events from an earthquake engineering perspective. *Journal of Security Education 1*(4): 159-167.

Bruneau, M. &Reinhorn, A. (2006). Overview of the resilience concept. *Proceedings of the 8th US National Conference on Earthquake Engineering*.

Bruneau, M., & Reinhorn, A. (2007). Exploring the concept of seismic resilience for acute care facilities. *Earthquake Spectra 23*(1): 41-62.

Building Seismic Safety Council (2003). The 2003 NEHRP recommended provisions for new buildings and other structures. Part I: Provisions, *FEMA 450*.

Burton, H. V., Deierlein, G., Lallemant, D., & Lin, T. (2015). Framework for incorporating probabilistic building performance in the assessment of community seismic resilience. *Journal of Structural Engineering*, 142(8), C4015007.

Burton, C. G. (2015). A validation of metrics for community resilience to natural hazards and disasters using the recovery from Hurricane Katrina as a case study. *Annals of the Association of American Geographers*, *105*(1), 67-86.

Campbell, K. W. (2003). Prediction of strong ground motion using the hybrid empirical method and its use in the development of ground-motion (attenuation) relations in eastern North America. *Bulletin of the Seismological Society of America*, 93(3), 1012-1033.

Chang, S. E. (2010). Urban disaster recovery: a measurement framework and its application to the 1995 Kobe earthquake. Disasters, 34(2), 303-327.

Cimellaro, G. P., Reinhorn, A.M. & Bruneau, M. (2010a). Framework for analytical quantification of disaster resilience. *Engineering Structures 32*(11): 3639-3649.

Cimellaro, G. P., Reinhorn, A.M. & Bruneau., M. (2010b). Seismic resilience of a hospital system. *Structure and Infrastructure Engineering 6*(1)-(2): 127-144.

Cimellaro, G. P. (2016). *Urban resilience for emergency response and recovery: fundamental concepts and applications* (Vol. 41). Springer.

Comerio, M.C. (1998). *Disaster hits home: New policy for urban housing recovery*. Berkely, CA: University of California Press.

Comerio, M. C. (2006). Estimating downtime in loss modeling. *Earthquake Spectra*, 22(2), 349-365.

Cornell, C. Allin, & Helmut Krawinkler. (2000). Progress and challenges in seismic performance assessment. *PEER Center News 3*(2): 1-3.

Cutter, S. L., Barnes, L., Berry, M., Burton, C., Evans, E., Tate, E., & Webb, J. (2008). A place-based model for understanding community resilience to natural disasters. *Global environmental change*, 18(4), 598-606.

Cutter, S. L., Ash, K. D., & Emrich, C. T. (2014). The geographies of community disaster resilience. Global environmental change, 29, 65-77.

Deshmukh, A. & Hastak, M. (2012). A framework for enhancing resilience of community by expediting post disaster recovery, *at International Conference on Disaster Management, Kumamoto*, Japan, August 2012.

Ellingwood B. R., Cutler, H., Gardoni, P., Peacock, W. G., van de Lindt, J. W. & Wang, N. (2016) The Centerville Virtual Community: A Fully Integrated Decision Model of Interacting Physical and Social Infrastructure Systems. *Sustainable and Resilient Infrastructure*. 1(3-4), 95-107.

Federal Emergency Management Agency (FEMA). 1997. FEMA 273, NEHRP Guidelines for the Seismic Rehabilitation of Buildings. Washington, DC

FEMA/NIBS. (2003). Multi-hazard Loss Estimation Methodology Earthquake Model (HAZUS-MH MR4): Technical Manual. Washington, D.C.

FEMA. (2012). FEMA P-58-1: Seismic Performance Assessment of Buildings. Volume 1– Methodology.

FEMA Training, FEMA.gov. , Chapter 3: Mitigation. https://training.fema.gov/hiedu/downloads/case%20study%20chapter%203.doc

Girard, C., & Peacock, W. G. (1997). Ethnicity and segregation: Post-hurricane relocation. *Hurricane Andrew: Ethnicity, gender and the sociology of disasters*, 191-205.

Goda, K. & Hong, H.P. (2008). Estimation of Seismic Loss for Spatially Distributed Buildings. *Earthquake Spectra 24* (4); 889-910.

Godschalk, D. (1999). *Natural hazard mitigation: Recasting disaster policy and planning*. Island Press.

González, A. D., Dueñas-Osorio, L., Sánchez-Silva, M., & Medaglia, A. L. (2015). The interdependent network design problem for optimal infrastructure system restoration. *Computer-Aided Civil and Infrastructure Engineering*.

Haas, J, Robert, K., & Martyn, B., eds. (1977). Reconstruction following disaster. *Cambridge Mass.: MIT Press.*

Holmes, T. (2016). Planning for Community Resilience: *A Handbook for Reducing Vulnerability to Disasters*, by Jamie Hicks Masterson, Walter Gillis Peacock, Shannon S. Van Zandt, Himanshu Grover, Lori Feild Schwarz, and John T. Cooper, Jr. (2014). Washington, DC: Island Press. 256 pages. Journal of the American Planning Association, 82(2), 214-215.

Hoshiya, M. (1981). Seismic damage restoration of underground water pipelines. In *A Paper prepared for Review Meeting of the US-Japan Cooperative Research Seismic Risk Analysis and Its Application to Reliability-Based Design of Lifeline Systems,* Honolulu, January l98l.

Isoyama, R., Iwata, T., & Watanabe, T. (1985). Optimization of post-earthquake restoration of city gas systems. In *Proc. of the Trilateral Seminar-Workshop on Lifeline Earthquake Engineering*, Taipei, Taiwan (pp. 3-17).

Isumi, M., Nomura, N., & Shibuya, T. (1985). Simulation of Post-Earthquake Restoration of Lifeline Systems. *International journal of mass emergencies and disasters*, *3*(1), 87-105.

Jayaram, N. & Baker, J.W. (2009). Correlation Model for Spatially Distributed Ground-motion Intensities. *Earthquake Engineering & Structural Dynamics*, *38*(15); 22.

Kameda, H. (1994). Multi-phase evaluation of lifeline system performance under earthquake environment. In *Proceedings of Second China-Japan-US Trilateral Symposium on Lifeline Earthquake Engineering*.

Kates, R. W., & Pijawka, D. (1977). From rubble to monument: the pace of reconstruction. *Reconstruction following disaster*, *1*.

Kozin, F., & Zhou, H. (1990). System study of urban response and reconstruction due to earthquake. *Journal of Engineering Mechanics*, *116*(9), 1959-1972.

Lee, R., & Kiremidjian, A.S. (2007). Uncertainty and correlation for loss assessment of spatially distributed systems. *Earthquake Spectra, 23*(4) :753-770.

Lin, P., & Wang, N. (2016). Building portfolio fragility functions to support scalable community resilience assessment. *Sustainable and Resilient Infrastructure, 1*(3-4), 108-122.

Lin, P., Wang, N., & Ellingwood, B. R. (2016). A risk de-aggregation framework that relates community resilience goals to building performance objectives. *Sustainable and Resilient Infrastructure*, *1*(1-2), 1-13.

Lin, P., & Wang, N. (2017a). Stochastic post-disaster functionality recovery of community building portfolios I: Modeling. *Structural Safety, 69*, 96-105.

Lin, P., & Wang, N. (2017b). Stochastic post-disaster functionality recovery of community building portfolios II: Application. *Structural Safety, 69*, 106-117.

Lin, Y. (2009). Development of algorithms to estimate post-disaster population dislocation: A research-based approach. Ph.D. thesis, Texas A & M University.

Lindell, M. K., Perry, R. W., Prater, C., & Nicholson, W. C. (2006). *Fundamentals of emergency management.* Washington, DC: FEMA.

Liu, H., Davidson, R. A., & Apanasovich, T. V. (2007). Statistical forecasting of electric power restoration times in hurricanes and ice storms. *Power Systems, IEEE Transactions on*, *22*(4), 2270-2279.

Mahsuli, M. and Haukaas, T. (2013). Seismic risk analysis with reliability methods, Part I: Models. *Structural Safety*, 42(1), pp. 54–62.

May, P. J., & Williams, W. (2012). Disaster policy implementation: Managing programs under shared governance. *Springer Science & Business Media.*

Miles, S. B., & Chang, S. E. (2003). Urban disaster recovery: A framework and simulation model.

Miles, S. B., & Chang, S. E. (2007). A simulation model of urban disaster recovery and resilience: Implementation for the 1994 Northridge earthquake.

Miles, S. B., & Chang, S. E. (2011). ResilUS: a community based disaster resilience model. *Cartography and Geographic Information Science*, 38(1), 36-51.

Miller, M., Baker, J., Lim, H. W., Song, J., & Jayaram, N. (2011). A FORM-based analysis of lifeline networks using a multivariate seismic intensity model. *In: 11th international conference on applications of statistics and probability in civil engineering (ICASP),*

NEHRP. (2009). Recommended seismic provisions for new buildings and other structures (FEMA P-750). *Federal Emergency Management Agency*, Washington, D.C.

NIST. (2015). Community resilience planning guide for buildings and infrastructure systems. Volume 1 and Volume 2.

Noda, S., Yamada, Y., & Iemura, H. (1981). Restoration of serviceability of a pipeline system. In *Lifeline Earthquake Engineering: The Current State of Knowledge, 1981* (pp. 225-240). ASCE.

Nojima, N., Ishikawa, Y., Okumura, T., & Sugito, M. (2001). Empirical estimation of lifeline outage time in seismic disaster. In *Proceedings of US-Japan Joint Workshop and Third Grantee Meeting, US-Japan Cooperative Research on Urban Earthquake Disaster Mitigation* (pp. 516-517).

Nojima, N., & Kameda, H. (1992). Optimal strategy by use of tree structure for post-earthquake restoration of lifeline network systems. In *Proceedings of the 10th World Conference on Earthquake Engineering* (pp. 5541-5546).

Oaks, D. S. (1990). The damage assessment process: the application of ATC-20. *The Loma Prieta earthquake, studies of short-term impacts. Program on environmental and behavior monograph*, *50*.

Ohlsen, C. & Rubin, C. (1993). *Planning for disaster recovery*. MIS report 25(7), 23. Washington, DC: International City Management Association.

Okuyama, Y., Hewings, G. J., & Sonis, M. (2004). Measuring economic impacts of disasters: interregional input-output analysis using sequential interindustry model. In *Modeling Spatial and Economic Impacts of Disasters* (pp. 77-101). Springer Berlin Heidelberg.

Olson, R.S. (2000). Toward a politics of disaster: Losses, values, agendas, and blame. *International Journal of Mass Emergencies and Disasters*, 18(2), 265–287.

Oregon. Seismic Safety Policy Advisory Commission (OSSPAC). (2013). The Oregon resilience plan: reducing risk and improving recovery for the next Cascadia earthquake and tsunami. The Commission.

Peacock, W. G., B. H. Morrow, & H. Gladwin. (1997). *Hurricane Andrew: Ethnicity, Gender, and the Sociology of Disasters*. London: Routledge.

Peacock, W., Lin, Y., Lu, J., & Zhang, Y. (2008). Household dislocation algorithm 2: an OLS through the origin approach. Hazard Reduction and Recovery Center. Texas A&M University. HRRC Reports: 08-04R.

Peacock, W. G., Husein, R., & Center, R. (2011). The adoption and implementation of hazard mitigation policies and strategies by coastal jurisdictions in Texas: The planning survey results.

Peacock, W. G., Van Zandt, S., Zhang, Y., & Highfield, W. E. (2014). Inequities in long-term housing recovery after disasters. *Journal of the American Planning Association*, *80*(4), 356-371.

Poland, C. (2009). The resilient city: Defining what San Francisco needs from its seismic mitigation polices. *San Francisco Planning and Urban Research Association report*, San Francisco, CA, USA.

Porter, K., & Ramer, K. (2012). Estimating earthquake-induced failure probability and downtime of critical facilities. *Journal of business continuity & emergency planning*, 5(4), 352-364.

Quarantelli, E. (1982). Sheltering and Housing after Major Community Disasters: Case Studies and General Observations. *OHIO STATE UNIV RESEARCH FOUNDATION COLUMBUS.*

Rodriguez-Llanes JM, Vos F, Yilmaz L, Guha-Sapir D (2013) Developing indicators and indicators systems of societal resilience to disasters: what prevent us from doing better? embrace project

Rose, A., & Guha, G. S. (2004). Computable general equilibrium modeling of electric utility lifeline losses from earthquakes. In *Modeling spatial and economic impacts of disasters* (pp. 119-141). Springer Berlin Heidelberg.

RS Means Company. (2015). Building construction cost data. *RS Means Company.*

Rubin, C. B. (1991). Disaster recovery after Hurricane Hugo in South Carolina. *Natural Hazards Research and Applications Information Center*, Institute of Behavioral Science, University of Colorado.

Shinozuka, M., Rose, A., & Eguchi, R. T. (1998). Engineering and socioeconomic impacts of earthquakes. *Buffalo, NY: Multidisciplinary Center for Earthquake Engineering Research.*

Smith, G. P., & Wenger, D. (2007). Sustainable disaster recovery: operationalizing an existing agenda. In *Handbook of disaster research* (pp. 234-257). Springer New York.

Steelman, Joshua, Junho Song, & Jerome F. Hajjar. (2007). Integrated Data Flow and Risk Aggregation for Consequence-Based Risk Management of Seismic Regional Loss. University of Illinois

UNISDR (2014). *Disaster Resilience Scorecard for Cities*. UNISDR, Geneva, Switzerland.

Vitoontus, S. & Ellingwood. B.R. (2013). Role of Correlation in Seismic Demand and Building Damage in Estimating Losses under Scenario Earthquakes. *Proc. Int. Conf. on Struct. Safety and Reliability (ICOSSAR 2013)*, New York, NY, Taylor & Francis, A.A. Balkema, The Netherlands.

Wang, M., & Takada, T. (2005). Macrospatial Correlation Model of Seismic Ground Motions. *Earthquake Spectra, 2*(4):1137-1156.

Whittaker, A., Deierlein, G., Hooper, J., & Merovich, A. (2004). Enginnering Demand Parameters for Structural Framing Systems. ATC 58 Structural Performance Products Team, Redwood City, CA.

Xiao, Y., & Van Zandt, S. (2012). Building community resiliency: Spatial links between household and business post-disaster return. *Urban Studies*, *49*(11), 2523-2542.

Yoshikawa, H., & Goda, K. (2013). Financial seismic risk analysis of building portfolios. Natural Hazards Review, 15(2), 112-120.

Zhang, Y., & Peacock, W. G. (2009). Planning for housing recovery? Lessons learned from Hurricane Andrew. *Journal of the American Planning Association*, *76*(1), 5-24.

Zhang, W., & Wang, N. (2016). Resilience-based risk mitigation for road networks. *Structural Safety*, *62*, 57-65.

Zhang, W., Wang, N., & Nicholson, C. (2017). Resilience-based post-disaster recovery strategies for road-bridge networks. *Structure and Infrastructure Engineering*, 1-10.

Zhang, W., Lin, P., Wang, N., Nicholson, C., & Xue, X. (2018). Probabilistic Prediction of Postdisaster Functionality Loss of Community Building Portfolios Considering Utility Disruptions. *Journal of Structural Engineering*, 144(4), 04018015.